Searches for third-generation squark production in fully hadronic final states in proton-proton collisions at $\sqrt{s} = 8$ TeV

The CMS collaboration

E-mail: cms-publication-committee-chair@cern.ch

ABSTRACT: Searches for third-generation squarks in fully hadronic final states are presented using data samples corresponding to integrated luminosities of 19.4 or 19.7 fb^{-1}, collected at a centre-of-mass energy of 8 TeV with the CMS detector at the LHC. Three mutually exclusive searches are presented, each optimized for a different decay topology. They include a multijet search requiring one fully reconstructed top quark, a dijet search requiring one or two jets originating from b quarks, and a monojet search. No excesses above the standard model expectations are seen, and limits are set on top and bottom squark production in the context of simplified models of supersymmetry.

Contents

1 Introduction

The standard model (SM) of particle physics has proven to be remarkably robust. Nonetheless, the SM has well-known shortcomings, such as an instability in the calculation of the Higgs boson mass known as the fine-tuning (or hierarchy) problem [1–5]. The discovery of

a Higgs boson with a mass of about $125\,\mathrm{GeV}$ [6–8] at the CERN LHC has reinforced the acuteness of this problem. These shortcomings suggest that the SM is merely a low-energy approximation of a deeper, more complete theory. Supersymmetry (SUSY) [9–15] is a widely considered extension of the SM that introduces an additional symmetry of nature between fermions and bosons. A new supersymmetric particle (sparticle) is proposed for each SM particle, with the same mass and quantum numbers but with a spin that differs by a half-integer unit. For example, squarks are the SUSY partners of quarks. Supersymmetric models contain extended Higgs sectors. The SUSY partners of the Higgs bosons are higgsinos. Neutral (charged) higgsinos mix with the SUSY partners of the neutral (charged) electroweak gauge bosons to form neutralinos $\widetilde{\chi}^0$ (charginos $\widetilde{\chi}^\pm$). Divergent quantum corrections to the Higgs boson mass due to virtual SM particles are cancelled by corresponding contributions from virtual sparticles [16–19], thus resolving the fine-tuning problem.

The symmetry proposed by SUSY cannot be exact, as no sparticles have yet been observed. However, the stabilising features of SUSY can survive with a modest amount of fine tuning if sparticles are not much heavier than their SM counterparts. For third-generation particles in particular, the mass difference between a particle and its corresponding sparticle should not be too large, in order for SUSY to provide a so-called "natural" solution [20–23] to the fine-tuning problem. Thus the SUSY partners of top and bottom quarks, the top and bottom squarks $\widetilde{t}$ and $\widetilde{b}$, respectively, might have masses below or around the TeV scale and be accessible at the LHC. In SUSY models with R-parity [24] conservation, top and bottom squarks can be pair produced, with each top or bottom squark initiating a decay chain in which the end products are SM particles and a stable lightest supersymmetric particle (LSP). In many SUSY scenarios the LSP is the lightest neutralino $\widetilde{\chi}^0_1$, which is weakly interacting and will escape detection, leading to a distinctive experimental signature of large momentum imbalance in the plane perpendicular to the beam axis.

This paper presents three complementary searches for the direct production of either a pair of top squarks ($\widetilde{t}\overline{\widetilde{t}}$) or bottom squarks ($\widetilde{b}\overline{\widetilde{b}}$) decaying to fully hadronic final states with large transverse momentum imbalance. The searches are based on proton-proton collision data collected using the CMS detector at the LHC at a centre-of-mass energy of $8\,\mathrm{TeV}$ and correspond to an integrated luminosity of 19.4 or $19.7\,\mathrm{fb}^{-1}$ depending on the study [25]. Each search is separately optimized for different kinematic regimes of top or bottom squark masses, as well as for mass differences between the squark and LSP, where the LSP is taken to be the $\widetilde{\chi}^0_1$. They are: (1) a search for top-squark pair production in multijet events with at least one tagged hadronically decaying top quark (hereafter referred to as the "multijet t-tagged" search), which is sensitive to scenarios with a large mass difference between the top squark and the LSP; (2) a search for dijet events with exactly one or two tagged bottom-quark jets (b jets) possibly accompanied by additional jets radiated in the initial state (hereafter referred to as the "dijet b-tagged" search), which is sensitive to scenarios with large or intermediate mass differences between the bottom squark and the LSP; and (3) a search for events with a single jet (hereafter referred to as the "monojet" search), which is sensitive to scenarios with highly compressed spectra, i.e. to scenarios in which

the mass difference between the top or bottom squark and the LSP is small. The results from the three searches are combined and interpreted in the context of simplified model spectra (SMS) [26]. Previous searches for top- and bottom-squark pair production at the LHC are presented in refs. [27–39].

This paper is organised in the following way. Section 2 describes the CMS detector, and section 3 discusses event reconstruction algorithms. The simulations of signal and background events are outlined in section 4. A summary of the strategies shared by all three searches, including common event selections and backgrounds, are discussed in section 5. The multijet t-tagged search is presented in section 6, the dijet b-tagged search in section 7, and the monojet search in section 8. Finally, the results are shown in section 9 and interpreted using SMS in section 10, with a summary in section 11. Additional information for model testing can be found in appendix A.

2   The CMS detector

The central feature of the CMS apparatus is a superconducting solenoid of 6 m internal diameter, providing a magnetic field of 3.8 T. Within the superconducting solenoid volume are a silicon pixel and strip tracker, a lead tungstate crystal electromagnetic calorimeter (ECAL), and a brass and scintillator hadron calorimeter (HCAL), each composed of a barrel and two endcap sections. Muons are measured in gas-ionization detectors embedded in the steel flux-return yoke outside the solenoid. Extensive forward calorimetry complements the coverage provided by the barrel and endcap detectors.

The polar angle θ, defined with respect to the anticlockwise-beam direction, the pseudorapidity η, defined as $\eta = -\ln[\tan(\theta/2)]$, and the azimuthal angle ϕ in the plane perpendicular to the beam axis, define the coordinates used to describe position within the detector. The transverse momentum vector $\vec{p}_T$ of a particle is defined as the projection of its four-momentum on to the plane perpendicular to the beams. Its magnitude is referred to as p_T.

The silicon tracker measures charged particles within the pseudorapidity range $|\eta| <$ 2.5. Isolated particles of $p_T = 100\,\text{GeV}$ emitted with $|\eta| < 1.4$ have track resolutions of 2.8% in p_T and 10 (30) μm in the transverse (longitudinal) impact parameter [40]. The ECAL and HCAL measure energy deposits in the pseudorapidity range $|\eta| < 3$. Quartz-steel forward calorimeters extend the coverage to $|\eta| = 5$. The HCAL, when combined with the ECAL, measures jets with a resolution $\Delta E/E \approx 100\%/\sqrt{E\,[\text{GeV}]} \oplus 5\%$ [41]. Muons are measured in the pseudorapidity range $|\eta| < 2.4$. Matching muons to tracks measured in the silicon tracker results in a relative transverse momentum resolution for muons with $20 < p_T < 100\,\text{GeV}$ of 1.3–2.0% in the barrel and better than 6% in the endcaps. The p_T resolution in the barrel is better than 10% for muons with p_T up to 1 TeV [42].

The events used in the searches presented here were collected using a two-tier trigger system: a hardware-based level-1 trigger and a software-based high-level trigger. A full description of the CMS detector and its trigger system can be found in ref. [43].

3   Event reconstruction

Events are reconstructed with the CMS particle-flow algorithm [44, 45]. Using an optimized combination of information from the tracker, the calorimeters, and the muon systems, each particle is identified as a charged hadron, neutral hadron, photon, muon, or electron. Charged hadrons that do not originate from the primary vertex, defined by the pp interaction vertex with the largest sum of charged-track p_T^2 values, are not considered. The remaining particles are clustered into jets using the anti-k_T algorithm with distance parameter 0.5 [46]. Calorimeter energy deposits corresponding to neutral particles originating from overlapping pp interactions, "pileup", is subtracted on an event-by-event basis using the jet-area method [47]. Jets are corrected to take into account the detector response as a function of jet p_T and η, using factors derived from simulation. The jets must satisfy loose identification criteria that remove calorimeter noise. An additional residual energy correction, derived from dijet and γ+jets events, is applied to account for differences in the jet energy scales [48] between simulation and data.

Both the multijet t-tagged and dijet b-tagged analyses employ tagging of b quark jets (b tagging). Utilising the precise inner tracking system of the CMS detector, the combined secondary vertex (CSV) algorithm [49] uses secondary vertices, track-based lifetime information, and jet kinematics to distinguish between jets from b quarks and those from light quarks or gluons.

In the multijet t-tagged analysis, a jet is tagged as a b quark jet if it satisfies $p_T > 30\,\text{GeV}$, $|\eta| < 2.4$, and the medium working point requirements of the algorithm [50]. Averaged over p_T in $t\bar{t}$ events, the b quark identification efficiency is 67% for the medium working point, and the probability for a jet originating from a light quark or gluon to be misidentified as a b quark jet is 1.4%. The dijet b-tagged analysis uses the loose and medium working point versions of the algorithm. The b-tagging efficiency is 80–85% (46–74%) for the loose (medium) working point [49], and the probability for a jet originating from a light quark or gluon to be misidentified as a b quark is 8–12% (1–2%). Values are quoted for jets with $p_T > 70\,\text{GeV}$ and are dependent on the jet p_T.

Muons are reconstructed by finding compatible track segments in the silicon tracker and the muon detectors [42]. Both the dijet b-tagged and multijet t-tagged analyses require muons to lie within $|\eta| < 2.1$, whereas the monojet analysis uses muons up to $|\eta| < 2.4$. Electron candidates are reconstructed from a cluster of energy deposits in the ECAL that is matched to a track in the silicon tracker [51]. Electron candidates are required to satisfy $|\eta| < 1.44$ or $1.56 < |\eta| < 2.5$, where the intermediate range of $|\eta|$ is excluded to avoid the transition region between the ECAL barrel and endcap, in which the reconstruction efficiency is difficult to model. Muon and electron candidates are required to originate within 2 mm of the beam axis in the transverse plane. In the monojet analysis, hadronically decaying τ leptons are reconstructed using the "hadron-plus-strips" algorithm [52], which reconstructs candidates with one or three charged pions and up to two neutral pions.

A relative lepton isolation parameter is defined as the sum of the p_T of all photons and all charged and neutral hadrons, computed in a cone of radius $\Delta R = \sqrt{(\Delta \eta)^2 + (\Delta \phi)^2} = 0.4$ around the lepton direction, divided by the lepton p_T. Values are corrected for the effect of

pileup. Lepton candidates with relative isolation values below 0.2 are considered isolated in the monojet and dijet b-tagged analyses.

In the multijet t-tagged analysis, a key ingredient for providing good background rejection and simultaneously preserving good signal selection involves vetoing prompt leptons from W or Z boson decays, while accepting possible secondary leptons from b quark decays. Hence events containing a muon or electron with $p_T > 5\,\text{GeV}$ are vetoed based on the spatial distribution of particles around the lepton. A directional isolation parameter Iso^{dir} is defined by considering particles in a region of radius ΔR centred on the lepton direction, where ΔR is 0.2 for muons and 0.2 (0.3) for electrons with $|\eta| \leq 1.44\,(>1.56)$. A sum is performed over the particle transverse momenta multiplied by the square of the angle in the η–ϕ plane between the particle and the p_T-weighted centroid of all particles contributing to the sum [53]. Leptons from heavy-quark decays usually are closer to hadronic activity in η–ϕ space than leptons from on-shell W or Z boson decays. The requirements on Iso^{dir} have been chosen to retain high rejection efficiency, especially for high-p_T leptons, and a small misidentification rate for leptons from b quark decays. This is the first CMS publication to make use of this variable.

The hermetic nature of the CMS detector allows event reconstruction over nearly the full solid angle. Conservation of momentum in the transverse plane can therefore be used to detect a momentum imbalance, which can be associated with particles that exit the detector without interaction. The missing transverse momentum vector $\vec{p}_T^{\text{miss}}$ is defined as the projection on the plane perpendicular to the beam axis of the negative vector sum of the momenta of all reconstructed particles in an event. Its magnitude is referred to as p_T^{miss}. For the monojet analysis, an alternative definition of $\vec{p}_T^{\text{miss}}$ is used, $\vec{p}_T^{\text{miss},\mu}$, which differs from the nominal definition in that the contribution of muons is excluded. This alternative definition allows the same trigger, for which missing transverse momentum is defined without muons, to be used for both signal and control samples, reducing systematic uncertainties. The alternative definition $\vec{p}_T^{\text{miss},\mu}$ is also used to evaluate some electroweak backgrounds for the multijet t-tagged and dijet b-tagged analyses, as described below.

4 Simulation of signal and background event samples

Monte Carlo (MC) simulations of signal and background events are used to optimize selection criteria, determine signal efficiencies, and develop background estimation techniques.

Within the context of natural SUSY, several SMS scenarios are examined. They are based on the pair production of top or bottom squarks followed by the decay of the top or bottom squarks according to $\widetilde{t} \to t\widetilde{\chi}_1^0$, $\widetilde{t} \to b\widetilde{\chi}_1^\pm$ with $\widetilde{\chi}_1^\pm \to bW^\pm$, $\widetilde{t} \to c\widetilde{\chi}_1^0$, and $\widetilde{b} \to b\widetilde{\chi}_1^0$, where $\widetilde{\chi}_1^\pm$ is the lightest chargino. The Feynman diagrams for these processes are shown in figure 1. Simulated samples of signal events are generated with the MADGRAPH 5.1.3.30 [54] event generator, with up to two additional partons incorporated at the matrix element level. All SUSY particles other than those included in the SMS scenario under consideration are assumed to be too heavy to participate in the interaction.

SM events are simulated using a number of MC event generators. Top-antitop quark pair production ($t\bar{t}$), W/Z +jets, Zγ, Wγ, $t\bar{t}$Z, and $t\bar{t}$W samples are produced using the
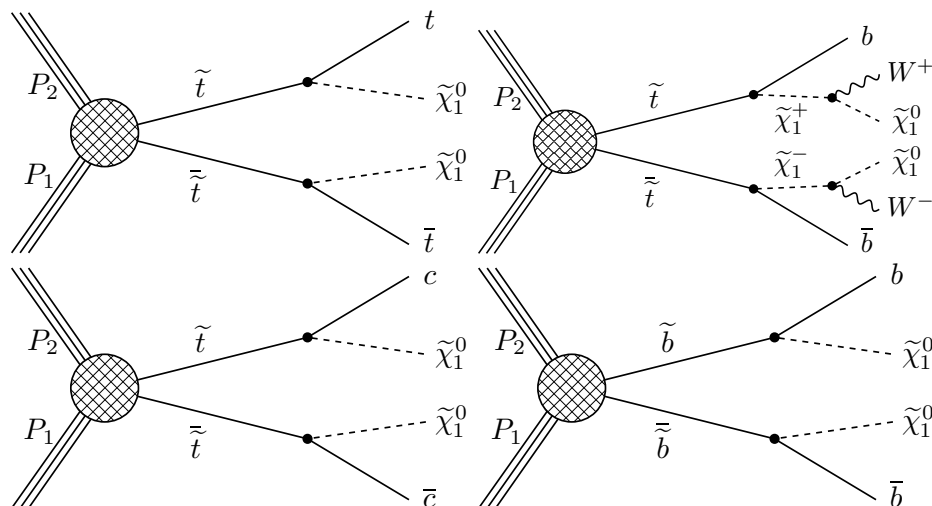
Figure 1. Feynman diagrams showing the pair production of top or bottom squarks followed by their decays according to $\widetilde{t} \to t\widetilde{\chi}_1^0$ (top, left), $\widetilde{t} \to b\widetilde{\chi}_1^\pm$ with $\widetilde{\chi}_1^\pm \to bW^\pm$ (top, right), $\widetilde{t} \to c\widetilde{\chi}_1^0$ (bottom, left), a flavour changing neutral current loop-induced process, and $\widetilde{b} \to b\widetilde{\chi}_1^0$ (bottom, right).

MADGRAPH5 event generator with CTEQ6L [55] parton distribution functions (PDFs). Single top quark events are generated with the POWHEG [56] program using the CT10 [57] and CTEQ66 [58] PDFs. Multijet events from QCD processes and events with WW, WZ and ZZ (diboson) production are simulated with the PYTHIA 6.4.24 [59] program using the CTEQ6L PDFs.

For both the signal and SM simulated samples, the parton shower, hadronization, and multiple-parton interactions are described using PYTHIA. Decays of τ leptons are handled by the TAUOLA 27.121.5 package [60]. The generated events are interfaced to the CMS fast detector simulation [61] for the signal samples and to a GEANT4-based [62] detector simulation for the SM background samples.

5 Search strategy

The analyses presented here are designed to be efficient for possible signals, while maintaining manageable background levels. All three searches require at least one high-p_T jet and a large value of p_T^{miss}. Background from QCD multijet events is reduced by a minimum angle between the directions of the $\vec{p}_T^{\mathrm{miss}}$ vector and highest p_T jet(s). Electroweak backgrounds are reduced by vetoing events with leptons. Use of b tagging and kinematic variables further distinguishes signal from background.

The sources of SM background, and the background evaluation procedures, are also similar in the three searches. Events with a Z boson that decays to neutrinos, denoted $Z(\nu\bar{\nu})$ +jets, contain genuine p_T^{miss} and constitute a significant background. This background is estimated using dimuon control samples, exploiting the similar kinematics of $Z \to \nu\bar{\nu}$ and $Z \to \mu^+\mu^-$ events as well as the known branching fractions. In regions where $t\bar{t}$ contamination is small, W +jets events with $W \to \mu\nu$ can similarly be used to estimate the $Z(\nu\bar{\nu})$

+jets background. Another significant source of background is from W +jets events when the W boson decays leptonically, denoted $W(\ell\nu)$ +jets events. Here, the lepton (electrons and muons, including those from leptonically decaying τ leptons) fails the lepton veto and hence is "lost", i.e. it is not isolated, not identified, or outside of the acceptance of the analysis. Hadronically decaying τ leptons (τ_{h}) from W boson decay in $\mathrm{t\bar{t}}$ and W +jets events form another significant background source. Both the lost-lepton and τ_{h} backgrounds are evaluated using single-muon control samples. Dijet and multijet backgrounds are reduced using topological selections, with the remaining contributions estimated using data control regions enhanced in QCD events. Very small backgrounds from processes such as diboson, $\mathrm{t\bar{t}Z}$, $\mathrm{t\bar{t}W}$, and single top quark are estimated from simulation. The data control regions used in the estimates of the SM backgrounds are defined in such a manner to minimize the contributions of signal events, and thus possible signal event contributions to control regions are ignored.

6 Search for top-squark pair production using top-quark tagging

This search for pairs of hadronically decaying top quarks with large $p_{\mathrm{T}}^{\mathrm{miss}}$ in the final state is motivated by the scenario of top-squark pair production, assuming that the mass difference between the top squark and the stable LSP is larger than the mass of the top quark, $m_{\tilde{\mathrm{t}}} - m_{\tilde{\chi}_1^0} \geq m_{\mathrm{t}}$. The decay channel $\tilde{\mathrm{t}} \to \mathrm{t}\tilde{\chi}_1^0$ is therefore kinematically available, allowing a search for top squarks through top quark tagging, which provides an important discriminant against the multijet background. If $\tilde{\chi}_1^{\pm}$ states exist with a mass between the top squark and the LSP masses, the top squark can also decay via $\tilde{\mathrm{t}} \to \mathrm{b}\tilde{\chi}_1^+ \to \mathrm{bW}^+\tilde{\chi}_1^0$ (plus its charge conjugate), yielding a different event signature since no top quark is produced. By requiring just one fully reconstructed top quark, the search maintains sensitivity to $\tilde{\mathrm{t}} \to \mathrm{t}\tilde{\chi}_1^0$ as well as $\tilde{\mathrm{t}} \to \mathrm{b}\tilde{\chi}_1^{\pm}$ decays.

6.1 Event selection

The event sample used for this analysis is collected by triggering on events with $p_{\mathrm{T}}^{\mathrm{miss}} >$ 80 GeV, where $p_{\mathrm{T}}^{\mathrm{miss}}$ is reconstructed using the particle-flow algorithm, and at least two central ($|\eta| < 2.6$) jets with $p_{\mathrm{T}} > 50$ GeV. This trigger is $(98 \pm 1)\%$ efficient as measured in data once the analysis requirements described below have been applied. The selected events are required to have: (i) no identified electrons or muons with $p_{\mathrm{T}} > 5$ GeV that are isolated according to the directional isolation parameter described in section 3; (ii) at least five jets with $p_{\mathrm{T}} > 30$ GeV and $|\eta| < 2.4$, of which the two highest p_{T} jets must have $p_{\mathrm{T}} > 70$ GeV and the next two highest p_{T} jets $p_{\mathrm{T}} > 50$ GeV; (iii) at least one b-tagged jet, $N_{\mathrm{b\ jets}} \geq 1$; and (iv) azimuthal angle $\Delta\phi(\vec{p}_{\mathrm{T}}^{\,j}, \vec{p}_{\mathrm{T}}^{\,\mathrm{miss}})$ between the directions of the three highest p_{T} jets and the $\vec{p}_{\mathrm{T}}^{\,\mathrm{miss}}$ vector larger than 0.5, 0.5, and 0.3, respectively, with $p_{\mathrm{T}}^1 > p_{\mathrm{T}}^2 > p_{\mathrm{T}}^3$. The electron and muon vetoes minimize backgrounds from SM $\mathrm{t\bar{t}}$ and W+jets production, where the W boson decays into a neutrino and a lepton. Events containing a hadronically decaying τ lepton are not explicitly rejected. The jet multiplicity and b-tagging requirements help to select signal events, since the SUSY signatures of interest tend to include multiple jets in the central η range, high-p_{T} leading jets and b jets.

The $\Delta\phi$ requirement strongly suppresses the background from QCD multijet events, which mostly arises from the mismeasurement of jet p_{T}, leading to large $\vec{p}_{\mathrm{T}}^{\mathrm{miss}}$ aligned along a jet axis. Events that satisfy the above requirements are denoted the "preselection" sample.

Reconstruction of hadronically decaying top quarks is performed as suggested in refs. [63–65]. To maximize signal acceptance, one "fully reconstructed" and one "partially reconstructed" top quark are required. The collection of five or more jets in the preselection sample is divided into all possible sets of three jets and a remnant, where the remnant must contain at least one b-tagged jet. The fully reconstructed top quark is one of the three-jet (trijet) combinations. The partially reconstructed top quark is then built from the remnant using the b-tagged jet as a seed. If the remnant contains multiple b-tagged jets, the one with highest p_{T} is used as the seed. Once events with two candidate top quarks are identified, they are used to form additional kinematical variables that distinguish between signal and the remaining SM background, which arises primarily from $t\bar{t}$ production.

6.1.1 Top quark reconstruction

To be considered as a fully reconstructed top quark, the trijet system must satisfy the following requirements. (i) Each jet must lie within a cone in (η, ϕ) space of radius 1.5 centred on the momentum direction formed by the trijet combination. The radius requirement implies a moderate Lorentz boost of the top quark as expected for the large $\Delta m = m_{\widetilde{\mathrm{t}}} - m_{\widetilde{\chi}_1^0}$ region targeted in this search. (ii) The trijet system mass ($m_{\text{3-jet}}$) must be within the range 80–270 GeV. (iii) The trijet system must satisfy one of the three following criteria:

(a) $\quad 0.2 < \arctan\left(\dfrac{m_{13}}{m_{12}}\right) < 1.3 \quad \text{and} \quad R_{\min} < \dfrac{m_{23}}{m_{\text{3-jet}}} < R_{\max},$

(b) $\quad R_{\min}^2\left[1 + \left(\dfrac{m_{13}}{m_{12}}\right)^2\right] < 1 - \left(\dfrac{m_{23}}{m_{\text{3-jet}}}\right)^2 < R_{\max}^2\left[1 + \left(\dfrac{m_{13}}{m_{12}}\right)^2\right] \quad \text{and} \quad \dfrac{m_{23}}{m_{\text{3-jet}}} > 0.35,$

(c) $\quad R_{\min}^2\left[1 + \left(\dfrac{m_{12}}{m_{13}}\right)^2\right] < 1 - \left(\dfrac{m_{23}}{m_{\text{3-jet}}}\right)^2 < R_{\max}^2\left[1 + \left(\dfrac{m_{12}}{m_{13}}\right)^2\right] \quad \text{and} \quad \dfrac{m_{23}}{m_{\text{3-jet}}} > 0.35.$

Here, m_{12}, m_{13}, and m_{23} are the dijet masses, where the jet indices 1, 2, and 3 are p_{T} ordered. The numerical constants have values $R_{\min} = 0.85(m_{\mathrm{W}}/m_{\mathrm{t}})$, $R_{\max} = 1.25(m_{\mathrm{W}}/m_{\mathrm{t}})$, $m_{\mathrm{W}} = 80.4$ GeV, and $m_{\mathrm{t}} = 173.4$ GeV [66].

The top quark tagging (t tagging) conditions of (a), (b), or (c) can be reduced (under certain approximations detailed in ref. [64]) to the requirement that $m_{23}/m_{\text{3-jet}}$, $m_{12}/m_{\text{3-jet}}$, or $m_{13}/m_{\text{3-jet}}$, respectively, be consistent with the $m_{\mathrm{W}}/m_{\mathrm{t}}$ ratio. The other conditions are motivated by the Lorentz structure of the tW coupling and suppress contributions from light-quark and gluon jets [64]. These t tagging conditions are illustrated in figure 2 for simulated SM $t\bar{t}$ (left) and QCD (right) events. The lower box defines the region dictated by the criterion (a), with the central dashed horizontal line representing the ratio $m_{\mathrm{W}}/m_{\mathrm{t}}$. Similarly, the curved regions defined by criteria (b) and (c) are also shown, where the central dashed line indicates where $m_{12}/m_{\text{3-jet}}$ is equal to $m_{\mathrm{W}}/m_{\mathrm{t}}$ for region (b), and where $m_{13}/m_{\text{3-jet}}$ is equal to $m_{\mathrm{W}}/m_{\mathrm{t}}$ for region (c). The requirement that events lie within
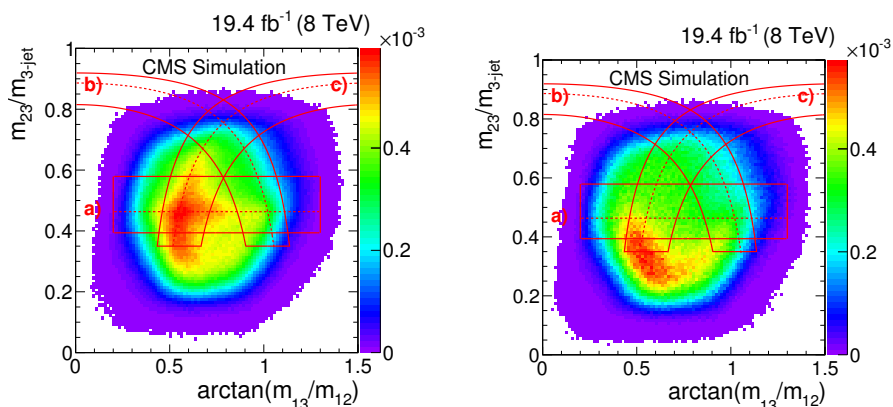
Figure 2. Distributions of $m_{23}/m_{3\text{-jet}}$ versus $\arctan(m_{13}/m_{12})$ for simulated SM $t\bar{t}$ (left), and multijet (right) events in the multijet t-tagged search. The red contours (a), (b), and (c) limit the regions in which conditions (a), (b) and (c) are satisfied, respectively. The central dashed lines represent where the ratios involved in conditions (a), (b) and (c) are equal to $m_{\mathrm{W}}/m_{\mathrm{t}}$, as described in the text.

the boundaries defined by (a), (b), or (c) is seen to be effective at selecting the SM $t\bar{t}$ events, which are very similar to signal events due to similar $m_{23}/m_{3\text{-jet}}$ and m_{13}/m_{12} ratios, while rejecting the bulk of the multijet background. If multiple trijet combinations satisfy these criteria, the triplet with mass closest to the top quark mass is selected. The four-momentum of the selected trijet system, $\mathrm{P}^{3\text{-jet}} = (E^{3\text{-jet}}, \vec{p}^{\,3\text{-jet}})$, is used in the subsequent calculation of kinematical variables that refine the event selection, described below.

The partial reconstruction of a second top quark is attempted in the remnant system, denoted R-sys. The four-momentum of the collective decay products in R-sys is denoted $\mathrm{P}^{\mathrm{R}\text{-sys}} = (E^{\mathrm{R}\text{-sys}}, \vec{p}^{\,\mathrm{R}\text{-sys}})$ and is constructed from either 3, 2, or 1 jet(s) in R-sys. If R-sys has ≥ 3 jets, all possible trijet combinations containing the b-tagged jet are considered. To retain maximum signal acceptance, the full reconstruction criteria of requirements (a), (b) and (c) are not used. Instead we merely select the trijet system with mass closest to that of the top quark. In addition, to reduce the misconstruction of top quark candidates, requirements are placed on the hadronic decay of the W boson candidate in the trijet system: excluding the b-tagged jet, the remaining pair of jets is required to have a dijet mass between 50 and 120 GeV. If this condition is satisfied, the four-momentum of the trijet system defines $\mathrm{P}^{\mathrm{R}\text{-sys}}$. Otherwise the trijet system is rejected and we examine 2-jet combinations involving the b-tagged jet. In the latter case, the separation between the b-tagged jet and the other jet is required to satisfy $\Delta R \equiv \sqrt{(\Delta\eta(\mathrm{b},j))^2 + (\Delta\phi(\mathrm{b},j))^2} \leq 2.0$ and the dijet mass must be less than the top quark mass. If multiple jet pairs satisfy these requirements, the pair with smallest ΔR is selected and the four-momentum of the pair defines $\mathrm{P}^{\mathrm{R}\text{-sys}}$. If no jet pair satisfies the requirements, the b-tagged jet is selected as the complete remnant system, and its four-momentum defines $\mathrm{P}^{\mathrm{R}\text{-sys}}$.

6.1.2 Kinematic requirements

After requiring one fully reconstructed and one partially reconstructed top quark, kinematic information is used to distinguish between signal and SM contributions. The M_{T2} [67, 68] variable, an extension of the transverse mass used for the W boson mass determination [69], is sensitive to the pair production of heavy particles with decay products that include undetected particles like neutrinos or the $\widetilde{\chi}_1^0$. The M_{T2} variable is constructed using $\mathrm{P}^{\text{3-jet}}$, $\mathrm{P}^{\text{R-sys}}$, and the $\vec{p}_{\mathrm{T}}^{\,\text{miss}}$ vectors in an event, assuming the undetected particles to be massless. The top-left plot in figure 3 shows a comparison of the shapes of the two M_{T2} distributions of simulated signal and SM $t\bar{t}$ events after applying the preselection criteria and requiring $p_{\mathrm{T}}^{\text{miss}} > 200\,\mathrm{GeV}$. The results for signal events are shown for various mass hypotheses for the top squark and LSP. For the $t\bar{t}$ background, the M_{T2} distribution peaks around the top quark mass and decreases relatively quickly for larger M_{T2} values. For the signal, the distribution peaks at higher values. As one of the top quarks is only partially reconstructed, the kinematic endpoint of M_{T2} is only approximately reconstructed. To reduce the SM $t\bar{t}$ background while maintaining good signal efficiency for a range of sparticle mass hypotheses, we require $M_{\mathrm{T2}} \geq 300\,\mathrm{GeV}$. The top-right plot in figure 3 shows the $p_{\mathrm{T}}^{\text{miss}}$ distribution in the same conditions.

The variable $M_{\mathrm{T}}^{\text{3-jet}}$, defined using the $\vec{p}_{\mathrm{T}}^{\,\text{miss}}$ and the fully reconstructed trijet system of the identified top quark,

$$(M_{\mathrm{T}}^{\text{3-jet}})^2 = (m^{\text{3-jet}})^2 + 2(E_{\mathrm{T}}^{\text{3-jet}} p_{\mathrm{T}}^{\text{miss}} - p_{\mathrm{T}}^{\text{3-jet}} p_{\mathrm{T}}^{\text{miss}} \cos\Delta\phi), \tag{6.1}$$

is also used to distinguish between signal and SM $t\bar{t}$ events, where $(E_{\mathrm{T}}^{\text{3-jet}})^2 \equiv (m^{\text{3-jet}})^2 + (p_{\mathrm{T}}^{\text{3-jet}})^2$. Here, $p_{\mathrm{T}}^{\text{3-jet}}$ is the magnitude of $\vec{p}^{\,\text{3-jet}}$ in the transverse plane and $\Delta\phi$ is the azimuthal angle between $\vec{p}_{\mathrm{T}}^{\,\text{miss}}$ and $\vec{p}^{\,\text{3-jet}}$. The variable $M_{\mathrm{T}}^{\text{R-sys}}$ is similarly defined using eq. (6.1), by replacing the "3-jet" variables with those of the partial top quark decay products in R-sys. The bottom row in figure 3 shows distributions of $M_{\mathrm{T}}^{\text{3-jet}}$ versus $M_{\mathrm{T}}^{\text{R-sys}}$ for SM $t\bar{t}$ simulated events (left) and for simulated events from a typical signal (right). All events are required to satisfy the preselection requirements and to have $p_{\mathrm{T}}^{\text{miss}} > 200\,\mathrm{GeV}$. For signal events, the $p_{\mathrm{T}}^{\text{miss}}$ requirement typically forces the two top quarks to lie in the hemisphere opposite to $\vec{p}_{\mathrm{T}}^{\,\text{miss}}$. This leads to larger values of $M_{\mathrm{T}}^{\text{3-jet}}$ and $M_{\mathrm{T}}^{\text{R-sys}}$ due to the large azimuthal angle differences involved. In contrast, for SM $t\bar{t}$ events, $\vec{p}_{\mathrm{T}}^{\,\text{miss}}$ typically lies close to one of the two top quarks, and thus either $M_{\mathrm{T}}^{\text{3-jet}}$ or $M_{\mathrm{T}}^{\text{R-sys}}$ tends to have a smaller value. The resulting correlations can be used to further reduce the SM $t\bar{t}$ background. Based on simulation, a simple linear requirement $(0.5M_{\mathrm{T}}^{\text{3-jet}} + M_{\mathrm{T}}^{\text{R-sys}}) \geq 500\,\mathrm{GeV}$ is imposed [see the diagonal lines in figure 3 (bottom)]. This requirement is found to be more effective than simple restrictions on $M_{\mathrm{T}}^{\text{3-jet}}$ and $M_{\mathrm{T}}^{\text{R-sys}}$ separately.

Four exclusive search regions are selected, defined by $200 \leq p_{\mathrm{T}}^{\text{miss}} \leq 350\,\mathrm{GeV}$ and $p_{\mathrm{T}}^{\text{miss}} > 350\,\mathrm{GeV}$ with exactly one or at least two b-tagged jets. The $N_{\text{b jets}} \geq 2$ requirement increases the sensitivity for high-mass top squark production. We further define a "baseline" selection $p_{\mathrm{T}}^{\text{miss}} > 200\,\mathrm{GeV}$ and $N_{\text{b jets}} \geq 1$ that encompasses all exclusive regions. Yields for different processes in each of the search regions are shown in table 1.
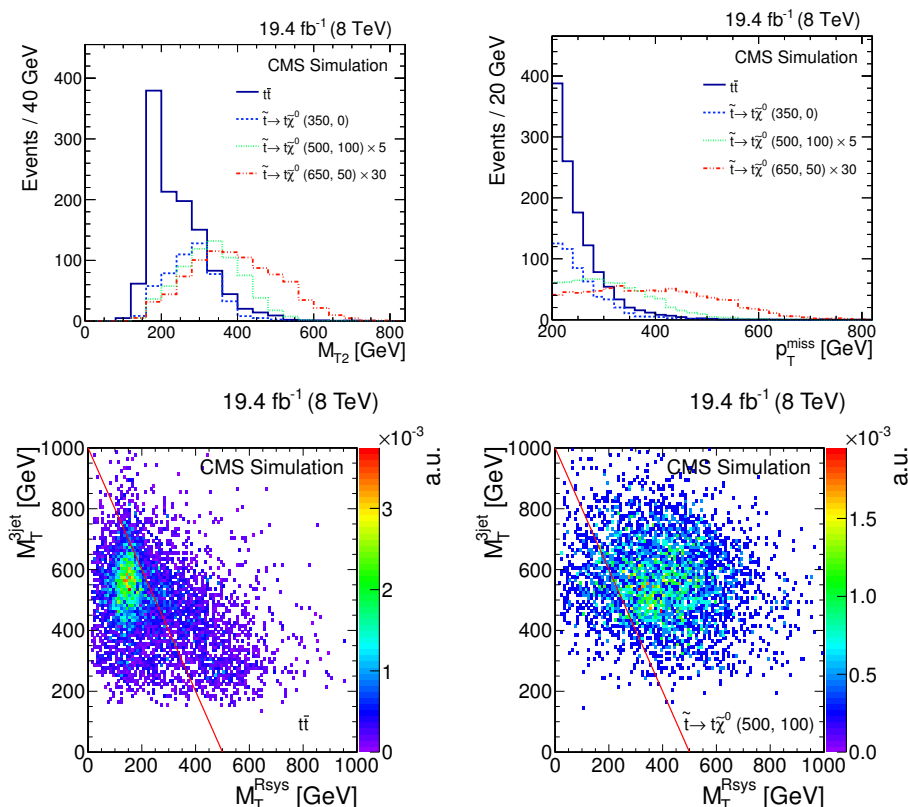
Figure 3. The top row shows one-dimensional distributions for M_{T2} (left) and p_T^{miss} (right) for the simulated processes of $t\bar{t}$ and three signal models in the multijet t-tagged search. The bottom row shows two-dimensional distributions of $M_T^{3\text{-jet}}$ versus $M_T^{R\text{-sys}}$ for $t\bar{t}$ (left) and a signal model with $(m_{\tilde{t}}, m_{\tilde{\chi}_1^0}) = (500, 100)\,\text{GeV}$ (right). Events below the lines are rejected. The distributions are shown after applying the preselection requirements together with a cut $p_T^{miss} > 200\,\text{GeV}$, and are normalized to equal area; the axis label "a.u." means arbitrary units.

6.2 Background predictions

The background is evaluated using a combination of control samples in data and results from MC simulation, following procedures established in refs. [70, 71]. The SM backgrounds from $t\bar{t}$, $W(\ell\nu)$ +jets, and QCD multijet production are estimated using data control regions. The background from $Z(\nu\bar{\nu})$ +jets production is estimated using simulated events that are scaled to match the data in control regions. The SM backgrounds from rare processes, such as $t\bar{t}Z$, WZ and ZZ production with at least one $Z \to \nu\bar{\nu}$ or $W \to \ell\nu$ decay, are small and estimated directly from simulation.

The background from SM events with a τ_h lepton is estimated from a data control sample selected using a trigger requiring a muon with $p_T > 17\,\text{GeV}$, $|\eta| < 2.1$ and at least three jets, each with $p_T > 30\,\text{GeV}$. To define the control sample, we require the muon to be isolated (as defined in section 3) and to have $p_T^\mu > 20\,\text{GeV}$ and $|\eta| < 2.1$. To select events with a $W \to \mu\nu$ candidate, the transverse mass $M_T = \sqrt{2p_T^\mu p_T^{miss}(1 - \cos\Delta\phi)}$ is required to be less than $100\,\text{GeV}$, where $\Delta\phi$ is the azimuthal angle between the $\vec{p}_T^{\,\mu}$ and the $\vec{p}_T^{\,miss}$

| | $200 < p_T^{\text{miss}} < 350\,\text{GeV}$ | $p_T^{\text{miss}} > 350\,\text{GeV}$ | $200 < p_T^{\text{miss}} < 350\,\text{GeV}$ | $p_T^{\text{miss}} > 350\,\text{GeV}$ |
	$N_{\text{b jets}} = 1$	$N_{\text{b jets}} = 1$	$N_{\text{b jets}} \geq 2$	$N_{\text{b jets}} \geq 2$
$t\bar{t}$	77.8 ± 4.0	12.6 ± 1.6	57.1 ± 3.5	6.3 ± 1.2
$W(\ell\nu)$ +jets	14.3 ± 2.3	4.6 ± 1.3	2.9 ± 1.0	1.1 ± 0.6
$Z(\nu\bar{\nu})$ +jets	13.4 ± 0.9	7.1 ± 0.5	3.2 ± 0.4	1.3 ± 0.2
Multijet	1.1 ± 0.6	$0.0^{+0.5}_{-0.0}$	$0.0^{+0.5}_{-0.0}$	$0.0^{+0.5}_{-0.0}$
Single top quark	7.0 ± 2.5	3.5 ± 1.7	5.2 ± 2.1	1.8 ± 1.2
$t\bar{t}Z$	2.7 ± 0.2	0.9 ± 0.1	2.8 ± 0.2	1.4 ± 0.2
$t\bar{t}W$	1.1 ± 0.2	0.2 ± 0.1	1.0 ± 0.2	0.1 ± 0.1
ZZ	0.5 ± 0.1	0.2 ± 0.1	0.1 ± 0.1	$0.0^{+0.1}_{-0.0}$
WZ	0.4 ± 0.2	0.1 ± 0.1	0.1 ± 0.1	$0.0^{+0.1}_{-0.0}$
WW	0.3 ± 0.2	0.1 ± 0.1	0.3 ± 0.2	$0.0^{+0.2}_{-0.0}$
Total	119.0 ± 5.4	29.3 ± 2.8	72.7 ± 4.2	12.0 ± 1.8
Signal (350, 0)	74.6 ± 4.8	3.8 ± 1.1	76.9 ± 4.9	7.5 ± 1.5
Signal (500, 100)	21.1 ± 0.8	13.9 ± 0.7	28.3 ± 1.0	19.8 ± 0.8
Signal (650, 50)	2.8 ± 0.1	6.5 ± 0.2	3.8 ± 0.1	9.3 ± 0.2

Table 1. For illustrative purposes, event yields from different MC simulated samples for each of the four exclusive search regions, defined by the multijet t-tagged analysis in the text, are shown. All numbers are scaled to an integrated luminosity of $19.4\,\text{fb}^{-1}$, and only statistical uncertainties are shown. The signal points correspond to $\widetilde{\tilde{t}} \to t\bar{t}\widetilde{\chi}^0_1\widetilde{\chi}^0_1$ and are labelled as $(m_{\widetilde{t}}, m_{\widetilde{\chi}^0_1})$ in units of GeV.

directions. Since the μ+jets and τ_{h} +jets events arise from the same physics processes, the hadronic component of the two samples is the same except for the response of the detector to the muon or τ_{h} lepton. To account for this difference, the muon in the data control sample is replaced by a simulated τ_{h} lepton (a "τ_{h} jet"). The resulting p_T^j is simulated using a $p_T^j/p_T^{\tau_{\text{h}}}$ response function obtained from MC simulated events. The τ_{h} jet in the MC simulated event is reconstructed and matched to the generated τ lepton, in bins of the generated τ lepton p_T. Corrections are applied to account for the trigger efficiency, acceptance and efficiency of the μ selection, M_T requirement efficiency, contamination from $\tau \to \mu\nu\nu$ decays, and the ratio of branching fractions $\mathcal{B}(W \to \tau_{\text{h}}\nu)/\mathcal{B}(W \to \mu\nu) = 0.65$ [66]. The N_{jets}, $\vec{p}_T^{\text{miss}}$, M_{T2}, $M_T^{\text{3-jet}}$, and $M_T^{\text{R-sys}}$ results for each event in the μ+jets data control sample are then recalculated with this simulated τ_{h} jet, and the search region selection criteria are applied to predict the τ_{h} background. The τ_{h} background estimation method is validated by applying it to simulated $t\bar{t}$ and W+jets samples. For the p_T^{miss} and M_{T2} variables, the predicted distributions reproduce the expected distributions within statistical uncertainties.

Due to the multiple sampling of the response template, the uncertainty in the prediction is evaluated with a set of pseudo-experiments using a bootstrap technique [72]. The main systematic uncertainties in the τ_{h} background estimation arise from the statistical precision of the validation method (6–21%), the μ acceptance (3–4%), and the τ_{h}-jet response function (2–3%) [52]. An additional uncertainty of 3–14% is assigned to the τ_{h}

background prediction to account for differences between the simulation and data for the efficiency of the M_{T} requirement, which arise as a consequence of finite resolution in $p_{\mathrm{T}}^{\mathrm{miss}}$ and because of uncertainties in the fraction of dileptonic $\mathrm{t\bar{t}}$ events.

The lost-lepton background arises from SM $\mathrm{t\bar{t}}$ and W+jets events. It is estimated using a μ+jets control sample selected with the same trigger and selection criteria as those used for the search, except requiring (rather than vetoing) exactly one well reconstructed, isolated muon with $p_{\mathrm{T}}^{\mu} > 5\,\mathrm{GeV}$. As in the estimation of the τ_{h} background, only events with $M_{\mathrm{T}} < 100\,\mathrm{GeV}$ are considered. Leptons lost due to non-identification and non-isolation are treated separately. The reconstruction and isolation efficiencies of the electrons and muons respectively, $\varepsilon_{\mathrm{reco}}^{\mathrm{e},\mu}$ and $\varepsilon_{\mathrm{iso}}^{\mathrm{e},\mu}$, are taken from $\mathrm{t\bar{t}}$ simulation in the lepton p_{T} bins after the baseline selection. To estimate the number of events with unidentified leptons in the search regions, the ratio $\left(1/\varepsilon_{\mathrm{iso}}^{\mu}\right)\left[(1 - \varepsilon_{\mathrm{reco}}^{\mathrm{e},\mu})/\varepsilon_{\mathrm{reco}}^{\mu}\right]$ is applied to the number of events in the control sample; similarly, the number of events with non-isolated leptons is estimated using $(\varepsilon_{\mathrm{reco}}^{\mathrm{e},\mu}/\varepsilon_{\mathrm{reco}}^{\mu})\left[(1 - \varepsilon_{\mathrm{iso}}^{\mathrm{e},\mu})/\varepsilon_{\mathrm{iso}}^{\mu}\right]$. The acceptance and efficiencies are validated with "tag-and-probe" studies of $\mathrm{Z} \to \ell^{+}\ell^{-}$ ($\ell = \mathrm{e}, \mu$) events in data and simulation [73]. The method is validated by predicting the lost-lepton background using a single-muon sample from simulated $\mathrm{t\bar{t}}$ and W+jets events. The predicted distributions and the true distributions (taken directly from the simulation) agree within the uncertainties.

The dominant uncertainties in the lost-lepton background prediction arise from the differences in lepton reconstruction and isolation efficiencies between data and MC simulation. The uncertainties due to lepton reconstruction efficiency are determined by comparing tag-and-probe efficiencies in $\mathrm{Z} \to \ell^{+}\ell^{-}$ events at the Z boson mass peak in data and simulation. For isolation uncertainties, the isolation variables in the simulation are scaled to match the distribution from the data, and the resulting differences in predictions are taken as a systematic uncertainty. Variations of the PDFs following the recommendation of refs. [74, 75] change the muon acceptance, but lead to less than 3% uncertainty in the final prediction. An additional uncertainty of 3% is assigned to account for possible differences between data and simulation for the M_{T} requirement, evaluated in the same manner as for the τ_{h} background.

The $\mathrm{Z}(\nu\bar{\nu})$+jets background is estimated from $\mathrm{Z}(\mu\mu)$+jets simulation, with a normalization that is adjusted to account for differences with respect to data using a scale factor $R_{\mathrm{data/MC}}^{\mu\mu}$ determined from a dimuon control sample. The dimuon control sample is selected using the preselection criteria of section 6.1, except that the lepton veto is removed and instead, a $\mu^{+}\mu^{-}$ pair is required to be present. The μ^{+} and μ^{-} must satisfy $p_{\mathrm{T}} > 20\,\mathrm{GeV}$, $|\eta| < 2.1$, a relative isolation parameter <0.2 (as defined in section 3), and the dimuon mass must lie in the Z boson mass range 71–111 GeV. To mimic the effect of neutrinos, $\vec{p}_{\mathrm{T}}^{\mathrm{miss},\mu}$ is used. The dimuon control sample includes events from $\mathrm{t\bar{t}}$ and $\mathrm{t\bar{t}Z}$ production, which must be subtracted. The $\mathrm{t\bar{t}}$ contribution is evaluated using simulation, with a normalization that is validated using a single-lepton (electron or muon) control sample with lepton $p_{\mathrm{T}} > 20\,\mathrm{GeV}$. In the single-lepton control sample, we also validate the normalization of the simulation after requiring either $N_{\mathrm{b\,jets}} = 1$ or $N_{\mathrm{b\,jets}} \geq 2$. The normalization in the single-muon control sample is found in all cases to be consistent with unity. A statistical uncertainty in this unit normalization (6–8%) is propagated as a systematic uncertainty

in the normalization of the $t\bar{t}$ contribution to the dimuon control sample. The $t\bar{t}Z$ contribution to the dimuon control sample is estimated directly from simulation. The $R^{\mu\mu}_{\text{data/MC}}$ scale factor is defined by the ratio of data to MC events in the dimuon control sample, after subtraction of the $t\bar{t}$ and $t\bar{t}Z$ components. The scale factor is found to be statistically consistent with unity for events with exactly zero b-tagged jets. Events with one b-tagged jet are found to have a scaling factor of 1.33 ± 0.17 (stat). In events with two or more b-tagged jets, the scaling factor is found to be 1.47 ± 0.49 (stat).

Systematic uncertainties in $R^{\mu\mu}_{\text{data/MC}}$ include uncertainties in the normalization and subsequent removal of the $t\bar{t}$ and $t\bar{t}Z$ processes (1–5%), uncertainties in the simulation to account for muon acceptance (10%), trigger efficiency uncertainties (1%), and data-versus-simulation shape disagreements. The shape disagreements are divided into an overall normalization uncertainty (26–33%) to account for discrepancies in the normalization due to the remaining event selection requirements, and a residual shape uncertainty (up to 80%) which accounts for potential normalization or shape discrepancies in the tails of the analysis variables. The residual shape uncertainty is taken from the envelope of a first-order polynomial fit to the data/MC ratio of the analysis variables. An asymmetric systematic uncertainty is assigned to account for the difference between this fit envelope and the overall normalization uncertainty.

The QCD multijet background is expected to be small due to the $p^{\text{miss}}_{\text{T}}$ and $\Delta\phi$ requirements. This background is estimated by measuring the number of QCD multijet events in a data control region and scaling the yield by a factor R_{QCD}, which translates the yield to the search region. The control region is identical to the search region except that one of the three highest p_{T} jets must fail the respective $\Delta\phi$ requirement specified in section 6.1. The R_{QCD} factor is defined as $R_{\text{QCD}} = R^{\text{SB}}_{\text{QCD}} F_{\text{SR}}$, where $R^{\text{SB}}_{\text{QCD}}$ is the ratio of the number of measured QCD multijet events found with the standard and inverted $\Delta\phi$ requirements in a sideband $175 < p^{\text{miss}}_{\text{T}} < 200\,\text{GeV}$, and F_{SR} is a MC-derived extrapolation factor that translates $R^{\text{SB}}_{\text{QCD}}$ to the search region $p^{\text{miss}}_{\text{T}} > 200\,\text{GeV}$. The analysis requires a reconstructed top quark, at least one b-tagged jet, and large $p^{\text{miss}}_{\text{T}}$, so the sideband and inverted $\Delta\phi$ control regions are dominated by $t\bar{t}$, $Z(\nu\bar{\nu})$+jets, and W+jets events. To determine the number of QCD multijet events in the sideband and control regions, the number of events observed in data is corrected for non-QCD contributions using the method described above for the $t\bar{t}$ contribution to the dimuon control sample in the $Z(\nu\bar{\nu})$+jets background estimate. Using simulation, the ratio of events in the standard and inverted $\Delta\phi$ regions is determined as a function of $p^{\text{miss}}_{\text{T}}$. The results are fit with a first-order polynomial. The F_{SR} factor, whose value is defined by the slope of this polynomial, is consistent with zero.

The statistical uncertainty from simulation, the jet energy scale uncertainty, and jet energy resolution uncertainty are combined to define a systematic uncertainty in R_{QCD}.

The individual contributions to the background, evaluated as described above, are listed in table 2 for each of the four search regions. Both statistical and systematic uncertainties are indicated. For the QCD multijet background, the predicted event yields for $N_{\text{b jets}} \geq 2$ are small, around 0.10 events. The corresponding total uncertainties of around 0.45 events are much larger, with about equal contributions from statistical and systematic terms, and so we merely quote these latter results as one standard deviation upper limits on the background estimates.

Background source	$N_{\text{b jets}}$	$200 \leq p_T^{\text{miss}} \leq 350\,\text{GeV}$	$p_T^{\text{miss}} > 350\,\text{GeV}$
$\tau \to$ hadrons	=1	$62.2 \pm 5.6 \pm 5.6$	$12.3 \pm 1.7 \pm 2.6$
Lost lepton	=1	$48 \pm 6 \pm 11$	$7.0 \pm 2.4^{+3.2}_{-3.1}$
$Z(\nu\bar{\nu})$ +jets	=1	$17.9 \pm 1.4^{+5.1}_{-8.4}$	$11.3 \pm 1.0^{+3.8}_{-5.5}$
Multijets	=1	$17 \pm 3 \pm 24$	$2.0 \pm 1.1 \pm 2.7$
Rare processes	=1	1.9 ± 0.9	0.8 ± 0.4
Total	=1	148^{+29}_{-24}	$33.4^{+7.0}_{-7.8}$
$\tau \to$ hadrons	≥ 2	$41.5 \pm 4.3 \pm 5.3$	$4.3 \pm 1.4^{+1.0}_{-1.1}$
Lost lepton	≥ 2	$32.6 \pm 5.1^{+8.6}_{-8.2}$	$1.2 \pm 0.8 \pm 0.5$
$Z(\nu\bar{\nu})$ +jets	≥ 2	$4.6 \pm 0.6^{+2.8}_{-2.4}$	$1.8 \pm 0.4^{+1.6}_{-1.0}$
Multijets	≥ 2	< 0.5	< 0.5
Rare processes	≥ 2	1.9 ± 0.9	1.2 ± 0.6
Total	≥ 2	81^{+13}_{-12}	$8.6^{+2.6}_{-2.4}$

Table 2. Predicted SM backgrounds corresponding to an integrated luminosity of $19.4\,\text{fb}^{-1}$ for all four of the multijet t-tagged search regions defined in the text. Both statistical and systematic uncertainties are quoted.

7 Search for bottom-squark pair production using bottom-quark tagging

We next describe the dijet b-tagged analysis. This analysis requires large p_T^{miss} and one or two jets identified as originating from bottom quarks. The possible presence of a hard light-flavour third jet, arising from initial-state radiation (ISR), is incorporated. The search is motivated by the possibility of bottom-squark pair production, where each bottom squark decays directly to the $\widetilde{\chi}_1^0$ LSP with the emission of a bottom quark, $\widetilde{b} \to b\widetilde{\chi}_1^0$. The signal production rate depends on the bottom squark mass, while the transverse momenta and hence the signal acceptance of the search depend on the mass difference $\Delta m = m_{\widetilde{b}} - m_{\widetilde{\chi}_1^0}$.

7.1 Event selection

The data used in the dijet b-tagged search are collected using the same trigger described in section 6.1 for the multijet t-tagged search. The trigger efficiency is measured to be larger than 95% after application of the selection criteria described below, as measured in data. A set of loose selection criteria are applied to define a baseline data set that is used in addition as a validation sample to compare data and simulation for various kinematic quantities. Exactly two central jets are required with $p_T > 70\,\text{GeV}$ and $|\eta| < 2.4$, and events are vetoed if they have an additional jet with $p_T > 50\,\text{GeV}$ and $|\eta| < 5.0$. One or both of the leading jets are required to be tagged as originating from a b quark, using the medium CSV algorithm working point. Events containing an isolated electron, muon, or track (representing single-prong τ-lepton decays or unidentified electrons or muons) with $p_T > 10\,\text{GeV}$ are rejected to suppress background processes such as $t\bar{t}$ and $W(\ell\nu)$+jets

production. In addition, the scalar sum H_T of the p_T values of the two highest-p_T jets (j_1 and j_2, with $p_T^{j_1} > p_T^{j_2}$) is required to be more than 250 GeV, and p_T^{miss} is required to be larger than 175 GeV. To reject QCD dijet events, we require $\Delta\phi(j_1, j_2) < 2.5$ radians. To further suppress the SM background from $t\bar{t}$ and $W(\ell\nu)$+jets events, the transverse mass defined by $M_T(j_2, p_T^{miss}) = \sqrt{[E_T^{j_2} + p_T^{miss}]^2 - [\vec{p}_T^{j_2} + \vec{p}_T^{miss}]^2}$ is required to be larger than 200 GeV.

Events are characterized using the boost-corrected contransverse mass M_{CT} [76, 77], which for processes involving two identical decays of heavy particles such as $\widetilde{b}\widetilde{\bar{b}} \to j_1 j_2 \widetilde{\chi}_1^0 \widetilde{\chi}_1^0$, is defined as $(M_{CT})^2 = [E_T^{j_1} + E_T^{j_2}]^2 - [\vec{p}_T^{j_1} - \vec{p}_T^{j_2}]^2 = 2 p_T^{j_1} p_T^{j_2} [1 + \cos\phi(j_1, j_2)]$. For signal events, the M_{CT} distribution is characterized by an endpoint at $(m_{\widetilde{b}}^2 - m_{\widetilde{\chi}_1^0}^2)/m_{\widetilde{b}}$.

To obtain sensitivity to different mass hypotheses, the search is conducted in four regions of M_{CT}: $M_{CT} < 250$, $250 < M_{CT} < 350$, $350 < M_{CT} < 450$, or $M_{CT} > 450$ GeV. For each M_{CT} region, we require either $N_{b\ jets} = 1$ or $N_{b\ jets} = 2$, for a total of eight exclusive search regions.

For $m_{\widetilde{b}} - m_{\widetilde{\chi}_1^0} \lesssim 100$ GeV, the p_T values of jets from the squark decay become too small to efficiently satisfy the selection requirements. However, events containing a high-p_T jet from ISR can provide a transverse boost to the recoiling $\widetilde{b}\widetilde{\bar{b}}$ system, enabling such events to satisfy the trigger and selection conditions. Additional search regions, hereafter denoted "ISR" search regions, are therefore considered by modifying the baseline selection requirements to allow an additional third jet from ISR: exactly three jets with $p_T > 30$ GeV and $|\eta| < 2.4$ are then required, where the two highest p_T jets must have $p_T > 70$ GeV and the highest p_T jet is required not to be b-tagged using the CSV loose definition. At least one of the two other jets must be b-tagged according to the medium CSV working point, and the events are classified according to whether one or both of these jets are so tagged, defining two ISR search regions. As in the nominal dijet case, events are rejected if they contain isolated leptons or tracks, or if $H_T < 250$ GeV. An additional requirement is $p_T^{non-b} > 250$ GeV, where p_T^{non-b} is the modulus of the vector sum over the transverse momenta of all jets that are not b-tagged. This requirement increases the probability of selecting events with hard ISR jets and is expected to be reasonably efficient for signal processes, as shown for two representative $\widetilde{b}\widetilde{\bar{b}} \to b\bar{b}\widetilde{\chi}_1^0\widetilde{\chi}_1^0$ mass hypotheses in figure 4. In addition, events must satisfy $p_T^{miss} > 250$ GeV. To reduce the multijet background, we require $\Delta\phi(\vec{p}_T^{j_i}, \vec{p}_T^{miss}) > 0.5$ radians, where $i = 1, 2, 3$. Finally, no requirement is placed on M_{CT} for the two ISR search regions.

For purposes of illustration, the background estimates predicted by simulation for the 10 search regions are listed in table 3. The contribution from QCD multijet production to the $N_{b\ jets} = 2$ search regions is expected to be negligible, so only the upper limits on this background contribution are quoted.

7.2 Background predictions

As compared to the multijet t-tagged search, due to jet multiplicity and lepton veto requirements including an isolated track veto, backgrounds involving top quarks are significantly reduced. Instead, in all 10 search regions the dominant background is from $Z(\nu\bar{\nu})$+jets events, followed in importance by contributions from W+jets and $t\bar{t}$ processes. The SM
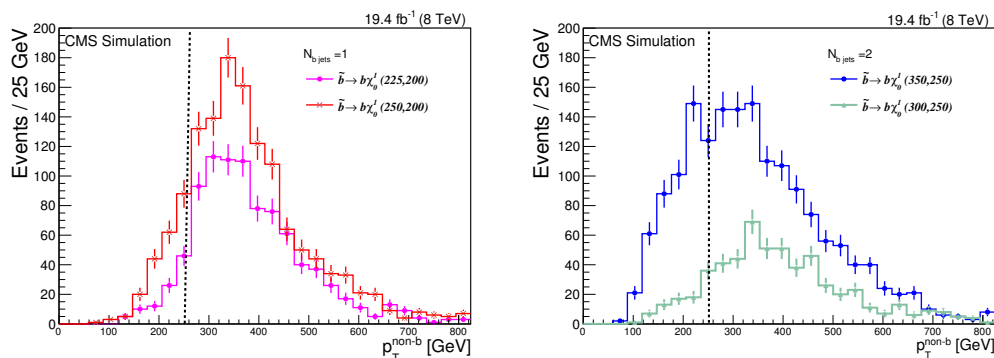
Figure 4. The distribution of $p_T^{\text{non-b}}$ (see text) for the ISR search regions with $N_{\text{b jets}} = 1$ (left) and $N_{\text{b jets}} = 2$ (right) in the dijet b-tagged analysis. The selection requirement $p_T^{\text{non-b}} > 250\,\text{GeV}$ is indicated by the vertical dashed lines.

	$N_{\text{b jets}}$	M_{CT} <250	M_{CT} $\in [250, 350]$	M_{CT} $\in [350, 450]$	M_{CT} >450	ISR
$Z(\nu\bar{\nu})$+jets	1	818±12	367.0±7.8	59.0±2.8	16.0±1.5	161.0±2.6
$W(\ell\nu)$+jets	1	398.0±8.4	149.0±4.9	17.0±1.5	6.0±0.9	90.0±3.4
$t\bar{t}$	1	221.0±2.5	176.0±2.2	17.0±0.7	2.2±0.2	71.0±1.4
Single top quark	1	33.0±3.7	13.0±2.3	0.3±0.3	<0.5	24.0±4.4
VV	1	18.0±0.7	17.0± 0.6	0.9±0.1	0.3±0.1	4.8±0.4
ttZ	1	0.8±0.1	0.5±0.1	0.2±0.1	<0.04	0.6±0.1
Multijets	1	12.0±8.2	6.0±6.0	<0.5	<0.5	0.3±0.4
Total	1	1500±17	729±11	94.0±3.2	25.0±1.6	352.0±6.2
Signal (275,250)	1	11.0±0.8	10.0±0.7	1.3±0.2	0.0±0.0	54.0±1.9
Signal (750,50)	1	0.6±0.1	1.1±0.1	1.7±0.2	2.7±0.2	3.1±0.3
$Z(\nu\bar{\nu})$+jets	2	58.0±3.2	28.1±2.1	4.8±0.8	1.1±0.3	7.7±0.5
$W(\ell\nu)$+jets	2	13.0±1.4	4.7±1.0	1.0±0.3	<0.2	2.7±0.6
$t\bar{t}$	2	12.1±0.6	11.0±0.5	1.8± 0.2	0.3±0.1	15±0.6
Single top quark	2	1.3±0.7	2.2±1.1	<0.5	<0.5	0.7±0.5
VV	2	1.5±0.1	3.2± 0.2	0.1±0.0	<0.1	0.2±0.1
ttZ	2	0.3±0.1	0.2± 0.1	<0.1	<0.1	0.2±0.1
Multijets	2	<0.5	<0.5	<0.5	<0.5	<0.5
Total	2	86.0±3.6	49.0±2.5	7.7±0.8	1.4±0.4	27.0±1.1
Signal (275,250)	2	1.5±0.2	1.4±0.2	0.0±0.0	0.0±0.0	4.6±0.6
Signal (750,50)	2	0.7±0.1	1.1±0.2	1.5±0.2	3.6±0.3	0.5±0.1

Table 3. Predicted background yields from simulation for the dijet b-tagged analysis. The results are scaled to an integrated luminosity of $19.4\,\text{fb}^{-1}$. The uncertainties are statistical. The results for the $\widetilde{\text{b}}\widetilde{\text{b}} \to \text{b}\bar{\text{b}}\widetilde{\chi}_1^0\widetilde{\chi}_1^0$ signal events are labelled as $(m_{\widetilde{\text{b}}}, m_{\widetilde{\chi}_1^0})$, in GeV, and the units of the M_{CT} variable are also GeV.

background due to these processes, as well as the contribution from single-top quark production, are determined using data with assistance from simulation. From studies with simulation and data control samples, the contribution of QCD multijet events is expected to be negligible. The contribution of diboson and $t\bar{t}Z$ events in the search regions is less than 3% and is estimated from simulation assuming a 50% systematic uncertainty.

For nine of the search regions, the eight M_{CT} search regions and the ISR search region with $N_{b\ jets} = 2$, the $Z(\nu\bar{\nu})$+jets background is evaluated using a control sample enriched in $W(\mu\nu)$ +jets events as they have similar kinematic properties. For this control sample, which is selected using an isolated muon trigger, the muon is required to have $p_T > 30\,\text{GeV}$ and $|\eta| < 2.1$ to ensure a trigger efficiency near unity. To exclude Drell-Yan processes, an event is vetoed if it contains an additional muon candidate that in combination with the required muon forms a system having invariant mass within $25\,\text{GeV}$ of the mass of the Z boson. To reject muons from decays-in-flight and from semileptonic decays within heavy-flavour jets, the selected muon must be separated by $\Delta R > 0.3$ from all jets. The remaining events are accepted and classified using the same criteria that define each of the nine search regions, except that a b-tag veto (using the loose CSV working point) is applied, to minimize the contribution of $t\bar{t}$ or single top quark processes. The muon $\vec{p}_T$ is removed from the event to mimic the signature of neutrinos from decays of the Z boson. All kinematic variables are modified accordingly, where $p_T^{\text{miss},\mu}$ is used. Selection thresholds for the resulting $p_T^{\text{miss},\mu}$, H_T, and $M_T(j_2, p_T^{\text{miss},\mu})$ variables are the same as those used to define the search regions. In the case of the doubly b-tagged ISR search region, the $p_T^{\text{non-b}}$ requirement (which, in this case, is effectively a requirement that the leading jet p_T be larger than $250\,\text{GeV}$) is common to both the search region and the control sample. The muon selection, in conjunction with the restrictions on $p_T^{\text{miss},\mu}$ and M_T, ensures that the contributions of QCD multijet events are negligible. The $\Delta\phi$ requirement thus has minimal impact and is not implemented for the control sample selection. The estimated number of $Z(\nu\bar{\nu})$+jets background events is:

$$N_{SR}^{\text{pred}}(Z \to \nu\bar{\nu}; M_{CT}, p_T^{\text{non-b}}, N_{b\ jets}) = N_{CR}^{\text{obs}}(M_{CT}, p_T^{\text{non-b}})\ R_{SR/CR}^{MC}(M_{CT}, p_T^{\text{non-b}}, N_{b\ jets}),$$

(7.1)

where $R_{SR/CR}^{MC}$ is the ratio of the number of $Z(\nu\bar{\nu}) + b$ jets events in the search region to the total number of events in the control sample, taken from simulation and determined separately for each search region defined by either M_{CT} and $N_{b\ jets}$ (in the case of the eight M_{CT} search regions) or by $p_T^{\text{non-b}}$ and $N_{b\ jets}$ (in the case of the doubly b-tagged ISR search region). The term $N_{CR}^{\text{obs}}(M_{CT}, p_T^{\text{non-b}}, N_{b\ jets})$ represents the number of events observed in data, in each control region. The number of simulated events in the control sample is corrected for differences between simulation and data in the muon isolation and identification efficiencies as a function of muon p_T, muon η, and trigger efficiency.

The $W(\mu\nu)$+jets control sample described above, when used to evaluate the $Z(\nu\bar{\nu})$+jets background in the $N_{b\ jets} = 1$ ISR search region, overlaps with the $W(\mu\nu)$+jets control sample used to evaluate the $Z(\nu\bar{\nu})$+jets background in the $N_{b\ jets} = 2$ ISR search region. Therefore, an alternative data control sample of $Z(\mu\mu)$+jets events is used to evaluate

this background in the $N_{\text{b jets}} = 1$ ISR region to provide sufficient discrimination between control regions. Using the same single-muon triggered control sample, we require the identical selection requirements as for the singly b-tagged ISR search region, except that we demand two opposite-sign, well-identified, isolated central ($|\eta| < 2.1$) muons with $p_{\text{T}} >$ 30 GeV and $p_{\text{T}} > 20$ GeV, respectively, that have an invariant dimuon mass between 76 and 106 GeV. One b-tagged jet is required using the medium CSV definition. In an analogous way to eq. (7.1), the number of $Z(\nu\bar{\nu})$+jets events is estimated by applying muon and trigger efficiencies, and by scaling the observed number of events in the control region by the factor $R_{\text{SR/CR}}^{\text{MC}}$, which is the ratio from simulation of the number of $Z \to \nu\bar{\nu}$ events in the search region to the total number of events in the control region.

Tests of the method are performed with simulation, treating MC events as data and comparing the predicted number of background events with the true number. Systematic uncertainties are assigned based on the level of agreement: 2–13% for the $N_{\text{b jets}} = 1$ search regions and 8–30% for the $N_{\text{b jets}} = 2$ search regions, where the uncertainties are dominated by the statistical precision available. To determine a systematic uncertainty in the number of non-$W(\mu\nu)$+jets events in the single-muon control sample, the production cross sections of Drell-Yan, diboson, $t\bar{t}$, and single-top simulation samples are varied up and down by 50%; less than 10% variation is observed for one or two b jets, across all search regions. The sensitivity of $R_{\text{SR/CR}}^{\text{MC}}$ in both the $W(\mu\nu)$+jets and $Z(\mu\mu)$+jets enriched control samples to muon isolation and identification is also studied. Varying these muon criteria within their uncertainties, and taking the deviations from the central values in each search bin, systematic uncertainties of 3–10% for $N_{\text{b jets}} = 1$ and 5–10% for $N_{\text{b jets}} = 2$ are assigned for both the M_{CT} and ISR search regions. Another source of systematic uncertainty in the ratio $R_{\text{SR/CR}}^{\text{MC}}$ can arise from differences between data and simulation in the production of Z bosons in association with one or two b jets. The data are observed to agree with the simulation to better than about 5% for $Z \to \mu^+\mu^-$ events having at least one b jet and covering M_{CT} values up to 250 GeV; we thus apply a 5% systematic uncertainty for all M_{CT} and ISR search regions. Other theoretical systematic uncertainties largely cancel in the ratio of cross sections but are nevertheless considered. Higher-order corrections from QCD are expected to be less than 5%, and the uncertainty from the choice of the PDFs is negligible as higher-order electroweak corrections are similar for W and Z boson production and largely cancel in the cross section ratios [78].

W+jets, $t\bar{t}$, and single-top processes make up the lost-lepton background, as defined in section 5. This lost-lepton background is evaluated together with the background due to τ_{h} events via control samples defined by the same dijet-with-$p_{\text{T}}^{\text{miss}}$ trigger used to define the 10 search regions. The event selection criteria for each control region are identical to those used to define the respective search region, except for the following three conditions. First, a single muon is required (rather than vetoed) using tight muon identification criteria. Second, in the cases of the eight M_{CT} search regions, the requirement on $\Delta\phi(\vec{p}_{\text{T}}^{\,j_1}, \vec{p}_{\text{T}}^{\,j_2})$ is removed. Third, in all 10 control regions, exactly one or exactly two jets must be b-tagged using the loose CSV working point. The prediction in each search region for the number of lost-lepton and τ_{h} background events due to W+jets, $t\bar{t}$, and single-top processes is

given by:

$$N_{\mathrm{SR}}^{\mathrm{pred}}(\text{lost-lep } \& \ \tau_{\mathrm{h}}; M_{\mathrm{CT}}, p_{\mathrm{T}}^{\text{non-b}}, N_{\mathrm{b \ jets}})$$
$$= N_{\mathrm{CR}}^{\mathrm{obs}}(M_{\mathrm{CT}}, p_{\mathrm{T}}^{\text{non-b}}, N_{\mathrm{b \ jets}}) \ R_{\mathrm{SR/CR}}^{\mathrm{MC}}(M_{\mathrm{CT}}, p_{\mathrm{T}}^{\text{non-b}}, N_{\mathrm{b \ jets}}), \qquad (7.2)$$

where the factor $R_{\mathrm{SR/CR}}^{\mathrm{MC}}$ (determined from simulation) is the ratio of the number of W+jets, $t\bar{t}$, and single-top events in a particular search region to the number of W+jets, $t\bar{t}$, single-top, diboson, and Drell-Yan events in the corresponding control region; finally, $N_{\mathrm{CR}}^{\mathrm{obs}}(M_{\mathrm{CT}}, N_{\mathrm{b \ jets}})$ represents the number of events observed in data for each control region.

The data and simulation samples as well as the control and search regions are all defined to be kinematically similar, so most of the uncertainties due to mismodelling of event kinematics or instrumental effects are expected to largely cancel. However, the relative $t\bar{t}$ and W+jets contribution depends on the b jet multiplicity, which can be different between a search region and its corresponding control region. The accuracies of the factors $R_{\mathrm{SR/CR}}^{\mathrm{MC}}$ are tested in data using two independent single-muon triggered samples containing exactly one b jet (expected to contain roughly equal $t\bar{t}$ and W+jets contribution) and exactly two b jets (expected to have a dominant $t\bar{t}$ contribution). A related source of uncertainty arises from possible differences in the modelling of lepton isolation and the isolated track veto between data and simulation. To probe this effect, the numbers of events with exactly one muon are predicted starting from a control sample with an isolated track and no isolated muon or electron using a transfer factor derived from MC. The average weighted uncertainty of the two studies results in 4–20% differences in the predicted background in various search regions. Statistical uncertainties in the transfer factors, due to the finite size of simulation samples, result in 2–16% and 10–80% uncertainties in the predicted backgrounds, for search regions with one and two b jets, respectively. Uncertainties related to the efficiency of the CSV algorithm to identify b jets result in 2–20% uncertainties in the final background predictions. And finally, uncertainties in the background prediction due to the contributions of dibosons and other rare processes, taken from simulation with 50% uncertainty, are less than 2% across all search regions. The predicted numbers of $t\bar{t}$, single-top, and $W(\ell\nu)$+jets events in the various search regions are listed in table 4, along with the statistical and total systematic uncertainties.

Background yields from QCD multijet processes are expected to be less than a percent of the total across all search bins. An estimate of the contribution from the QCD background is made by measuring the number of multijet events in a QCD enriched control region, and scaling this number by a transfer factor. The control regions are identical to the search regions except that the $\Delta\phi(\vec{p}_{\mathrm{T}}^{\,j_1}, \vec{p}_{\mathrm{T}}^{\,j_2})$ requirement is inverted (for the dijet search regions), and $\Delta\phi(\vec{p}_{\mathrm{T}}^{\,j_{1,2,3}}, \vec{p}_{\mathrm{T}}^{\,\mathrm{miss}})$ is inverted (for the ISR search regions). In the case of the dijet searches, the transfer factor is taken from a zero b-jet sideband. In the case of the ISR searches, the transfer factor is taken from a sideband defined by $175 < p_{\mathrm{T}}^{\mathrm{miss}} < 200\,\mathrm{GeV}$.

From studies from simulation, QCD events in the region with the standard $\Delta\phi$ requirement survive only because of mismeasurement, where under-measurement of one of the two leading jets results in it being reconstructed as the third jet, where the third leading jet of the event must have $p_{\mathrm{T}} < 50\,\mathrm{GeV}$. This behaviour is observed to have no correlation

with the b quark content of events. A dijet sideband region with zero b jets is therefore used to estimate the number of QCD events in the search regions. This dijet sideband is divided into two regions: a QCD subdominant sideband region for which $\Delta\phi(\vec{p}_T^{\,j_1}, \vec{p}_T^{\,j_2}) < 2.5$ together with $\Delta\phi(\vec{p}_T^{\,j_3}, \vec{p}_T^{\,\mathrm{miss}}) < 0.3$ to enrich the QCD content, and a QCD dominant sideband region defined by $\Delta\phi(\vec{p}_T^{\,j_1}, \vec{p}_T^{\,j_2}) > 2.5$. In the QCD subdominant sideband region, the contribution from non-QCD processes (Z+jets, $t\bar{t}$, and W+jets events) is significant and is subtracted (via simulation normalized to data) from the observed numbers of events. Contributions from non-QCD processes in the QCD dominant sideband region are negligible. The QCD transfer factors, characterized in bins of M_{CT} and $N_{\mathrm{b\ jets}}$ for the eight dijet searches, are then defined as the ratio of the number of multijet events between these two sideband regions.

Using a method similar to the QCD background determination in the multijet t-tagged search, described in section 6.2, the ISR sideband of $175 < p_T^{\mathrm{miss}} < 200\,\mathrm{GeV}$ is divided into two regions: a regular sideband region for which $\Delta\phi(\vec{p}_T^{\,j_{1,2,3}}, \vec{p}_T^{\,\mathrm{miss}}) > 0.5$, and an inverted sideband region for which $\Delta\phi(\vec{p}_T^{\,j_{1,2,3}}, \vec{p}_T^{\,\mathrm{miss}}) < 0.5$. While QCD processes dominate the inverted sideband region (due to the $\Delta\phi(\vec{p}_T^{\,j_{1,2,3}}, \vec{p}_T^{\,\mathrm{miss}}) > 0.5$ requirement), non-QCD processes dominate the regular sideband region (due to the large p_T^{miss} conditions). Using simulation, Z+jets, $t\bar{t}$, and W+jets processes are subtracted from the data yields for both sideband regions. The QCD transfer factors are then defined by the ratio of the remaining data yield in the regular sideband region to the remaining data yield in the inverted sideband region. Due to possible correlations between p_T^{miss} and $\Delta\phi(\vec{p}_T^{\,j_{1,2,3}}, \vec{p}_T^{\,\mathrm{miss}})$, the transfer factors are parametrized as a linear function of p_T^{miss} using simulation. The transfer factor is then extrapolated from the value obtained in the sideband to the value at the average expected p_T^{miss} from QCD processes in the ISR search regions.

The systematic uncertainty in the QCD background prediction comes from (i) the limited number of observed events in the data control samples, as well as (ii) the limited number of simulated non-QCD events that are subtracted from the sideband regions used to determine the transfer factors. For the ISR search regions, uncertainties associated with the determination of the linear parametrization of the transfer factor are propagated as an additional source of systematic uncertainty in the QCD background prediction.

The background yields using the methods outlined above are summarized in table 4.

8 Search for top- and bottom-squark pair production in compressed spectrum scenarios

We next describe the monojet search. Given the lack of observation of a SUSY signature in more conventional searches, it is important to search for SUSY with compressed mass spectra, i.e., SUSY scenarios in which the parent sparticles are close in mass to the daughter sparticles. Small mass splittings $\Delta m = m_{\widetilde{t}} - m_{\widetilde{\chi}_1^0}$ or $\Delta m = m_{\widetilde{b}} - m_{\widetilde{\chi}_1^0}$ between the top or bottom squark and the LSP leave little visible energy in the detector, making signal events difficult to distinguish from SM background. However, events with an energetic ISR jet recoiling against the $\vec{p}_T^{\,\mathrm{miss}}$ vector from the LSP can provide a clear signal for compressed events. We thus perform a search for events with a single jet and significant p_T^{miss}.

	$N_{\text{b jets}}$	M_{CT} <250	M_{CT} $\in [250, 350]$	M_{CT} $\in [350, 450]$	M_{CT} >450	ISR
$Z(\nu\overline{\nu})$ +jets	1	848±12±79	339±8±52	48.0±3.0±6.0	8.1±1.6±1.7	176±24±21
$t\overline{t}$, $W(\ell\nu)$ +jets	1	645±24±57	381±17±38	36.0±4.9±5.7	7.8±2.6±2.0	171±5±25
QCD multijets	1	25.0±9.4±5.2	16.0±7.4±2.8	0.0±1.0±1.2	negligible	3.2±0.2±4.6
Rare processes	1	18.0±9.2	18.0±8.9	1.1±0.5	0.3±0.1	5.4±2.7
Total	1	1540±100	754±68	85±10	16.0±4.1	356±41
$Z(\nu\overline{\nu})$ +jets	2	60.0±3.4±7.1	28.0±2.4±3.8	3.9±0.9±1.0	0.7±0.6±0.6	6.6±0.4±1.2
$t\overline{t}$, $W(\ell\nu)$ +jets	2	29.0±2.9±5.5	17.0±2.5±3.3	2.4±0.9±0.6	0.0±0.2±0.2	19.0±1.8±3.4
QCD multijets	2	1.9±0.7±0.4	1.2±0.8±0.2	0.0±0.1±0.1	negligible	0.4±0.1±0.7
Rare processes	2	1.8±0.9	3.4±1.7	0.1±0.1	0.1±0.1	0.4±0.4
Total	2	93±10	50.0±6.4	6.5±1.7	1.0±0.9	26.0±4.1

Table 4. Predicted SM backgrounds corresponding to an integrated luminosity of 19.4 fb^{-1} for the 10 dijet b-tagged search regions defined in the text, with M_{CT} given in units of GeV. The first uncertainty is statistical and the second systematic.

For $m_{\widetilde{t}} - m_{\widetilde{\chi}_1^0} < m_W$, the dominant $\widetilde{t}$ decay mode is the flavour changing neutral-current process $\widetilde{t} \to c\widetilde{\chi}_1^0$. In the case of the $\widetilde{b}$, the kinematically similar decay $\widetilde{b} \to b\widetilde{\chi}_1^0$ dominates for compressed scenarios, so the monojet topology is used to search for both top and bottom squarks. The search represents an optimization of the studies presented in refs. [79–81]. Relative to these previous studies, we increase the threshold on N_{jets}, and define search regions using the p_{T} of the highest p_{T} jet rather than $p_{\text{T}}^{\text{miss}}$.

8.1 Event selection

Data used in the analysis are selected by a combination of two triggers. The first trigger requires $p_{\text{T}}^{\text{miss},\mu} > 120$ GeV, where $p_{\text{T}}^{\text{miss},\mu}$ is calculated using calorimetric information only. The second trigger requires a jet to satisfy $p_{\text{T}} > 80$ GeV, $|\eta| < 2.6$, and to have less than 95% of the jet momentum carried by neutral hadrons. In addition, the second trigger requires $p_{\text{T}}^{\text{miss},\mu} > 105$ GeV, where $p_{\text{T}}^{\text{miss},\mu}$ is calculated using the particle-flow algorithm. Selection criteria of $p_{\text{T}}^{\text{miss},\mu} > 250$ GeV, and a leading jet (which has the highest momentum of all jets in the event and is denoted j_1) with $p_{\text{T}}^{j_1} > 110$ GeV and $|\eta| < 2.4$, ensure a fully efficient trigger. To suppress the instrumental and beam-related backgrounds, and to remove noisy events and misidentified high-p_{T} electrons and photons, events are rejected based on the properties of j_1: if less than 20% of its energy is carried by charged hadrons, or if more than 70% of its energy is carried by either neutral hadrons or photons, the event is rejected.

Although event selection is based upon a single high-momentum jet, signal acceptance is increased by accepting events in which there is a second jet j_2 originating from ISR. In addition, the signal also has soft final-state jets produced by the charm or bottom quarks originating from the sparticle decays. Ideally, these soft jets should not be taken into account in the jet counting. To suppress them a p_{T} threshold is introduced for the jet counting. Figure 5 shows the p_{T} distribution of charm quarks, taken from simulation, for
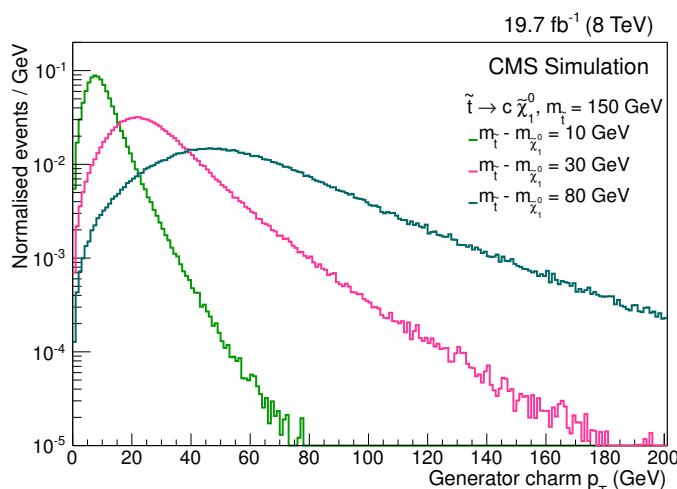
Figure 5. Charm quark p_T distribution for charm quarks emitted in the decay of top squarks of mass 150 GeV, for mass differences, $m_{\tilde{t}} - m_{\tilde{\chi}_1^0} = 10, 30, 80$ GeV in the monojet analysis.

a few representative mass hypotheses in the process $\tilde{\tilde{t}}\tilde{\bar{t}} \to c\bar{c}\tilde{\chi}_1^0\tilde{\chi}_1^0$. Placing the jet counting threshold at 60 GeV for jets with $|\eta| < 4.5$ provides a compromise between a high threshold to reject soft jets and a low threshold to reject QCD multijet events. Using this threshold condition, events with up to two jets are accepted. To suppress the QCD dijet background, $\Delta\phi(\vec{p}_T^{j_1}, \vec{p}_T^{j_2})$ is required to be less than 2.5. To reduce electroweak and top backgrounds, events with electrons satisfying $p_T > 10$ GeV and $|\eta| < 2.5$, or muons reconstructed with $p_T > 10$ GeV and $|\eta| < 2.4$, are rejected. Events with a well-identified τ_h lepton with $p_T > 20$ GeV and $|\eta| < 2.3$ are removed. The analysis is performed in search regions that reflect the hardness of the radiated jet in an event, in seven inclusive regions of leading jet p_T: $p_T^{j_1} > 250, 300, 350, 400, 450, 500$, and 550 GeV.

Following the above selection criteria, expected event yields from various SM processes, as predicted by simulation in each of the search regions, are shown in table 5.

8.2 Background predictions

The dominant SM backgrounds are due to $Z(\nu\bar{\nu})$+jets and $W(\ell\nu)$+jets processes. These backgrounds are estimated from data, utilizing a control sample of μ+jets events in which $Z(\mu\mu)$ and $W(\mu\nu)$ events are used to estimate the $Z(\nu\bar{\nu})$+jets and $W(\ell\nu)$+jets backgrounds, respectively. Small contributions from diboson, QCD multijet, and $t\bar{t}$ events are estimated using simulation corrected for any differences between simulation and data. Very small backgrounds arising from single top quark and $Z \to \ell^+\ell^-$ processes are taken from simulation directly.

The $Z(\nu\bar{\nu})$+jets background is estimated using a data control sample of dimuon events, selected using the same trigger as the search regions. The redefinition of the p_T^{miss} to exclude muons and mimic neutrinos at both the trigger level and in analysis variables allows the use of the same trigger, not possible in the multijet t-tagged or dijet b-tagged analyses, and reduces systematic uncertainties. The $Z(\mu\mu)$+jets enriched control sample is selected

$p_T^{j_1}$ (GeV)	>250	>300	>350	>400	>450	>500	>550
Z($\nu\bar{\nu}$)+jets	22600±56	11100±37	5230±24	2620±17	1340±12	727±8.7	406±6.5
W($\ell\nu$)+jets	13600±70	6870±50	3180±34	1500±23	751±17	376±12	204±8.7
WW,WZ,ZZ	819±27	546±18	332±12	181.0±6.5	92.0±3.4	61.0±2.3	34.0±1.2
t$\bar{t}$	639.0±5.7	369.0±4.3	206.0±3.2	113.0±2.4	64.0±1.8	36.0±1.3	21.0±1.0
Multijets	602±19	344±15	178±10	91.0±7.3	48.0±5.2	27.0±4.0	18.0±3.5
Single top quark	172.0±7.6	97.0±5.7	49.0±4.1	21.0±2.7	11.0±2.2	5.2±1.4	3.2±1.2
Z($\ell^+\ell^-$)+jets	127.0±6.1	75.0±4.7	40.0±3.5	25.0±2.8	17.0±2.4	11.0±2.0	7.4±1.6
Total	38600±96	19400±67	9220±45	4550±31	2320±22	1240±16	693±12
Signal (200, 120)	1130±22	663±17	352 ±12	193.0 ±9.2	111.0±7.0	62.9±5.1	35.5 ±3.9
Signal (250, 240)	1640±15	1070±12	657.0±9.6	403.0±7.5	256.0±6.0	156.0±4.6	98.0±3.7

Table 5. Predicted background yields from simulation for the monojet analysis. The results are scaled to an integrated luminosity of 19.7 fb^{-1}. The uncertainties are statistical. The results for the $\widetilde{\widetilde{t}}t \to c\bar{c}\tilde{\chi}_1^0\tilde{\chi}_1^0$ signal events are labelled as $(m_{\tilde{t}}, m_{\tilde{\chi}_1^0})$, in GeV.

by applying the full signal selection, except for the muon veto, instead demanding two oppositely charged muons with $p_T > 20$ GeV and $|\eta| < 2.4$. At least one of the muons must be isolated, and the dimuon reconstructed invariant mass must lie within a window of 60–120 GeV, to be consistent with the Z boson mass. The number of observed dimuon events in the data control sample ($N^{\rm obs}$) is corrected for non-Z($\mu\mu$) processes ($N^{\rm bgd}$), estimated using simulation. The event yield is corrected for the acceptance (A) and efficiency (ϵ) of the muon selection criteria, taken from Z($\mu\mu$) simulation and corrected for differences in muon identification between data and simulation. The number of Z($\nu\bar{\nu}$)+jets events is estimated using:

$$N(\text{Z}(\nu\bar{\nu})+\text{jets}) = \frac{N^{\rm obs} - N^{\rm bgd}}{A\epsilon}\,R, \tag{8.1}$$

where R is the ratio of branching fractions of Z $\to \nu\bar{\nu}$ to Z $\to \mu^+\mu^-$ decays [66], corrected for the contributions of virtual photon exchange in the Z +jets sample and for the Z mass window requirement.

The uncertainty in the prediction includes both statistical and systematic contributions: (i) the statistical uncertainty in the number of Z $\to \mu^+\mu^-$+jets events in the data and simulation, (ii) a 50% uncertainty from each of the non-Z backgrounds estimated using simulation, (iii) uncertainties associated with PDF choice (2%) [55, 82, 83] as recommended in refs. [74, 75], (iv) a 2% uncertainty due to hadronization, and (v) a 2% uncertainty in R. The statistical uncertainty in the number of Z($\mu\mu$)+jets events, 2–17%, dominates the total uncertainty, which ranges from 5% to 19%.

The background due to lost leptons from W +jets events is estimated using a single-muon control sample enriched in W($\mu\nu$)+jets events selected with the same trigger as the search regions. The full signal selection is applied, except that the muon veto is replaced by the requirement of a well-identified muon with $p_T > 20$ GeV and $|\eta| < 2.4$. The transverse mass of the muon-$\vec{p}_T^{\rm miss,\mu}$ system, as defined in section 6.2, is required

to satisfy $50 < M_\text{T} < 100\,\text{GeV}$. Analogously to the $\text{Z}(\nu\bar\nu)$+jets background estimation, the observed single-muon event yield in data (N^obs) is corrected for non-$\text{W}(\mu\nu)$ processes using simulation (N^bgd), and for the acceptance (A') and efficiency (ϵ') of the single-muon selection criteria using W +jets simulation, where differences between muon identification in data and simulation are taken into account. The total $\text{W}(\mu\nu)$+jets event yield is:

$$N(\text{W}(\mu\nu)+\text{jets}) = \frac{N^\text{obs} - N^\text{bgd}}{A'\epsilon'}. \tag{8.2}$$

The total lost-lepton and τ_h background is estimated by extrapolating the $\text{W}(\mu\nu)$ event yield to the total $\text{W}(\ell\nu)$ event yield using $p_\text{T}^{j_1}$-dependent generator level ratios of $\text{W}(\mu\nu)$ to $\text{W}(\text{e}\nu)$ and $\text{W}(\tau_\text{h}\nu)$ events, correcting for the inefficiencies of lepton vetoes used in the signal event selection (taken from W +jets simulation).

The uncertainty in the prediction includes both statistical and systematic contributions: (i) the uncertainties in the numbers of single-muon events in the data and simulation samples, (ii) a 50% uncertainty in each simulated non-W +jets contribution to the control sample, and (iii) statistical and systematic uncertainties (from PDFs) incorporated in the total uncertainties in acceptances and efficiencies. Statistical uncertainties in the number of $\text{W}(\mu\nu)$+jets events (1–8.6%) and uncertainties in the acceptance and efficiency values (4.5–7.1%) dominate the total uncertainty, which ranges from 5.7% to 12.0%.

The background from QCD multijet production is expected to be small, contributing $\approx$2% to the total background yield, and is predicted using the simulation normalized to data in control regions. The normalization is determined from a QCD-enriched control sample, defined using events that satisfy the signal event selection criteria except that the $\Delta\phi(\vec{p}_\text{T}^{\,j_1}, \vec{p}_\text{T}^{\,j_2}) < 2.5$ and $N_\text{jets} < 3$ requirements are not applied in order to maintain a sufficient number of events in the control sample, which is defined by $\Delta\phi(\vec{p}_\text{T}^{\,j_2}, \vec{p}_\text{T}^{\,\text{miss},\mu}) < 0.3$, a region enriched with mismeasured jets. The contribution from non-QCD dijet and multijet processes is subtracted from the data yield using simulation that has been normalized to data in QCD-free regions. A set of $p_\text{T}^{j_1}$-dependent data-MC scale factors are extracted and applied to the simulated QCD yield in the search regions, using the ratio of QCD events found in data to the yield predicted using simulation in the control sample.

A systematic uncertainty of 50% in the unnormalized QCD simulation is applied. The uncertainty in the scale factors determined from data includes both statistical and systematic components, arising from a 50% uncertainty assigned to each of the non-QCD contributions that are subtracted from the data yield in the control region. The total uncertainty, including statistical uncertainties, in the QCD background prediction is $\approx$ 60% in each search region. A cross check of this prediction is performed in a QCD-rich sideband region defined by $\Delta\phi(\vec{p}_\text{T}^{\,j_3}, \vec{p}_\text{T}^{\,\text{miss},\mu}) < 0.3$ and found to agree within the uncertainties with the observed number of events.

The $t\bar{t}$ contribution to total background is small ($\approx$2%) and is estimated using simulation that has been validated using data. A control sample of events with $p_\text{T}^{\text{miss},\mu} > 250\,\text{GeV}$, $p_\text{T}^{j_1} > 110\,\text{GeV}$, and $\Delta\phi(\vec{p}_\text{T}^{\,j_1}, \vec{p}_\text{T}^{\,j_2}) < 2.5$ is derived from the same trigger as used for the search regions. A $t\bar{t}$-rich sample is created by then requiring an identified electron and an identified muon of opposite sign. The invariant mass of the eμ system must be greater than

	$p_{\mathrm{T}}^{j_1} > 250\,\mathrm{GeV}$	$p_{\mathrm{T}}^{j_1} > 300\,\mathrm{GeV}$	$p_{\mathrm{T}}^{j_1} > 350\,\mathrm{GeV}$	$p_{\mathrm{T}}^{j_1} > 400\,\mathrm{GeV}$
Z($\nu\bar{\nu}$)+jets	21200±450±1000	10100±300±510	4600±210±250	2250±150±130
W($\ell\nu$)+jets	12300±120±690	5940±89±360	2690±62±170	1250±40±80
t$\bar{t}$	602±300	344±170	178±89	91±46
Z($\ell^+\ell^-$)+jets	127±64	75±38	40±20	25±13
Single top quark	172±86	97±49	49±24	21±10
Multijets	786±470	508±310	304±180	162±99
Diboson	639±320	369±180	206±100	113±56
Total	35900±1500	17400±800	8060±440	3910±250

	$p_{\mathrm{T}}^{j_1} > 450\,\mathrm{GeV}$	$p_{\mathrm{T}}^{j_1} > 500\,\mathrm{GeV}$	$p_{\mathrm{T}}^{j_1} > 550\,\mathrm{GeV}$
Z($\nu\bar{\nu}$)+jets	1250±110±84	663±80±48	334±57±28
W($\ell\nu$)+jets	637±28±44	301±19±22	150±13±13
t$\bar{t}$	48±24	27±14	18.0±9.0
Z($\ell^+\ell^-$)+jets	17.0±8.3	11.0±5.6	7.4±3.7
Single top quark	11.0±5.7	5.2±2.6	3.2±1.6
Multijets	80±49	52±32	28±18
Diboson	64±32	36±18	21±10
Total	2100±160	1100±100	563±71

Table 6. SM background predictions for the monojet search regions defined in the text, corresponding to an integrated luminosity of 19.7 fb^{-1}. For the Z($\nu\bar{\nu}$)+jets and W($\ell\nu$)+jets terms, the first uncertainty is statistical and the second is systematic. The uncertainties in the remaining backgrounds include both statistical and systematic terms.

60 GeV. The data and simulation in the control region are found to agree within $3 \pm 20\%$, so no additional scale factor is applied to the next-to-next-to-leading-order cross section estimate [84] used to normalize the yield to the integrated luminosities of the search samples. To be consistent with the other small background estimations, a 50% uncertainty is assigned that includes statistical and systematic uncertainties. Diboson processes contribute $\approx$2% to the total background. The number of WW, WZ, and ZZ events are estimated using simulation, normalized to the luminosity with next-to-leading-order (NLO) cross sections [85] and assigned a 50% uncertainty, while Zγ and Wγ events are estimated from data. They are treated inclusively as part of the Z($\nu\bar{\nu}$)+jets and W($\ell\nu$)+jets backgrounds, which is found to agree with simulation within 15%. Single top quark and Z $\to \ell^+\ell^-$+jets events account for $< 1\%$ of total background and are estimated directly from simulation. A 50% uncertainty is assigned to background predictions estimated from simulation.

The total background yields using the methods outlined above are shown in table 6 in each of the inclusive search regions.

Search regions	$N_{\text{b jets}}$					
	≥ 0		1		2	
Multijet t-tagged search			SM Pred.	Obs.	SM Pred.	Obs.
$p_{\text{T}}^{\text{miss}} \in [200, 350]\,\text{GeV}$			148^{+29}_{-24}	141	81^{+13}_{-12}	68
$p_{\text{T}}^{\text{miss}} > 350\,\text{GeV}$			$33.4^{+7.0}_{-7.8}$	30	$8.6^{+2.6}_{-2.4}$	15
Dijet b-tagged search			SM Pred.	Obs.	SM Pred.	Obs.
$M_{\text{CT}} < 250\,\text{GeV}$			1540 ± 100	1560	93 ± 10	101
$M_{\text{CT}} \in [250, 350]\,\text{GeV}$			754 ± 68	807	50.0 ± 6.4	55
$M_{\text{CT}} \in (350, 450]\,\text{GeV}$			85 ± 10	101	6.5 ± 1.7	8
$M_{\text{CT}} > 450\,\text{GeV}$			16.0 ± 4.1	23	1.0 ± 0.9	1
ISR			356 ± 41	359	26.0 ± 4.1	28
Monojet search	SM Pred.	Obs.				
$p_{\text{T}}^{j_1} > 250\,\text{GeV}$	35900 ± 1500	36600				
$p_{\text{T}}^{j_1} > 300\,\text{GeV}$	17400 ± 800	17600				
$p_{\text{T}}^{j_1} > 350\,\text{GeV}$	8060 ± 440	8120				
$p_{\text{T}}^{j_1} > 400\,\text{GeV}$	3910 ± 250	3900				
$p_{\text{T}}^{j_1} > 450\,\text{GeV}$	2100 ± 160	1900				
$p_{\text{T}}^{j_1} > 500\,\text{GeV}$	1100 ± 110	1000				
$p_{\text{T}}^{j_1} > 550\,\text{GeV}$	563 ± 71	565				

Table 7. Event yields for the different search regions defined in sections 6.1, 7.1, and 8.1. The multijet t-tagged search requires a combination of exclusive and inclusive bins in number of b-tagged jets ($N_{\text{b jets}} = 1$, $N_{\text{b jets}} \geq 2$), whereas the dijet b-tagged searches require exclusive bins ($N_{\text{b jets}} = 1, 2$); the monojet search makes no requirements on b-tagged jets ($N_{\text{b jets}} \geq 0$). The SM background predictions and the yields observed in data correspond to integrated luminosities of 19.4, 19.4, and 19.7 fb^{-1} for the multijet t-tagged, dijet b-tagged, and monojet searches, respectively. The quoted uncertainties in the SM predictions reflect the total (statistical and systematic) uncertainties quadratically summed over all different background contributions.

9 Results

Each search region definition was optimized and the SM backgrounds were evaluated before the data in the search regions were examined. Table 7 shows the observed yields compared with the SM background predictions in each of the 21 search regions defined by the three analyses. All search regions are consistent with predictions of the SM, and no significant excesses are observed.

Figure 6 shows distributions of some key variables in the multijet t-tagged search, for data and for the expected SM background estimated using the methods outlined in section 6.2. The hatched bands show both the statistical and systematic uncertainties from the predictions, taken from table 7. The $p_{\text{T}}^{\text{miss}}$ distribution (figure 6, left) is obtained after applying the baseline selection criteria described in section 6.1. The M_{T2} distribution (figure 6, centre) is obtained using the baseline selection criteria without the $0.5 M_{\text{T}}^{\text{3-jet}} + M_{\text{T}}^{\text{R-sys}} \geq 500\,\text{GeV}$ requirement, and the $0.5 M_{\text{T}}^{\text{3-jet}} + M_{\text{T}}^{\text{R-sys}}$ distribution (figure 6, right)
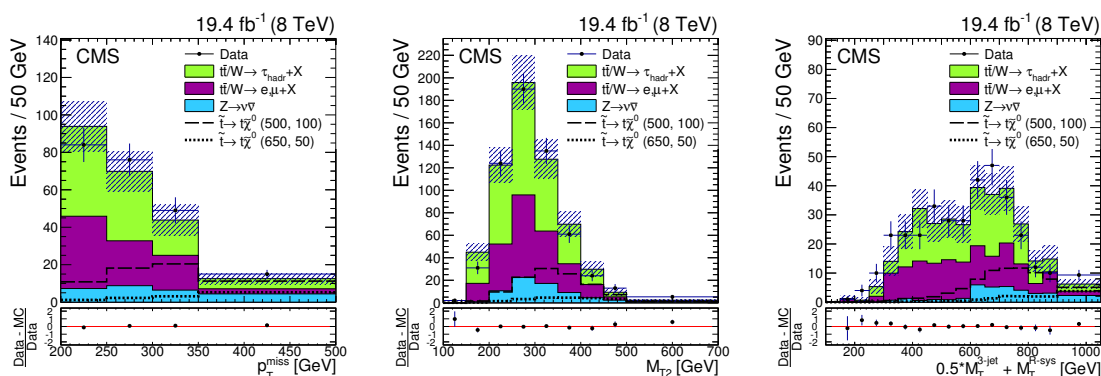
Figure 6. The p_T^{miss} (left), M_{T2} (centre), and $0.5M_T^{3\text{-}jet} + M_T^{R\text{-}sys}$ (right) distributions from data (black dots), and predicted backgrounds (solid filled areas) in the multijet t-tagged search, where the total (statistical and systematic) uncertainty in the background prediction is shown by the hatched band. The distributions of two representative signals $(m_{\widetilde{t}}, m_{\widetilde{\chi}_1^0}) = (500, 100)$ and $(650, 50)\,\mathrm{GeV}$ are overlaid (dashed and dotted lines respectively). The leftmost bin of each distribution contains the overflow.

is obtained using the baseline selection criteria without the $M_{T2} \geq 300\,\mathrm{GeV}$ requirement. The distributions simulated for two representative signal mass hypotheses for the case of $\widetilde{t}\widetilde{\bar{t}} \to t\bar{t}\widetilde{\chi}_1^0\widetilde{\chi}_1^0$ production, scaled to an integrated luminosity of $19.4\,\mathrm{fb}^{-1}$, are superimposed for comparison. The QCD prediction is not included in the plots shown in figure 6 since its contribution is negligible.

Distributions of some representative variables sensitive to signals in the dijet b-tagged search are shown in figure 7, after the baseline selection criteria (section 7.1) have been applied. The top (bottom) row shows results requiring $N_{b\,jets} = 1$ ($N_{b\,jets} = 2$). The left-hand plots show the M_{CT} distributions, and the right hand plots the p_T^{miss} distributions. The distributions of two representative signals for $\widetilde{b}\widetilde{\bar{b}} \to b\bar{b}\widetilde{\chi}_1^0\widetilde{\chi}_1^0$, scaled to an integrated luminosity of $19.4\,\mathrm{fb}^{-1}$, are superimposed for comparison. While the total background prediction in table 7 is obtained using the methods outlined in section 7.2, the background distributions in figure 7 are taken from simulation and normalized to an integrated luminosity of $19.4\,\mathrm{fb}^{-1}$.

Figure 8 shows the discriminating distributions in the monojet search, after the baseline selection criteria described in section 8.1 have been applied. The left plot shows the $p_T^{miss,\mu}$ distribution and the right plot the transverse momentum of the leading jet. Analogously to figure 7, the background distributions are taken directly from simulation and normalized to an integrated luminosity of $19.7\,\mathrm{fb}^{-1}$.

These three searches are individually designed to optimize the sensitivity to new physics for various signal topologies and third-generation sparticle mass hypotheses. In figure 6, the data are observed to agree with the SM background predictions, and in figures 7 and 8, with the SM background simulations, both with respect to overall normalization and shape.
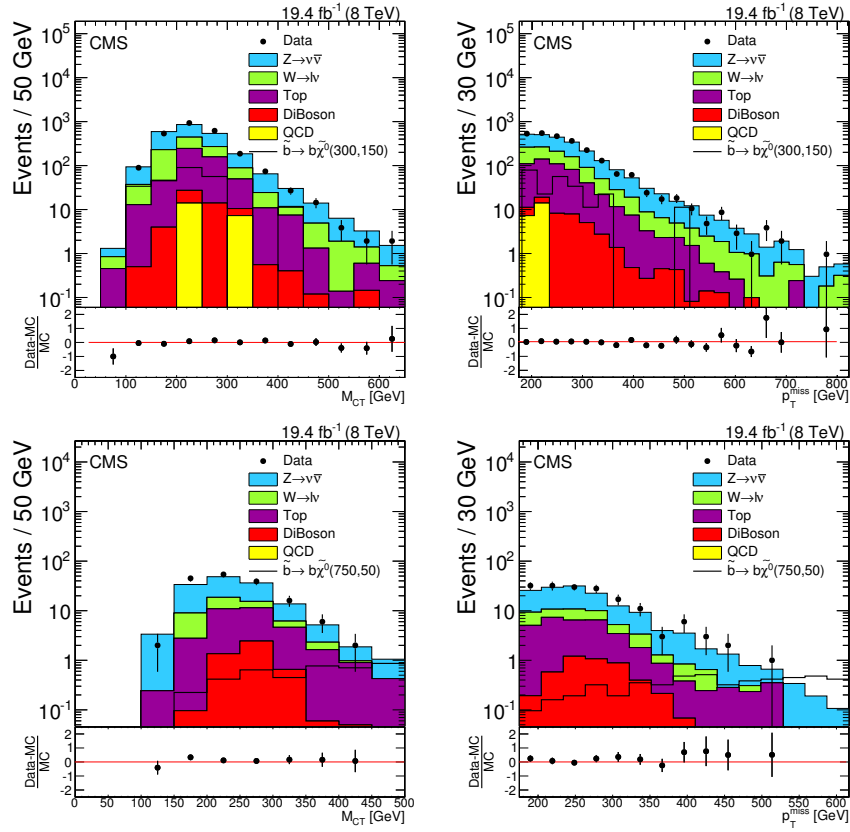
Figure 7. Distributions of (left column) M_{CT} and (right column) p_T^{miss} in data and MC simulation for baseline selected events in the dijet b-tagged search, with (top row) $N_{b\,jets} = 1$ and (bottom row) $N_{b\,jets} = 2$. Also shown (lines) are the corresponding distributions for two representative signals, $(m_{\tilde{b}}, m_{\tilde{\chi}_1^0}) = (750, 50)$ and $(300, 150)$ GeV. Statistical uncertainties are shown for the data.
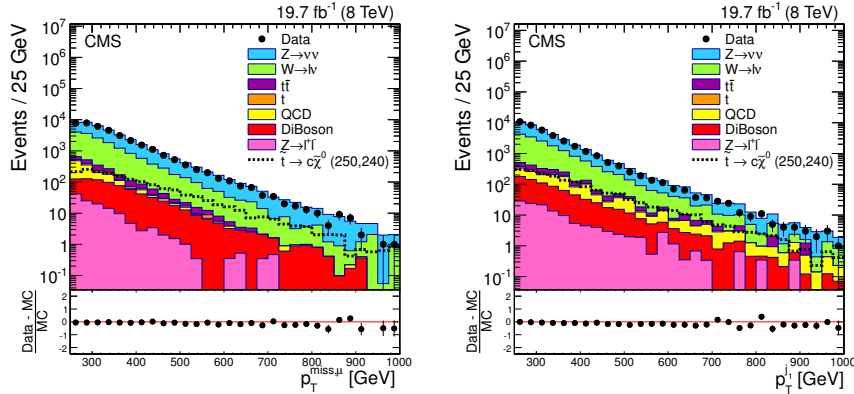
Figure 8. Distributions of (left) $p_T^{miss,\mu}$ and (right) leading jet p_T in the baseline monojet search region, $p_T^{j_1} > 250$ GeV, for data and SM backgrounds. Background distributions are taken from simulation, and normalized to an integrated luminosity of 19.7 fb^{-1}. A representative signal distribution for $\tilde{t} \to c\tilde{\chi}_1^0$ is also shown (in the dotted line), where $m_{\tilde{t}} = 250$ GeV and $m_{\tilde{\chi}_1^0} = 240$ GeV. Statistical uncertainties are shown for the data.

10 Interpretation

No significant deviations from the standard model predictions are observed. Results are interpreted as limits on SMS [26] involving the pair production of top and bottom squarks. Alternative decays of the top squark are studied, either $\widetilde{t} \to t\widetilde{\chi}_1^0$ or $\widetilde{t} \to c\widetilde{\chi}_1^0$, for a variety of top squark and LSP masses. We also study the case when there is an intermediate chargino state between the top squark and the LSP, $\widetilde{t} \to b\widetilde{\chi}_1^\pm \to bW^\pm \widetilde{\chi}_1^0$, where the LSP is assumed to be higgsino-like and nearly degenerate in mass with the lightest chargino: $m_{\widetilde{\chi}_1^\pm} - m_{\widetilde{\chi}_1^0} = 5\,\text{GeV}$. For this case, we investigate different branching fractions $\mathcal{B}(\widetilde{t} \to t\widetilde{\chi}_1^0) = 1 - \mathcal{B}(\widetilde{t} \to b\widetilde{\chi}_1^\pm)$ for the decay of the top squark. Finally, we study the decay of the bottom squark via the channel $\widetilde{b} \to b\widetilde{\chi}_1^0$ for different bottom squark and LSP masses.

The CL_s method [86, 87] is used to estimate the lower mass exclusion limits at 95% confidence level (CL) for third-generation squark pair production. Signal samples are produced as discussed in section 4, where the modelling of ISR within MadGraph has been re-weighted to account for observed differences between data and simulation [34], and a corresponding signal uncertainty assigned. Other sources of uncertainty arise from the jet energy scale, the PDFs [75, 88], and the integrated luminosity [25]. Signal cross sections include re-summation of soft-gluon emission at next-to-leading-logarithmic accuracy (NLO+NLL) [89–93]. Theoretical uncertainties are dominated by PDF uncertainties, and calculations are detailed in ref. [88].

The multijet t-tagged analysis and the dijet b-tagged analysis both define mutually exclusive search and control regions. Because those two analyses are statistically independent of each other, they are combined using the CL_s method, assuming fully correlated systematic uncertainties as nuisance parameters. On the other hand, when choosing between the results from the monojet analysis and the dijet b-tagged analysis, the analysis with the best *a priori* expected limit is selected for any particular point in the bottom squark versus neutralino mass plane. There is no overlap between the monojet and multijet t-tagged search regions and hence no special treatment is required when displaying the results of the two analyses on the same mass plane.

Figure 9 displays the 95% CL exclusion limits for top squark and LSP $\widetilde{\chi}_1^0$ masses, for either the $\widetilde{t}\widetilde{t} \to t\bar{t}\widetilde{\chi}_1^0\widetilde{\chi}_1^0$ or $\widetilde{t}\widetilde{t} \to c\bar{c}\widetilde{\chi}_1^0\widetilde{\chi}_1^0$ simplified models, whichever is kinematically allowed. The black diagonal dashed lines show the various kinematic regimes for top squark decay, from left to right: $m_{\widetilde{t}} > m_{\widetilde{\chi}_1^0}$ and $m_{\widetilde{t}} - m_{\widetilde{\chi}_1^0} < m_W$ dominated by $\widetilde{t}\widetilde{t} \to c\bar{c}\widetilde{\chi}_1^0\widetilde{\chi}_1^0$; $m_W < m_{\widetilde{t}} - m_{\widetilde{\chi}_1^0} < m_t$ dominated by $\widetilde{t}\widetilde{t} \to t\widetilde{\chi}_1^0\bar{b}\widetilde{\chi}_1^\pm \to t\bar{b}W^\pm\widetilde{\chi}_1^0\widetilde{\chi}_1^0$; and finally $m_{\widetilde{t}} > m_t + m_{\widetilde{\chi}_1^0}$, dominated by $\widetilde{t}\widetilde{t} \to t\bar{t}\widetilde{\chi}_1^0\widetilde{\chi}_1^0$.

While the multijet t-tagged search is combined with the dijet b-tagged search, the dijet b-tagged search does not contribute to the case in which the top squark decays to a top quark and the LSP with 100% branching fraction. This is primarily due to the jet veto requirements of the dijet b-tagged analysis, together with the high transverse momenta requirements for jets. The observed 95% CL exclusion limits (solid lines) are shown with the uncertainty bounds due to the uncertainty on the theoretical signal cross section (thinner, solid lines) $\pm 1\sigma_\text{th}$. The expected 95% CL exclusion limits (dashed lines)
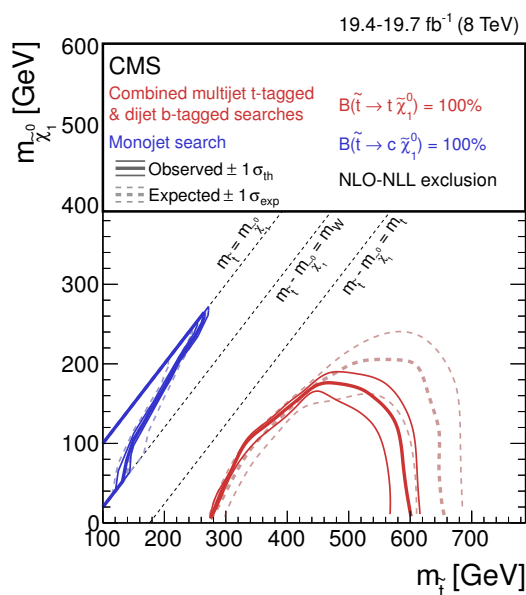
Figure 9. Expected and observed 95% CL exclusion limits in the $(m_{\tilde{t}}, m_{\tilde{\chi}_1^0})$ mass plane for top-squark pair production, assuming 100% branching fraction to the decay $\tilde{t} \to t\tilde{\chi}_1^0$, or, in the case of a highly compressed spectrum, to $\tilde{t} \to c\tilde{\chi}_1^0$. The $\pm 1\sigma_{\exp}$ and $\pm 1\sigma_{\rm th}$ limit curves are also shown. The combined results from the dijet b-tagged and multijet t-tagged searches and the result from the monojet search are displayed separately. The dashed black diagonal lines mark the borders of the various kinematic regimes leading to different top squark decays as described in the text.

are shown with their associated uncertainty (thinner, dashed lines) $\pm 1\sigma_{\exp}$. Exclusion lines are shown in red for the combined multijet t-tagged and dijet b-tagged searches, and in blue for the monojet search. The maximum lower limit on the top squark mass is expected to be about 620 GeV and is observed to be about 560 GeV, in the case of a massless LSP. In the region for which $m_{\tilde{t}} - m_{\tilde{\chi}_1^0} > m_{\rm W}$, the maximum lower limit on the LSP mass is expected to be just over 150 GeV for a top squark mass of 580 GeV, and is observed to be about 180 GeV for a top squark mass of 460 GeV. In the case of highly compressed spectra, when $m_{\tilde{t}}$ is close to $m_{\tilde{\chi}_1^0}$, the strip below the kinematically allowed diagonal line, $m_{\tilde{t}} = m_{\tilde{\chi}_1^0}$, and above the blue solid line is excluded, roughly up to 250 GeV in the top squark and LSP mass.

Figure 10 shows the same results as figure 9, except also considering a chargino $\tilde{\chi}_1^\pm$ intermediate in mass to the top squark and LSP. A 50% branching fraction to the chargino decay channel, $\tilde{t} \to b\tilde{\chi}_1^\pm$, is assumed; the other 50% of top squarks decay via $\tilde{t} \to t\tilde{\chi}_1^0$. In this case, both the dijet b-tagged and the multijet t-tagged analyses contribute to the expected and observed limits. The sensitivity of the dijet b-tagged analysis to this model derives from the near degeneracy of the $\tilde{\chi}_1^\pm$ and $\tilde{\chi}_1^0$ ($m_{\tilde{\chi}_1^\pm} - m_{\tilde{\chi}_1^0} = 5\,{\rm GeV}$). The decay products of the chargino result in large missing transverse momentum together with other particles that are too soft to be reconstructed as a hard jet. The dijet b-tagged analysis therefore primarily contributes to the moderately compressed regions, $m_{\rm W} < m_{\tilde{t}} - m_{\tilde{\chi}_1^0} < m_{\rm t}$, whereas the multijet t-tagged analysis remains mainly sensitive to the bulk region. For
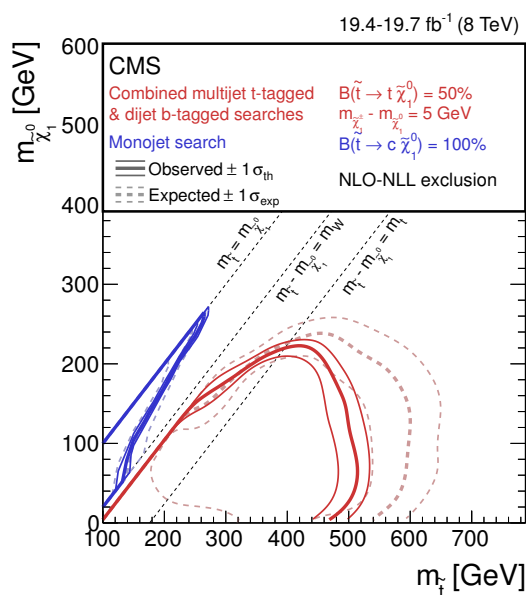
Figure 10. Expected and observed 95% CL exclusion limits in the $(m_{\widetilde{t}}, m_{\widetilde{\chi}_1^0})$ mass plane for top-squark pair production, assuming 50% branching fraction to the decay $\widetilde{t} \to t\widetilde{\chi}_1^0$, with the remaining 50% of decays proceeding via $\widetilde{t} \to b\widetilde{\chi}_1^\pm$ and where the mass difference between the $\widetilde{\chi}_1^\pm$ and $\widetilde{\chi}_1^0$ is taken to be 5 GeV. In the case of a highly compressed spectrum, 100% branching fraction to $\widetilde{t} \to c\widetilde{\chi}_1^0$ is assumed. The $\pm 1\sigma_{\mathrm{exp}}$ and $\pm 1\sigma_{\mathrm{th}}$ limit curves are also shown. The combined results from the dijet b-tagged and multijet t-tagged searches and the result from the monojet search are displayed separately. The dashed black diagonal lines mark the borders of the various kinematic regimes leading to different top squark decays as described in the text.

an LSP mass less than about 150 GeV, the lower limit on the top squark mass is expected to be about 540 GeV, and is observed to vary between about 460 and 480 GeV. In the bulk region, the lower limit on the LSP mass is expected to be about 200 GeV for a top squark mass near 440 GeV, and is observed to be slightly lower, at about 200 GeV for a top squark mass near 400 GeV.

Figure 11 is similar to figure 10, except that the branching fraction $\mathcal{B}(\widetilde{t} \to t\widetilde{\chi}_1^0) = 1 - \mathcal{B}(\widetilde{t} \to b\widetilde{\chi}_1^\pm)$ is varied between 1.0 and 0.0 in steps of 0.25. For clarity, only the curves of the observed lower limits are displayed. As the branching fraction $\mathcal{B}(\widetilde{t} \to t\widetilde{\chi}_1^0)$ is reduced from 1.0 to 0.0, the dijet b-tagged analysis becomes more sensitive, excluding higher LSP higgsino masses, up to nearly 300 GeV (for a top squark mass near 480 GeV) in the case of pure $\widetilde{t} \to b\widetilde{\chi}_1^\pm$ decays ($\mathcal{B} = 0.0$). Correspondingly, the multijet t-tagged analysis becomes less sensitive because the events fail the $N_{\mathrm{jets}} \geq 5$ requirement. For $\mathcal{B} = 0.0$, the top squark mass is excluded up to 610 GeV, when the higgsino mass is about 170 GeV.

Finally, figure 12 shows the 95% CL exclusion limits, in the LSP mass versus bottom squark mass plane, for the simplified model $\widetilde{b}\widetilde{\overline{b}} \to b\overline{b}\widetilde{\chi}_1^0\widetilde{\chi}_1^0$ with $\mathcal{B}(\widetilde{b} \to b\widetilde{\chi}_1^0) = 1.0$. The black diagonal dashed line shows the allowed kinematic region for bottom squark decay, $m_{\widetilde{b}} > m_{\widetilde{\chi}_1^0}$. The dijet b-tagged analysis is combined with the monojet analysis by choosing the analysis with the best expected limit at each point in the mass plane. We expect to
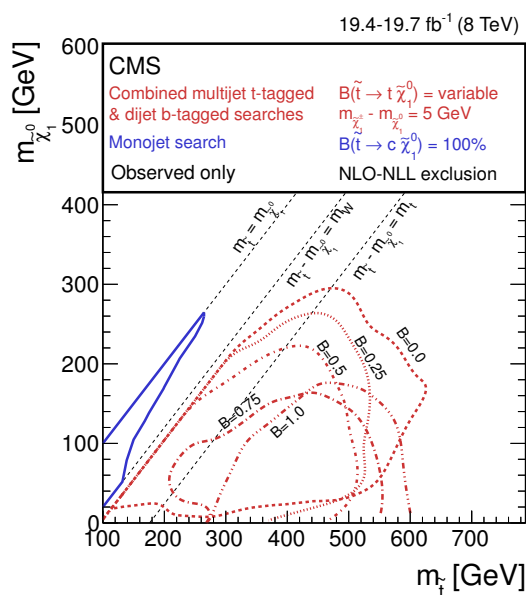
Figure 11. Various observed 95% CL mass exclusion limit curves for top-squark pair production, assuming different branching fractions of the two top squark decays $\widetilde{t} \to t\widetilde{\chi}_1^0$ and $\widetilde{t} \to b\widetilde{\chi}_1^\pm$. The mass difference between the $\widetilde{\chi}_1^\pm$ and $\widetilde{\chi}_1^0$ is taken to be 5 GeV. A branching fraction ($\mathcal{B}$) of 1.0 implies all decays are via $\widetilde{t} \to t\widetilde{\chi}_1^0$, repeating the observed multijet t-tagged limit shown in figure 9, and conversely, $\mathcal{B} = 0.0$ implies all decays proceed through $\widetilde{t} \to b\widetilde{\chi}_1^\pm$. The combined results from the dijet b-tagged and multijet t-tagged searches and the result from the monojet search are displayed separately. The dashed black diagonal lines mark the borders of the various kinematic regimes leading to different top squark decays as described in the text.

exclude the bottom squark up to 680 GeV for the case of a massless LSP, and are able to exclude it to 650 GeV. In the bulk region, the four M_{CT} binned search regions in which $N_{\mathrm{b\ jets}} = 2$ provide the best sensitivity. We expect to exclude the LSP to 320 GeV and are able to exclude it to 330 GeV for a bottom squark mass near 480 GeV. For mass points very close to the kinematically allowed boundary, the monojet search provides a thin strip of exclusion ranging up to about 250 GeV along the diagonal. Otherwise, significant coverage is extended from the bulk region well into the compressed spectra region via the dijet b-tagged ISR search region with $N_{\mathrm{b\ jets}} = 2$.

11 Summary

Three complementary searches have been presented for third-generation squarks in fully hadronic final states, corresponding to integrated luminosities of 19.4 or 19.7 fb^{-1} of proton-proton collision data, collected at $\sqrt{s} = 8$ TeV by the CMS experiment at the CERN LHC. By exploiting different search techniques, the separate analyses probe similar physics processes in a variety of phase space regions, across the top/bottom squark and neutralino mass planes, including alternative SUSY scenarios in which there exists an intermediate chargino state. No significant excesses above the predictions from the standard model are
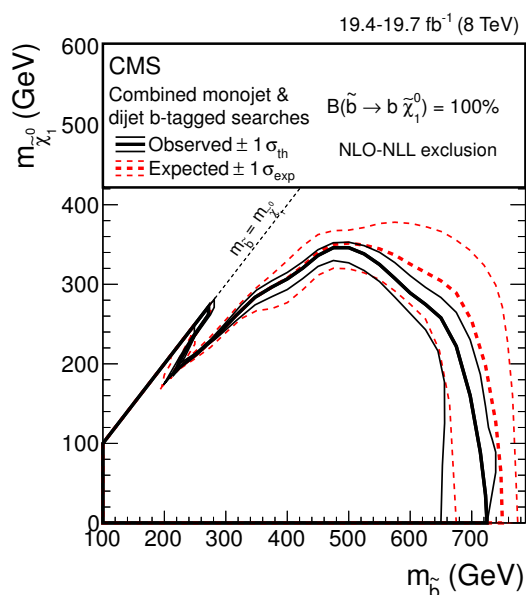
Figure 12. Expected and observed 95% CL exclusion limits in the $(m_{\widetilde{b}}, m_{\widetilde{\chi}_1^0})$ mass plane for bottom-squark pair production, assuming 100% branching fraction to the decay $\widetilde{b} \to b\widetilde{\chi}_1^0$. The $\pm 1\sigma_{\mathrm{exp}}$ and $\pm 1\sigma_{\mathrm{th}}$ limit curves are also shown. The combined results from dijet b-tagged and monojet searches are displayed, taking the best expected limit from either search at each point in the mass plane. The black diagonal line marks the border of the kinematically allowed region.

observed, and 95% CL exclusion limits are placed on top and bottom squark masses. A dedicated t-tagging search excludes the process $\widetilde{\overline{t}}\widetilde{t} \to t\overline{t}\widetilde{\chi}_1^0\widetilde{\chi}_1^0$ with $m_{\widetilde{t}} \le 560\,\mathrm{GeV}$ for $m_{\widetilde{\chi}_1^0} \approx 0\,\mathrm{GeV}$. A dedicated b-tagging search excludes the process $\widetilde{\overline{b}}\widetilde{b} \to b\overline{b}\widetilde{\chi}_1^0\widetilde{\chi}_1^0$ with $m_{\widetilde{b}} \le 650\,\mathrm{GeV}$ for $m_{\widetilde{\chi}_1^0} \approx 0\,\mathrm{GeV}$. The process $\widetilde{\overline{t}}\widetilde{t} \to t\widetilde{\chi}_1^0\overline{b}\widetilde{\chi}_1^- \to t\overline{b}W^-\widetilde{\chi}_1^0\widetilde{\chi}_1^0$ and its charge conjugate are excluded for different branching fractions of the top squark decay, and the two analyses are combined to exclude the region $m_{\widetilde{t}} \le 460\,\mathrm{GeV}$ with $m_{\widetilde{\chi}_1^0} \le 150\,\mathrm{GeV}$ and $\mathcal{B}(\widetilde{t} \to t\widetilde{\chi}_1^0) = 0.5$ assuming the $\widetilde{\chi}_1^0$ and $\widetilde{\chi}_1^\pm$ to be nearly mass degenerate. A dedicated monojet search in the compressed region of the top (bottom) squark versus LSP mass plane excludes $\widetilde{\overline{t}}\widetilde{t} \to c\overline{c}\widetilde{\chi}_1^0\widetilde{\chi}_1^0$ ($\widetilde{\overline{b}}\widetilde{b} \to b\overline{b}\widetilde{\chi}_1^0\widetilde{\chi}_1^0$) production for $m_{\widetilde{t}}(m_{\widetilde{b}}) \le 250\,\mathrm{GeV}$ and $m_{\widetilde{t}} - m_{\widetilde{\chi}_1^0}(m_{\widetilde{b}} - m_{\widetilde{\chi}_1^0}) < 10\,\mathrm{GeV}$, and analogously for $m_{\widetilde{t}}(m_{\widetilde{b}}) \le 120\,\mathrm{GeV}$ and $m_{\widetilde{t}} - m_{\widetilde{\chi}_1^0}(m_{\widetilde{b}} - m_{\widetilde{\chi}_1^0}) < 80\,\mathrm{GeV}$.

Acknowledgments

## A   Information for additional model testing

Information needed to enable additional model testing is provided here.

Figure 13 shows the search regions that give the best expected 95% CL limit for top-squark pair production assuming different branching fractions to the top squark decays $\widetilde{t} \to t\widetilde{\chi}_1^0$ and $\widetilde{t} \to b\widetilde{\chi}_1^\pm$ in the $(m_{\widetilde{t}}, m_{\widetilde{\chi}_1^0})$ mass plane. The top-left hand plot of figure 13 illustrates the optimal search region assuming $\mathcal{B}(\widetilde{t} \to t\widetilde{\chi}_1^0) = 1.0$. Contributions only come from the multijet t-tagged analysis. The top-right hand plot illustrates the optimal search region assuming $\mathcal{B}(\widetilde{t} \to t\widetilde{\chi}_1^0) = 0.5$. Here, the multijet t-tagged analysis has no sensitivity when the top squark mass is less than the top mass, so the dijet b-tagged search dominates. At large top squark mass the multijet t-tagged analysis dominates. The bottom plot of figure 13 illustrates the optimal search region assuming $\mathcal{B}(\widetilde{t} \to t\widetilde{\chi}_1^0) = 0.0$ (all top squarks decay via $\widetilde{t} \to b\widetilde{\chi}_1^\pm$), in which contributions only come from the dijet b-tagged analysis.

Figure 14 similarly shows the search regions in the monojet analysis that give the best expected 95% CL limit for the top squark decay $\widetilde{t} \to c\widetilde{\chi}_1^0$ in the $(m_{\widetilde{t}}, m_{\widetilde{\chi}_1^0})$ mass plane, and bottom squark decay $\widetilde{b} \to b\widetilde{\chi}_1^0$ in the $(m_{\widetilde{b}}, m_{\widetilde{\chi}_1^0})$ mass plane. Typically, harder jet thresholds are found to give better expected limits close to the diagonal, and softer jet thresholds are better for lower $\widetilde{t}$ and $\widetilde{b}$ masses.

Figure 15 shows the analysis giving the best expected 95% CL limit for bottom squark decay $\widetilde{b} \to b\widetilde{\chi}_1^0$ in the $(m_{\widetilde{b}}, m_{\widetilde{\chi}_1^0})$ mass plane when the results from the monojet and dijet b-tagged analyses are combined. Figure 16 shows the individual 95% CL exclusion limits for the dijet b-tagged and monojet searches for $\widetilde{b}\overline{\widetilde{b}} \to b\bar{b}\widetilde{\chi}_1^0\widetilde{\chi}_1^0$. The monojet search gives the better exclusion close to the diagonal, showing the kinematic limit of mass degeneracy between the bottom squark and LSP. The dijet b-tagged search, including "ISR" regions, dominate in the rest of the parameter space.

Cut flow tables detailing the fraction of total events passing event selections at each step are also shown. Table 8 shows the signal acceptance × efficiency for different top squark and LSP mass hypotheses at each stage event selection in the multijet t-tagged search. Similarly, tables 9, 10, and 11 show the signal acceptance × efficiency for different third-generation squark and LSP mass hypotheses at each stage of the event selection in the dijet b-tagged and monojet searches. In these tables, "Event cleaning" (the first of the cuts applied to events) are the requirements used to remove events with badly measured p_T^{miss}, beam halo, detector noise, etc.
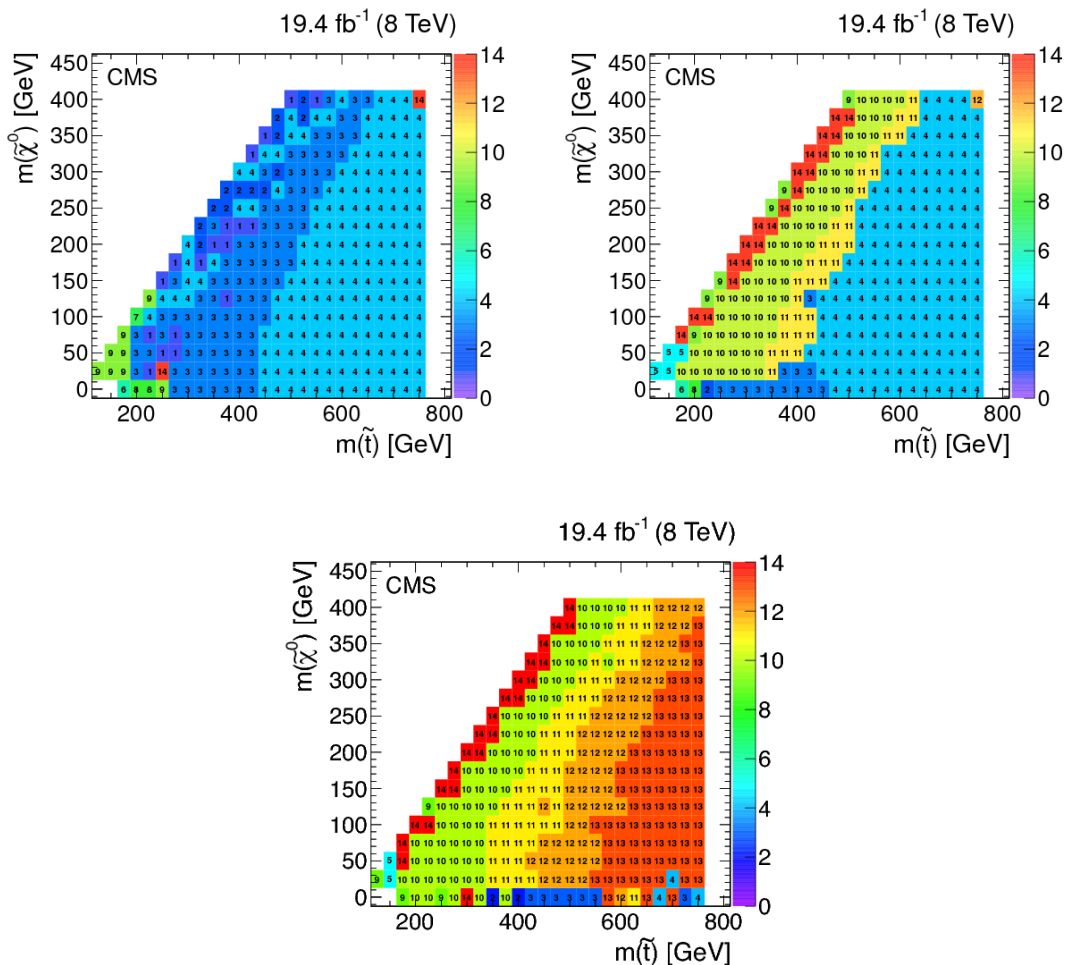
Figure 13. The search region from the combined multijet t-tagged and dijet b-tagged analyses resulting in the best 95% CL expected limit is indicated by a number and shown on the colour scale in the $(m_{\tilde{t}}, m_{\tilde{\chi}_1^0})$ mass plane. Search regions are numbered as follows. Regions labelled 1–4 are for the multijet t-tagged analysis: (1) 1b + $200 \leq p_T^{miss} \leq 350$; (2) 1b + $p_T^{miss} > 350$; (3) 2b + $200 < p_T^{miss} < 350$; and (4) 2b + $p_T^{miss} > 350$ GeV. Numbers 5-14 are from the dijet b-tagged analysis. Regions labelled 5-9 are for those search regions with 1 b tag: (5) $M_{CT} < 250$; (6) $250 < M_{CT} < 350$; (7) $350 < M_{CT} < 450$; (8) $M_{CT} > 450$ GeV and (9) the ISR region. Regions labelled 10–14 are for similar regions with 2 b tags. In the top left-hand plot, the optimal search regions are shown for the best expected limit curve in figure 9 in which $\mathcal{B}(\tilde{t} \to t\tilde{\chi}_1^0) = 1.0$ is assumed, i.e. all top squarks decay via $\tilde{t} \to t\tilde{\chi}_1^0$. In the top right-hand plot, the optimal search regions are shown for the expected limit curve in figure 10 in which $\mathcal{B}(\tilde{t} \to t\tilde{\chi}_1^0) = 0.5$ is assumed. In the bottom plot, the optimal search regions are shown for the expected limit curve shown in figure 11, i.e. all top squarks decay via $\tilde{t} \to b\tilde{\chi}_1^\pm$.

| t-tagged event selection	$\widetilde{t}\widetilde{t} \to t\widetilde{\chi}_1^0\bar{b}\widetilde{\chi}_1^\pm \to t\bar{b}W^\pm\widetilde{\chi}_1^0\widetilde{\chi}_1^0$					
	$\mathcal{B}(\widetilde{t} \to t\widetilde{\chi}_1^0) = 0.0$		$\mathcal{B}(\widetilde{t} \to t\widetilde{\chi}_1^0) = 0.5$		$\mathcal{B}(\widetilde{t} \to t\widetilde{\chi}_1^0) = 1.0$	
	(500,125) GeV	(650,25) GeV	(500,125) GeV	(650,25) GeV	(500,125) GeV	(650,25) GeV
Event cleaning	98.02 ± 0.09	97.35 ± 0.10	98.05 ± 0.04	97.29 ± 0.05	98.13 ± 0.08	97.44 ± 0.10
μ veto	87.16 ± 0.21	76.60 ± 0.27	79.58 ± 0.13	74.36 ± 0.14	72.16 ± 0.28	72.50 ± 0.29
e veto	83.60 ± 0.23	64.21 ± 0.31	68.77 ± 0.14	59.72 ± 0.16	55.41 ± 0.31	55.55 ± 0.32
$N_{\text{jets}}(p_{\text{T}} > 70\,\text{GeV}) \geq 2$	74.49 ± 0.27	61.72 ± 0.31	61.02 ± 0.15	57.06 ± 0.16	49.55 ± 0.31	52.72 ± 0.32
$N_{\text{jets}}(p_{\text{T}} > 50\,\text{GeV}) \geq 4$	14.99 ± 0.22	30.17 ± 0.29	23.86 ± 0.13	32.76 ± 0.15	31.16 ± 0.29	34.55 ± 0.31
$N_{\text{jets}}(p_{\text{T}} > 30\,\text{GeV}) \geq 5$	9.11 ± 0.18	22.06 ± 0.27	17.54 ± 0.12	25.63 ± 0.14	26.25 ± 0.28	28.49 ± 0.29
$\Delta\phi(\vec{p}_{\text{T}}^{\,j}, \vec{p}_{\text{T}}^{\,\text{miss}})(j = 1,2,3)$ $\geq 0.5, 0.5, 0.3$	7.47 ± 0.17	17.39 ± 0.24	14.77 ± 0.11	21.54 ± 0.13	22.46 ± 0.26	24.98 ± 0.28
$N_{\text{b jets}} \geq 1$	6.77 ± 0.16	15.48 ± 0.23	13.09 ± 0.11	19.12 ± 0.13	19.63 ± 0.25	21.81 ± 0.26
$p_{\text{T}}^{\text{miss}} > 200\,\text{GeV}$	4.79 ± 0.13	11.84 ± 0.21	8.54 ± 0.09	15.02 ± 0.11	12.21 ± 0.20	17.60 ± 0.24
Top tagger, $M_{\text{T2}} \geq 300\,\text{GeV}$, $(0.5M_{\text{T}}^{\text{3-jet}} + M_{\text{T}}^{\text{R-sys}})$ $\geq 500\,\text{GeV}$	0.96 ± 0.06	1.89 ± 0.09	3.01 ± 0.05	5.15 ± 0.07	4.87 ± 0.13	8.37 ± 0.18
$N_{\text{b jets}} = 1$, $p_{\text{T}}^{\text{miss}} \in [200, 350]\,\text{GeV}$	0.18 ± 0.03	0.31 ± 0.04	0.63 ± 0.02	0.67 ± 0.03	1.19 ± 0.07	1.06 ± 0.07
$N_{\text{b jets}} = 1$, $p_{\text{T}}^{\text{miss}} \geq 350\,\text{GeV}$	0.23 ± 0.03	0.52 ± 0.05	0.58 ± 0.02	1.38 ± 0.04	0.93 ± 0.06	2.49 ± 0.10
$N_{\text{b jets}} \geq 2$, $p_{\text{T}}^{\text{miss}} \in [200, 350]\,\text{GeV}$	0.32 ± 0.04	0.46 ± 0.04	0.99 ± 0.03	0.99 ± 0.03	1.64 ± 0.08	1.34 ± 0.07
$N_{\text{b jets}} \geq 2$, $p_{\text{T}}^{\text{miss}} \geq 350\,\text{GeV}$	0.23 ± 0.03	0.61 ± 0.05	0.80 ± 0.03	2.11 ± 0.05	1.11 ± 0.07	3.48 ± 0.12

Table 8. Signal acceptance $\times$ efficiency, shown in %, for each step of the event selection of the multijet t-tagged analysis. Two representative mass points are shown: $(m_{\widetilde{t}}, m_{\widetilde{\chi}_1^0}) = (500,125)$ and $(650,25)\,\text{GeV}$, for $\widetilde{t}\widetilde{t} \to t\widetilde{\chi}_1^0\bar{b}\widetilde{\chi}_1^\pm \to t\bar{b}W^\pm\widetilde{\chi}_1^0\widetilde{\chi}_1^0$ with $\mathcal{B}(\widetilde{t} \to t\widetilde{\chi}_1^0) = 0.0$, 0.5 and 1.0. Only statistical uncertainties are shown.
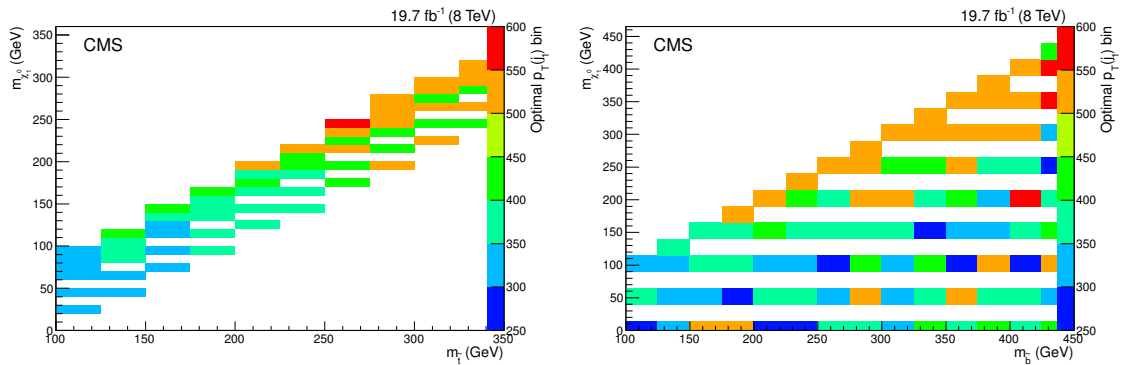
Figure 14. The search region resulting in the best 95% CL expected limit for the monojet search, in the $(m_{\widetilde{t}}, m_{\widetilde{\chi}_1^0})$ mass plane for $\widetilde{t}\widetilde{t} \to c\bar{c}\widetilde{\chi}_1^0\widetilde{\chi}_1^0$ (left) and the $(m_{\widetilde{b}}, m_{\widetilde{\chi}_1^0})$ mass plane for $\widetilde{b}\widetilde{b} \to b\bar{b}\widetilde{\chi}_1^0\widetilde{\chi}_1^0$ (right).
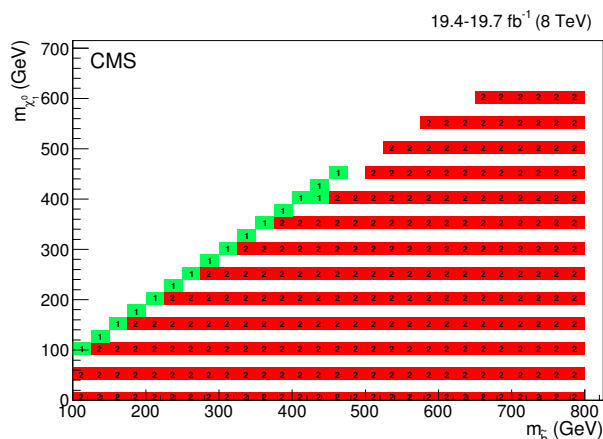
Figure 15. The search resulting in the best 95% CL expected limit, for different sparticle mass hypotheses for the process $\widetilde{b}\widetilde{b} \to b\bar{b}\widetilde{\chi}_1^0\widetilde{\chi}_1^0$. Bins shown in green ('1') are where the monojet search gives the best expected limit, and those shown in red ('2') are where the dijet b-tagged search gives the best expected limit.
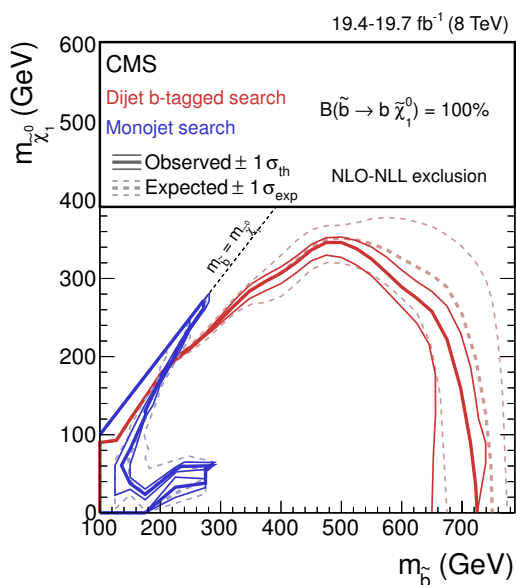
Figure 16. Expected and observed 95% CL exclusion limits in the mass plane $(m_{\widetilde{b}}, m_{\widetilde{\chi}_1^0})$, for bottom-squark pair production, assuming 100% branching fraction to the decay $\widetilde{b} \to b\widetilde{\chi}_1^0$. The $\pm 1\,\sigma_{\mathrm{exp}}$ and $\pm 1\,\sigma_{\mathrm{th}}$ limit curves are also shown. Limits for the dijet b-tagged search and monojet search are superimposed, to illustrate where in the parameter space each search dominates. The black diagonal line shows the region of parameter space for bottom squark decay; $m_{\widetilde{b}} > m_{\widetilde{\chi}_1^0}$.

M_{CT} event selection	$\widetilde{\mathrm{b}}\widetilde{\mathrm{b}} \to \mathrm{b}\bar{\mathrm{b}}\widetilde{\chi}^0_1\widetilde{\chi}^0_1$		$\widetilde{\mathrm{t}}\widetilde{\mathrm{t}} \to \mathrm{t}\widetilde{\chi}^0_1\bar{\mathrm{b}}\widetilde{\chi}^\pm_1 \to \mathrm{t}\bar{\mathrm{b}}\mathrm{W}^\pm\widetilde{\chi}^0_1\widetilde{\chi}^0_1$			
	$\mathcal{B}(\widetilde{\mathrm{b}} \to \mathrm{b}\widetilde{\chi}^0_1) = 1.0$		$\mathcal{B}(\widetilde{\mathrm{t}} \to \mathrm{t}\widetilde{\chi}^0_1) = 0.0$		$\mathcal{B}(\widetilde{\mathrm{t}} \to \mathrm{t}\widetilde{\chi}^0_1) = 0.5$	
	(275,250) GeV	(700,100) GeV	(250,125) GeV	(500,125) GeV	(250,125) GeV	(500,125) GeV
Event cleaning	91.50 ±0.11	92.92 ±0.13	91.63 ±0.08	93.54 ±0.18	91.63 ±0.06	92.87 ±0.07
$N_{\mathrm{jets}}(p_{\mathrm{T}} > 70\,\mathrm{GeV}) = 2$	2.01±0.30	37.62 ±0.38	3.22±0.17	31.71±0.29	15.86±0.11	23.73 ±0.17
e, μ veto	1.97±0.28	36.01±0.36	3.19±0.17	31.60±0.29	13.62±0.12	19.09 ±0.15
IsoTrk Veto	1.87±0.26	33.64±0.34	2.92±0.15	30.63±0.28	12.08±0.12	16.62± 0.14
3rd Jet Veto	1.24±0.21	23.1±0.22	2.34±0.13	21.24±0.33	6.57 ±0.08	7.32±0.09
$H_{\mathrm{T}} > 250\,\mathrm{GeV}$	0.56±0.14	22.13±0.20	1.13±0.10	20.91±0.32	2.76 ±0.04	6.41±0.08
$p_{\mathrm{T}}^{\mathrm{miss}} > 175\,\mathrm{GeV}$	0.13±0.10	16.41±0.18	0.92±0.09	17.83±0.26	0.55±0.03	4.81±0.07
$M_{\mathrm{T}} > 200\,\mathrm{GeV}$	0.074±0.009	14.4 ±0.15	0.86±0.08	16.24±0.25	0.25±0.03	3.9 ±0.05
$\Delta\phi(\mathrm{b}_1,\mathrm{b}_2) < 2.5$	0.071±0.009	13.0±0.14	0.86±0.08	16.21±0.25	0.86±0.04	3.49±0.06
$N_{\mathrm{b\,jets}} = 1$	0.039±0.007	6.42 ±0.09	0.033±0.001	5.92±0.13	0.19±0.02	2.89±0.04
$N_{\mathrm{b\,jets}} = 2$	0.002±0.001	5.2±0.08	0.002±0.001	6.49±0.16	0.02±0.001	1.56 ±0.03
$N_{\mathrm{b\,jets}} = 1,$ $M_{\mathrm{CT}} < 250\,\mathrm{GeV}$	0.027±0.005	1.74±0.08	0.017±0.001	0.68±0.03	0.14±0.01	0.92± 0.04
$N_{\mathrm{b\,jets}} = 1,$ $M_{\mathrm{CT}} \in [250, 350]\,\mathrm{GeV}$	0.011±0.004	2.82±0.09	0.015±0.001	1.12±0.07	0.04±0.003	1.28±0.05
$N_{\mathrm{b\,jets}} = 1,$ $M_{\mathrm{CT}} \in [250, 350]\,\mathrm{GeV}$	0.001±0.0006	1.73±0.08	0.001±0.0006	1.56±0.08	0.01±0.001	0.61±0.03
$N_{\mathrm{b\,jets}} = 1,$ $M_{\mathrm{CT}} > 450\,\mathrm{GeV}$	0.00±0.00	0.13±0.06	0.00±0.00	2.54±0.09	0.00±0.00	0.06±0.004
$N_{\mathrm{b\,jets}} = 2,$ $M_{\mathrm{CT}} < 250\,\mathrm{GeV}$	0.001±0.005	1.29±0.06	0.002±0.0006	0.44±0.02	0.02±0.001	0.50±0.03
$N_{\mathrm{b\,jets}} = 2,$ $M_{\mathrm{CT}} \in [250, 350]\,\mathrm{GeV}$	0.001±0.005	1.98±0.09	0.001±0006	1.21±0.07	0.002±0.001	0.72±0.04
$N_{\mathrm{b\,jets}} = 2,$ $M_{\mathrm{CT}} \in [250, 350]\,\mathrm{GeV}$	0.00±0.00	1.52±0.08	0.00±0.00	1.58±0.08	0.0±0.00	0.38±0.04
$N_{\mathrm{b\,jets}} = 2,$ $M_{\mathrm{CT}} > 450\,\mathrm{GeV}$	0.00±0.00	0.15±0.03	0.00±0.00	3.21±0.11	0.00±0.00	0.00±0.00

Table 9. Signal acceptance × efficiency, shown in %, for each step of the event selection of the dijet b-tagged analysis, for the M_{CT} search regions. Two representative mass points are shown; $(m_{\widetilde{\mathrm{b}}},\ m_{\widetilde{\chi}^0_1}) = (275,250)$ and $(700,100)\,\mathrm{GeV}$ for $\widetilde{\mathrm{b}}\widetilde{\mathrm{b}} \to \mathrm{b}\bar{\mathrm{b}}\widetilde{\chi}^0_1\widetilde{\chi}^0_1$ with $\mathcal{B}(\widetilde{\mathrm{b}} \to \mathrm{b}\widetilde{\chi}^0_1) = 1.0$, and $(m_{\widetilde{\mathrm{t}}},\ m_{\widetilde{\chi}^0_1}) = (250,125)$ and $(500,125)\,\mathrm{GeV}$ for $\widetilde{\mathrm{t}}\widetilde{\mathrm{t}} \to \mathrm{t}\widetilde{\chi}^0_1\bar{\mathrm{b}}\widetilde{\chi}^\pm_1 \to \mathrm{t}\bar{\mathrm{b}}\mathrm{W}^\pm\widetilde{\chi}^0_1\widetilde{\chi}^0_1$ with $\mathcal{B}(\widetilde{\mathrm{t}} \to \mathrm{t}\widetilde{\chi}^0_1) = 0.0,\ 0.5$. The dijet b-tagged analysis has no sensitivity to the $\mathcal{B}(\widetilde{\mathrm{t}} \to \mathrm{t}\widetilde{\chi}^0_1) = 1.0$ case so it is not shown. Only statistical uncertainties are shown.

ISR event selection	$\widetilde{\mathrm{b}}\overline{\widetilde{\mathrm{b}}} \to \mathrm{b}\bar{\mathrm{b}}\widetilde{\chi}_1^0\widetilde{\chi}_1^0$		$\widetilde{\mathrm{t}}\overline{\widetilde{\mathrm{t}}} \to \mathrm{t}\widetilde{\chi}_1^0\bar{\mathrm{b}}\widetilde{\chi}_1^\pm \to \mathrm{t}\bar{\mathrm{b}}\mathrm{W}^\pm\widetilde{\chi}_1^0\widetilde{\chi}_1^0$			
	$\mathcal{B}(\widetilde{\mathrm{b}} \to \mathrm{b}\widetilde{\chi}_1^0) = 1.0$		$\mathcal{B}(\widetilde{\mathrm{t}} \to \mathrm{t}\widetilde{\chi}_1^0) = 0.0$		$\mathcal{B}(\widetilde{\mathrm{t}} \to \mathrm{t}\widetilde{\chi}_1^0) = 0.5$	
	(275,250) GeV	(700,100) GeV	(250,125) GeV	(500,125) GeV	(250,125) GeV	(500,125) GeV
Event cleaning	94.40±0.07	96.50±0.17	94.62±0.14	95.28±0.15	94.61±0.08	95.34±0.08
$N_{\mathrm{jets}}(p_{\mathrm{T}} > 30\,\mathrm{GeV}) == 3$	9.98±0.31	28.90±0.29	28.57±0.26	31.52±0.29	36.72±0.25	29.61 ±0.21
$1^{st}, 2^{nd}$ jets ($p_{\mathrm{T}} > 70\,\mathrm{GeV}$)	2.50±0.14	27.60±0.28	17.21±0.21	27.90± 0.26	14.91±0.14	21.63 ±0.19
e, μ and IsoTrk veto	2.40±0.14	27.50±0.28	15.84±0.20	24.08±0.23	9.42±0.11	14.48± 0.16
$H_{\mathrm{T}} > 250\,\mathrm{GeV}$	1.40±0.09	27.20±0.28	9.46±0.12	23.13 ±0.23	7.58±0.09	10.21±0.12
$p_{\mathrm{T}}^{\mathrm{miss}} > 175\,\mathrm{GeV}$	0.90±0.07	22.10±0.24	0.73±0.10	12.10±0.17	0.43±0.04	4.77±0.07
$\mathrm{Min}(\Delta\phi(j_{1,2,3}, p_{\mathrm{T}}^{\mathrm{miss}})) > 0.5$	0.36±0.04	17.30±0.19	0.58±0.08	9.72±0.15	0.36±0.04	3.1±0.06
$N_{\mathrm{b\,jets}} = 1$ (2nd or 3rd jets)	0.13±0.01	3.4±0.12	0.29±0.06	2.10 ±0.09	0.090±0.008	1.26±0.02
$N_{\mathrm{b\,jets}} = 2$ (2nd and 3rd jets)	0.0080±0.0002	0.43±0.02	0.09±0.04	0.29±0.07	0.015±0.001	0.43±0.03
$N_{\mathrm{b\,jets}} = 1$, $p_{\mathrm{T}}^{\mathrm{non\text{-}b}} > 250\,\mathrm{GeV}$	0.087±0.003	2.60±0.09	0.14±0.09	1.44±0.08	0.070±0.008	0.87±0.06
$N_{\mathrm{b\,jets}} = 2$, $p_{\mathrm{T}}^{\mathrm{non\text{-}b}} > 250\,\mathrm{GeV}$	0.0060±0002	0.37±0.02	0.050±0.007	0.24±0.04	0.012±0.001	0.16±0.02

Table 10. Signal acceptance × efficiency, shown in %, for each step of the event selection of the dijet b-tagged analysis, for the ISR search regions. Two representative mass points are shown; ($m_{\widetilde{\mathrm{b}}}$, $m_{\widetilde{\chi}_1^0}$) = (275,250) and (700,100) GeV, for $\widetilde{\mathrm{b}}\overline{\widetilde{\mathrm{b}}} \to \mathrm{b}\bar{\mathrm{b}}\widetilde{\chi}_1^0\widetilde{\chi}_1^0$ with $\mathcal{B}(\widetilde{\mathrm{b}} \to \mathrm{b}\widetilde{\chi}_1^0) = 1.0$, and ($m_{\widetilde{\mathrm{t}}}$, $m_{\widetilde{\chi}_1^0}$) = (250,125) and (500,125) GeV, for $\widetilde{\mathrm{t}}\overline{\widetilde{\mathrm{t}}} \to \mathrm{t}\widetilde{\chi}_1^0\bar{\mathrm{b}}\widetilde{\chi}_1^\pm \to \mathrm{t}\bar{\mathrm{b}}\mathrm{W}^\pm\widetilde{\chi}_1^0\widetilde{\chi}_1^0$ with $\mathcal{B}(\widetilde{\mathrm{t}} \to \mathrm{t}\widetilde{\chi}_1^0) = 0.0, 0.5$. The dijet b-tagged analysis has no sensitivity to the $\mathcal{B}(\widetilde{\mathrm{t}} \to \mathrm{t}\widetilde{\chi}_1^0) = 1.0$ case so it is not shown. Only statistical uncertainties are shown.

Monojet event selection	$\widetilde{\mathrm{b}}\overline{\widetilde{\mathrm{b}}} \to \mathrm{b}\bar{\mathrm{b}}\widetilde{\chi}_1^0\widetilde{\chi}_1^0$		$\widetilde{\mathrm{t}}\overline{\widetilde{\mathrm{t}}} \to \mathrm{c}\bar{\mathrm{c}}\widetilde{\chi}_1^0\widetilde{\chi}_1^0$	
	$\mathcal{B}(\widetilde{\mathrm{b}} \to \mathrm{b}\widetilde{\chi}_1^0) = 1.0$		$\mathcal{B}(\widetilde{\mathrm{t}} \to \mathrm{c}\widetilde{\chi}_1^0) = 1.0$	
	(250, 240) GeV	(150, 50) GeV	(250, 240) GeV	(200, 120) GeV
Event cleaning	98.61 ± 0.24	98.79 ± 0.02	97.54 ± 0.14	99.21 ± 0.03
$p_{\mathrm{T}}^{\mathrm{miss}} > 200\,\mathrm{GeV}$	7.41 ± 0.49	2.37 ± 0.02	7.17 ± 0.25	4.29 ± 0.06
Noisy events	6.90 ± 0.47	2.22 ± 0.02	6.68 ± 0.24	4.01 ± 0.06
$p_{\mathrm{T}}(j_1) > 110\,\mathrm{GeV}$	6.58 ± 0.46	2.08 ± 0.02	6.35 ± 0.23	3.71 ± 0.06
$N_{\mathrm{jets}} < 3$	5.78 ± 0.44	1.39 ± 0.02	5.56 ± 0.22	2.30 ± 0.04
$\Delta\phi(j_1, j_2) < 2.5$	5.58 ± 0.43	1.170 ± 0.015	5.36 ± 0.21	1.96 ± 0.04
μ veto	5.57 ± 0.43	1.170 ± 0.015	5.36 ± 0.21	1.96 ± 0.04
e veto	5.57 ± 0.43	1.160 ± 0.015	5.36 ± 0.21	1.96 ± 0.04
τ_{h} veto	5.52 ± 0.43	1.14 ± 0.015	5.30 ± 0.21	1.93 ± 0.04
$p_{\mathrm{T}}^{\mathrm{miss}}$ & $p_{\mathrm{T}}(j_1) > 250\,\mathrm{GeV}$	2.08 ± 0.27	0.222 ± 0.006	2.04 ± 0.13	0.42 ± 0.02
$p_{\mathrm{T}}(j_1) > 300\,\mathrm{GeV}$	1.32 ± 0.21	0.122 ± 0.005	1.32 ± 0.11	0.25 ± 0.01
$p_{\mathrm{T}}(j_1) > 350\,\mathrm{GeV}$	0.80 ± 0.17	0.058 ± 0.003	0.81 ± 0.08	0.13 ± 0.01
$p_{\mathrm{T}}(j_1) > 400\,\mathrm{GeV}$	0.49 ± 0.13	0.027 ± 0.002	0.50 ± 0.07	0.072 ± 0.008
$p_{\mathrm{T}}(j_1) > 450\,\mathrm{GeV}$	0.31 ± 0.11	0.016 ± 0.002	0.32 ± 0.05	0.041 ± 0.006
$p_{\mathrm{T}}(j_1) > 500\,\mathrm{GeV}$	0.19 ± 0.08	0.009 ± 0.001	0.19 ± 0.04	0.023 ± 0.005
$p_{\mathrm{T}}(j_1) > 550\,\mathrm{GeV}$	0.12 ± 0.07	0.006 ± 0.001	0.12 ± 0.03	0.013 ± 0.003

Table 11. Signal acceptance × efficiency, shown in %, for each step of the event selection of the monojet analysis. Two representative mass points are shown; ($m_{\widetilde{\mathrm{b}}}$, $m_{\widetilde{\chi}_1^0}$) = (250,240) and (150,50) GeV for $\widetilde{\mathrm{b}}\overline{\widetilde{\mathrm{b}}} \to \mathrm{b}\bar{\mathrm{b}}\widetilde{\chi}_1^0\widetilde{\chi}_1^0$ where $\mathcal{B}(\widetilde{\mathrm{b}} \to \mathrm{b}\widetilde{\chi}_1^0) = 1.0$, and ($m_{\widetilde{\mathrm{t}}}$, $m_{\widetilde{\chi}_1^0}$) = (250,240) GeV and (200,120) for $\widetilde{\mathrm{t}}\overline{\widetilde{\mathrm{t}}} \to \mathrm{c}\bar{\mathrm{c}}\widetilde{\chi}_1^0\widetilde{\chi}_1^0$, where $\mathcal{B}(\widetilde{\mathrm{t}} \to \mathrm{c}\widetilde{\chi}_1^0) = 1.0$. Only statistical uncertainties are shown.

References

[1] E. Witten, *Dynamical breaking of supersymmetry*, *Nucl. Phys.* **B 188** (1981) 513 [INSPIRE].

[2] M. Dine, W. Fischler and M. Srednicki, *Supersymmetric technicolor*, *Nucl. Phys.* **B 189** (1981) 575 [INSPIRE].

[3] S. Dimopoulos and S. Raby, *Supercolor*, *Nucl. Phys.* **B 192** (1981) 353 [INSPIRE].

[4] S. Dimopoulos and H. Georgi, *Softly broken supersymmetry and* SU(5), *Nucl. Phys.* **B 193** (1981) 150 [INSPIRE].

[5] R.K. Kaul and P. Majumdar, *Cancellation of quadratically divergent mass corrections in globally supersymmetric spontaneously broken gauge theories*, *Nucl. Phys.* **B 199** (1982) 36 [INSPIRE].

[6] CMS collaboration, *Observation of a new boson at a mass of 125 GeV with the CMS experiment at the LHC*, *Phys. Lett.* **B 716** (2012) 30 [arXiv:1207.7235] [INSPIRE].

[7] ATLAS collaboration, *Observation of a new particle in the search for the Standard Model Higgs boson with the ATLAS detector at the LHC*, *Phys. Lett.* **B 716** (2012) 1 [arXiv:1207.7214] [INSPIRE].

[8] CMS collaboration, *Precise determination of the mass of the Higgs boson and tests of compatibility of its couplings with the standard model predictions using proton collisions at 7 and 8 TeV*, *Eur. Phys. J.* **C 75** (2015) 212 [arXiv:1412.8662] [INSPIRE].

[9] J. Wess and B. Zumino, *Supergauge transformations in four-dimensions*, *Nucl. Phys.* **B 70** (1974) 39 [INSPIRE].

[10] H.P. Nilles, *Supersymmetry, supergravity and particle physics*, *Phys. Rept.* **110** (1984) 1 [INSPIRE].

[11] H.E. Haber and G.L. Kane, *The search for supersymmetry: probing physics beyond the standard model*, *Phys. Rept.* **117** (1985) 75 [INSPIRE].

[12] R. Barbieri, S. Ferrara and C.A. Savoy, *Gauge models with spontaneously broken local supersymmetry*, *Phys. Lett.* **B 119** (1982) 343 [INSPIRE].

[13] S. Dawson, E. Eichten and C. Quigg, *Search for supersymmetric particles in hadron-hadron collisions*, *Phys. Rev.* **D 31** (1985) 1581 [INSPIRE].

[14] S.P. Martin, *A supersymmetry primer*, *Adv. Ser. Direct. High Energy Phys.* **21** (2010) 1 [hep-ph/9709356] [INSPIRE].

[15] D.J.H. Chung et al., *The soft supersymmetry breaking Lagrangian: theory and applications*, *Phys. Rept.* **407** (2005) 1 [hep-ph/0312378] [INSPIRE].

[16] R. Barbieri and G.F. Giudice, *Upper bounds on supersymmetric particle masses*, *Nucl. Phys.* **B 306** (1988) 63 [INSPIRE].

[17] B. de Carlos and J.A. Casas, *One loop analysis of the electroweak breaking in supersymmetric models and the fine tuning problem*, *Phys. Lett.* **B 309** (1993) 320 [hep-ph/9303291] [INSPIRE].

[18] S. Dimopoulos and G.F. Giudice, *Naturalness constraints in supersymmetric theories with nonuniversal soft terms*, *Phys. Lett.* **B 357** (1995) 573 [hep-ph/9507282] [INSPIRE].

[19] R. Barbieri, G.R. Dvali and L.J. Hall, *Predictions from a U(2) flavor symmetry in supersymmetric theories*, *Phys. Lett.* **B 377** (1996) 76 [hep-ph/9512388] [INSPIRE].

[20] N. Sakai, *Naturalness in supersymmetric Guts*, *Z. Phys.* **C 11** (1981) 153 [INSPIRE].

[21] M. Papucci, J.T. Ruderman and A. Weiler, *Natural SUSY endures*, *JHEP* **09** (2012) 035 [arXiv:1110.6926] [INSPIRE].

[22] C. Brust, A. Katz, S. Lawrence and R. Sundrum, *SUSY, the third generation and the LHC*, *JHEP* **03** (2012) 103 [arXiv:1110.6670] [INSPIRE].

[23] A. Delgado, G.F. Giudice, G. Isidori, M. Pierini and A. Strumia, *The light stop window*, *Eur. Phys. J.* **C 73** (2013) 2370 [arXiv:1212.6847] [INSPIRE].

[24] G.R. Farrar and P. Fayet, *Phenomenology of the Production, Decay and Detection of New Hadronic States Associated with Supersymmetry*, *Phys. Lett.* **B 76** (1978) 575 [INSPIRE].

[25] CMS collaboration, *CMS luminosity based on pixel cluster counting-summer 2013 update*, CMS-PAS-LUM-13-001 (2013).

[26] CMS collaboration, *Interpretation of searches for supersymmetry with simplified models*, *Phys. Rev.* **D 88** (2013) 052017 [arXiv:1301.2175] [INSPIRE].

[27] ATLAS collaboration, *Search for a supersymmetric partner to the top quark in final states with jets and missing transverse momentum at $\sqrt{s} = 7$ TeV with the ATLAS detector*, *Phys. Rev. Lett.* **109** (2012) 211802 [arXiv:1208.1447] [INSPIRE].

[28] ATLAS collaboration, *Search for direct top squark pair production in final states with one isolated lepton, jets and missing transverse momentum in $\sqrt{s} = 7$ TeV pp collisions using $4.7 fb^{-1}$ of ATLAS data*, *Phys. Rev. Lett.* **109** (2012) 211803 [arXiv:1208.2590] [INSPIRE].

[29] ATLAS collaboration, *Search for a heavy top-quark partner in final states with two leptons with the ATLAS detector at the LHC*, *JHEP* **11** (2012) 094 [arXiv:1209.4186] [INSPIRE].

[30] ATLAS collaboration, *Search for direct top-squark pair production in final states with two leptons in pp collisions at $\sqrt{s} = 8$ TeV with the ATLAS detector*, *JHEP* **06** (2014) 124 [arXiv:1403.4853] [INSPIRE].

[31] ATLAS collaboration, *Search for direct third-generation squark pair production in final states with missing transverse momentum and two b-jets in $\sqrt{s} = 8$ TeV pp collisions with the ATLAS detector*, *JHEP* **10** (2013) 189 [arXiv:1308.2631] [INSPIRE].

[32] ATLAS collaboration, *Measurement of spin correlation in top-antitop quark events and search for top squark pair production in pp collisions at $\sqrt{s} = 8$ TeV Using the ATLAS detector*, *Phys. Rev. Lett.* **114** (2015) 142001 [arXiv:1412.4742] [INSPIRE].

[33] ATLAS collaboration, *Search for pair-produced third-generation squarks decaying via charm quarks or in compressed supersymmetric scenarios in pp collisions at $\sqrt{s} = 8$ TeV with the ATLAS detector*, *Phys. Rev.* **D 90** (2014) 052008 [arXiv:1407.0608] [INSPIRE].

[34] CMS collaboration, *Search for top-squark pair production in the single-lepton final state in pp collisions at $\sqrt{s} = 8$ TeV*, *Eur. Phys. J.* **C 73** (2013) 2677 [arXiv:1308.1586] [INSPIRE].

[35] CMS collaboration, *Search for supersymmetry in hadronic final states with missing transverse energy using the variables α_T and b-quark multiplicity in pp collisions at $\sqrt{s} = 8$ TeV*, *Eur. Phys. J.* **C 73** (2013) 2568 [arXiv:1303.2985] [INSPIRE].

[36] CMS collaboration, *Search for new physics in events with same-sign dileptons and b jets in pp collisions at $\sqrt{s} = 8$ TeV*, *JHEP* **03** (2013) 037 [arXiv:1212.6194] [INSPIRE].

[37] CMS collaboration, *Search for top squark and higgsino production using diphoton Higgs boson decays*, *Phys. Rev. Lett.* **112** (2014) 161802 [arXiv:1312.3310] [InSPIRE].

[38] CMS collaboration, *Search for top-squark pairs decaying into Higgs or Z bosons in pp collisions at $\sqrt{s} = 8\,TeV$*, *Phys. Lett.* **B 736** (2014) 371 [arXiv:1405.3886] [InSPIRE].

[39] CMS collaboration, *Searches for supersymmetry based on events with b jets and four W bosons in pp collisions at 8 TeV*, *Phys. Lett.* **B 745** (2015) 5 [arXiv:1412.4109] [InSPIRE].

[40] CMS collaboration, *Description and performance of track and primary-vertex reconstruction with the CMS tracker*, 2014 *JINST* **9** P10009 [arXiv:1405.6569] [InSPIRE].

[41] CMS collaboration, *Energy calibration and resolution of the cms electromagnetic calorimeter in pp collisions at $\sqrt{s} = 7\,TeV$*, 2013 *JINST* **8** P09009 [arXiv:1306.2016] [InSPIRE].

[42] CMS collaboration, *Performance of CMS muon reconstruction in pp collision events at $\sqrt{s} = 7\,TeV$*, 2012 *JINST* **7** P10002 [arXiv:1206.4071] [InSPIRE].

[43] CMS collaboration, *The CMS experiment at the CERN LHC*, 2008 *JINST* **3** S08004 [InSPIRE].

[44] CMS collaboration, *Particle-flow event reconstruction in CMS and performance for jets, taus and MET*, CMS-PAS-PFT-09-001 (2009).

[45] CMS collaboration, *Commissioning of the particle-flow event reconstruction with the first LHC collisions recorded in the CMS detector*, CMS-PAS-PFT-10-001 (2010).

[46] M. Cacciari, G.P. Salam and G. Soyez, *The anti-k_t jet clustering algorithm*, *JHEP* **04** (2008) 063 [arXiv:0802.1189] [InSPIRE].

[47] M. Cacciari, G.P. Salam and G. Soyez, *FastJet user manual*, *Eur. Phys. J.* **C 72** (2012) 1896 [arXiv:1111.6097] [InSPIRE].

[48] CMS collaboration, *Determination of jet energy calibration and transverse momentum resolution in CMS*, 2011 *JINST* **6** P11002 [arXiv:1107.4277] [InSPIRE].

[49] CMS collaboration, *Algorithms for b Jet identification in CMS*, CMS-PAS-BTV-09-001 (2009).

[50] CMS collaboration, *Performance of b tagging at $\sqrt{s} = 8\,TeV$ in multijet, ttbar and boosted topology events*, CMS-PAS-BTV-13-001 (2013).

[51] CMS collaboration, *Performance of electron reconstruction and selection with the CMS detector in proton-proton collisions at $\sqrt{s} = 8\,TeV$*, arXiv:1502.02701 [InSPIRE].

[52] CMS collaboration, *Performance of tau-lepton reconstruction and identification in CMS*, 2012 *JINST* **7** P01001 [arXiv:1109.6034] [InSPIRE].

[53] CMS collaboration, *Scalar top quark search with jets and missing momentum in pp collisions at $\sqrt{s} = 7\,TeV$*, CMS-PAS-SUS-11-030 (2011).

[54] J. Alwall et al., *The automated computation of tree-level and next-to-leading order differential cross sections and their matching to parton shower simulations*, *JHEP* **07** (2014) 079 [arXiv:1405.0301] [InSPIRE].

[55] J. Pumplin et al., *New generation of parton distributions with uncertainties from global QCD analysis*, *JHEP* **07** (2002) 012 [hep-ph/0201195] [InSPIRE].

[56] S. Frixione, P. Nason and C. Oleari, *Matching NLO QCD computations with parton shower simulations: the POWHEG method*, *JHEP* **11** (2007) 070 [arXiv:0709.2092] [InSPIRE].

[57] H.-L. Lai et al., *New parton distributions for collider physics*, *Phys. Rev.* **D 82** (2010) 074024 [arXiv:1007.2241] [InSPIRE].

[58] P.M. Nadolsky et al., *Implications of CTEQ global analysis for collider observables*, *Phys. Rev.* **D 78** (2008) 013004 [arXiv:0802.0007] [inSPIRE].

[59] T. Sjöstrand, S. Mrenna and P.Z. Skands, *PYTHIA 6.4 physics and manual*, *JHEP* **05** (2006) 026 [hep-ph/0603175] [inSPIRE].

[60] N. Davidson, G. Nanava, T. Przedzinski, E. Richter-Was and Z. Was, *Universal interface of TAUOLA technical and physics documentation*, *Comput. Phys. Commun.* **183** (2012) 821 [arXiv:1002.0543] [inSPIRE].

[61] CMS collaboration, *The fast simulation of the CMS detector at LHC*, *J. Phys. Conf. Ser.* **331** (2011) 032049 [inSPIRE].

[62] GEANT4 collaboration, S. Agostinelli et al., *GEANT4: A Simulation toolkit*, *Nucl. Instrum. Meth.* **A 506** (2003) 250 [inSPIRE].

[63] D.E. Kaplan, K. Rehermann, M.D. Schwartz and B. Tweedie, *Top tagging: a method for identifying boosted hadronically decaying top quarks*, *Phys. Rev. Lett.* **101** (2008) 142001 [arXiv:0806.0848] [inSPIRE].

[64] T. Plehn, M. Spannowsky, M. Takeuchi and D. Zerwas, *Stop reconstruction with tagged tops*, *JHEP* **10** (2010) 078 [arXiv:1006.2833] [inSPIRE].

[65] D.E. Kaplan, K. Rehermann and D. Stolarski, *Searching for direct stop production in hadronic top data at the LHC*, *JHEP* **07** (2012) 119 [arXiv:1205.5816] [inSPIRE].

[66] Particle Data Group collaboration, K.A. Olive et al., *Review of Particle Physics*, *Chin. Phys.* **C 38** (2014) 090001.

[67] C.G. Lester and D.J. Summers, *Measuring masses of semiinvisibly decaying particles pair produced at hadron colliders*, *Phys. Lett.* **B 463** (1999) 99 [hep-ph/9906349] [inSPIRE].

[68] A. Barr, C. Lester and P. Stephens, *A variable for measuring masses at hadron colliders when missing energy is expected; m_{T2}: the truth behind the glamour*, *J. Phys.* **G 29** (2003) 2343 [hep-ph/0304226] [inSPIRE].

[69] UA1 collaboration, G. Arnison et al., *Experimental observation of isolated large transverse energy electrons with associated missing energy at $\sqrt{s} = 540\,GeV$*, *Phys. Lett.* **B 122** (1983) 103 [inSPIRE].

[70] CMS collaboration, *Search for new physics with jets and missing transverse momentum in pp collisions at $\sqrt{s} = 7\,TeV$*, *JHEP* **08** (2011) 155 [arXiv:1106.4503] [inSPIRE].

[71] CMS collaboration, *Search for new physics in the multijet and missing transverse momentum final state in proton-proton collisions at $\sqrt{s} = 7\,TeV$*, *Phys. Rev. Lett.* **109** (2012) 171803 [arXiv:1207.1898] [inSPIRE].

[72] B. Efron, *CBMS-NSF Regional Conference Series in Applied Mathematics. Vol. 38: The Jackknife, The Bootstrap and Other Resampling Plans*, SIAM, Philadelphia U.S.A. (1982).

[73] CMS collaboration, *Measurement of the inclusive W and Z production cross sections in pp collisions at $\sqrt{s} = 7\,TeV$*, *JHEP* **10** (2011) 132 [arXiv:1107.4789] [inSPIRE].

[74] S. Alekhin et al., *The PDF4LHC Working Group Interim Report*, arXiv:1101.0536 [inSPIRE].

[75] M. Botje et al., *The PDF4LHC Working Group Interim Recommendations*, arXiv:1101.0538 [inSPIRE].

[76] D.R. Tovey, *On measuring the masses of pair-produced semi-invisibly decaying particles at hadron colliders*, *JHEP* **04** (2008) 034 [arXiv:0802.2879] [inSPIRE].

[77] G. Polesello and D.R. Tovey, *Supersymmetric particle mass measurement with the boost-corrected contransverse mass*, *JHEP* **03** (2010) 030 [arXiv:0910.0174] [INSPIRE].

[78] S.A. Malik and G. Watt, *Ratios of W and Z cross sections at large boson p_T as a constraint on PDFs and background to new physics*, *JHEP* **02** (2014) 025 [arXiv:1304.2424] [INSPIRE].

[79] CMS collaboration, *Search for dark matter, extra dimensions and unparticles in monojet events in protonproton collisions at $\sqrt{s} = 8$ TeV*, *Eur. Phys. J.* **C 75** (2015) 235 [arXiv:1408.3583] [INSPIRE].

[80] CMS collaboration, *Search for New Physics with a Mono-Jet and Missing Transverse Energy in pp Collisions at $\sqrt{s} = 7$ TeV*, *Phys. Rev. Lett.* **107** (2011) 201804 [arXiv:1106.4775] [INSPIRE].

[81] CMS collaboration, *Search for dark matter and large extra dimensions in monojet events in pp collisions at $\sqrt{s} = 7$ TeV*, *JHEP* **09** (2012) 094 [arXiv:1206.5663] [INSPIRE].

[82] A.D. Martin, W.J. Stirling, R.S. Thorne and G. Watt, *Parton distributions for the LHC*, *Eur. Phys. J.* **C 63** (2009) 189 [arXiv:0901.0002] [INSPIRE].

[83] R.D. Ball et al., *Impact of heavy quark masses on parton distributions and LHC phenomenology*, *Nucl. Phys.* **B 849** (2011) 296 [arXiv:1101.1300] [INSPIRE].

[84] N. Kidonakis, *Differential and total cross sections for top pair and single top production*, in *20th International Workshop on Deep-Inelastic Scattering and Related Subjects*, DESY-PROC-2012-02 (2012) [arXiv:1205.3453].

[85] J.M. Campbell, R.K. Ellis and C. Williams, *Vector boson pair production at the LHC*, *JHEP* **07** (2011) 018 [arXiv:1105.0020] [INSPIRE].

[86] A.L. Read, *Presentation of search results: The CL_s technique*, *J. Phys.* **G 28** (2002) 2693 [INSPIRE].

[87] T. Junk, *Confidence level computation for combining searches with small statistics*, *Nucl. Instrum. Meth.* **A 434** (1999) 435 [hep-ex/9902006] [INSPIRE].

[88] M. Krämer et al., *Supersymmetry production cross sections in pp collisions at $\sqrt{s} = 7$ TeV*, arXiv:1206.2892 [INSPIRE].

[89] W. Beenakker, R. Höpker, M. Spira and P.M. Zerwas, *Squark and gluino production at hadron colliders*, *Nucl. Phys.* **B 492** (1997) 51 [hep-ph/9610490] [INSPIRE].

[90] A. Kulesza and L. Motyka, *Threshold resummation for squark-antisquark and gluino-pair production at the LHC*, *Phys. Rev. Lett.* **102** (2009) 111802 [arXiv:0807.2405] [INSPIRE].

[91] A. Kulesza and L. Motyka, *Soft gluon resummation for the production of gluino-gluino and squark-antisquark pairs at the LHC*, *Phys. Rev.* **D 80** (2009) 095004 [arXiv:0905.4749] [INSPIRE].

[92] W. Beenakker et al., *Soft-gluon resummation for squark and gluino hadroproduction*, *JHEP* **12** (2009) 041 [arXiv:0909.4418] [INSPIRE].

[93] W. Beenakker et al., *Squark and gluino hadroproduction*, *Int. J. Mod. Phys.* **A 26** (2011) 2637 [arXiv:1105.1110] [INSPIRE].

The CMS collaboration

Yerevan Physics Institute, Yerevan, Armenia

V. Khachatryan, A.M. Sirunyan, A. Tumasyan

Institut für Hochenergiephysik der OeAW, Wien, Austria

W. Adam, E. Asilar, T. Bergauer, J. Brandstetter, E. Brondolin, M. Dragicevic, J. Erö, M. Flechl, M. Friedl, R. Frühwirth[1], V.M. Ghete, C. Hartl, N. Hörmann, J. Hrubec, M. Jeitler[1], V. Knünz, A. König, M. Krammer[1], I. Krätschmer, D. Liko, I. Mikulec, D. Rabady[2], B. Rahbaran, H. Rohringer, J. Schieck[1], R. Schöfbeck, J. Strauss, W. Treberer-Treberspurg, W. Waltenberger, C.-E. Wulz[1]

National Centre for Particle and High Energy Physics, Minsk, Belarus

V. Mossolov, N. Shumeiko, J. Suarez Gonzalez

Universiteit Antwerpen, Antwerpen, Belgium

S. Alderweireldt, T. Cornelis, E.A. De Wolf, X. Janssen, A. Knutsson, J. Lauwers, S. Luyckx, S. Ochesanu, R. Rougny, M. Van De Klundert, H. Van Haevermaet, P. Van Mechelen, N. Van Remortel, A. Van Spilbeeck

Vrije Universiteit Brussel, Brussel, Belgium

S. Abu Zeid, F. Blekman, J. D'Hondt, N. Daci, I. De Bruyn, K. Deroover, N. Heracleous, J. Keaveney, S. Lowette, L. Moreels, A. Olbrechts, Q. Python, D. Strom, S. Tavernier, W. Van Doninck, P. Van Mulders, G.P. Van Onsem, I. Van Parijs

Université Libre de Bruxelles, Bruxelles, Belgium

P. Barria, C. Caillol, B. Clerbaux, G. De Lentdecker, H. Delannoy, D. Dobur, G. Fasanella, L. Favart, A.P.R. Gay, A. Grebenyuk, A. Léonard, A. Mohammadi, L. Perniè, A. Randle-conde, T. Reis, T. Seva, L. Thomas, C. Vander Velde, P. Vanlaer, J. Wang, F. Zenoni

Ghent University, Ghent, Belgium

K. Beernaert, L. Benucci, A. Cimmino, S. Crucy, A. Fagot, G. Garcia, M. Gul, J. Mccartin, A.A. Ocampo Rios, D. Poyraz, D. Ryckbosch, S. Salva Diblen, M. Sigamani, N. Strobbe, F. Thyssen, M. Tytgat, W. Van Driessche, E. Yazgan, N. Zaganidis

Université Catholique de Louvain, Louvain-la-Neuve, Belgium

S. Basegmez, C. Beluffi[3], G. Bruno, R. Castello, A. Caudron, L. Ceard, G.G. Da Silveira, C. Delaere, T. du Pree, D. Favart, L. Forthomme, A. Giammanco[4], J. Hollar, A. Jafari, P. Jez, M. Komm, V. Lemaitre, A. Mertens, C. Nuttens, L. Perrini, A. Pin, K. Piotrzkowski, A. Popov[5], L. Quertenmont, M. Selvaggi, M. Vidal Marono

Université de Mons, Mons, Belgium

N. Beliy, T. Caebergs, G.H. Hammad

Centro Brasileiro de Pesquisas Fisicas, Rio de Janeiro, Brazil

W.L. Aldá Júnior, G.A. Alves, L. Brito, M. Correa Martins Junior, T. Dos Reis Martins, C. Hensel, C. Mora Herrera, A. Moraes, M.E. Pol, P. Rebello Teles

Universidade do Estado do Rio de Janeiro, Rio de Janeiro, Brazil

E. Belchior Batista Das Chagas, W. Carvalho, J. Chinellato[6], A. Custódio, E.M. Da Costa, D. De Jesus Damiao, C. De Oliveira Martins, S. Fonseca De Souza, L.M. Huertas Guativa, H. Malbouisson, D. Matos Figueiredo, L. Mundim, H. Nogima, W.L. Prado Da Silva, J. Santaolalla, A. Santoro, A. Sznajder, E.J. Tonelli Manganote[6], A. Vilela Pereira

Universidade Estadual Paulista [a]**, Universidade Federal do ABC** [b]**, São Paulo, Brazil**

S. Ahuja, C.A. Bernardes[b], S. Dogra[a], T.R. Fernandez Perez Tomei[a], E.M. Gregores[b], P.G. Mercadante[b], S.F. Novaes[a], Sandra S. Padula[a], D. Romero Abad, J.C. Ruiz Vargas

Institute for Nuclear Research and Nuclear Energy, Sofia, Bulgaria

A. Aleksandrov, V. Genchev[2], R. Hadjiiska, P. Iaydjiev, A. Marinov, S. Piperov, M. Rodozov, S. Stoykova, G. Sultanov, M. Vutova

University of Sofia, Sofia, Bulgaria

A. Dimitrov, I. Glushkov, L. Litov, B. Pavlov, P. Petkov

Institute of High Energy Physics, Beijing, China

M. Ahmad, J.G. Bian, G.M. Chen, H.S. Chen, M. Chen, T. Cheng, R. Du, C.H. Jiang, R. Plestina[7], F. Romeo, S.M. Shaheen, J. Tao, C. Wang, Z. Wang

State Key Laboratory of Nuclear Physics and Technology, Peking University, Beijing, China

C. Asawatangtrakuldee, Y. Ban, G. Chen, Q. Li, S. Liu, Y. Mao, S.J. Qian, D. Wang, M. Wang, Q. Wang, Z. Xu, D. Yang, F. Zhang[8], L. Zhang, Z. Zhang, W. Zou

Universidad de Los Andes, Bogota, Colombia

C. Avila, A. Cabrera, L.F. Chaparro Sierra, C. Florez, J.P. Gomez, B. Gomez Moreno, J.C. Sanabria

University of Split, Faculty of Electrical Engineering, Mechanical Engineering and Naval Architecture, Split, Croatia

N. Godinovic, D. Lelas, D. Polic, I. Puljak

University of Split, Faculty of Science, Split, Croatia

Z. Antunovic, M. Kovac

Institute Rudjer Boskovic, Zagreb, Croatia

V. Brigljevic, K. Kadija, J. Luetic, L. Sudic

University of Cyprus, Nicosia, Cyprus

A. Attikis, G. Mavromanolakis, J. Mousa, C. Nicolaou, F. Ptochos, P.A. Razis, H. Rykaczewski

Charles University, Prague, Czech Republic

M. Bodlak, M. Finger, M. Finger Jr.[9]

Academy of Scientific Research and Technology of the Arab Republic of Egypt, Egyptian Network of High Energy Physics, Cairo, Egypt

A. Ali[10], R. Aly, S. Aly, Y. Assran[11], A. Ellithi Kamel[12], A. Lotfy, R. Masod[10]

National Institute of Chemical Physics and Biophysics, Tallinn, Estonia

B. Calpas, M. Kadastik, M. Murumaa, M. Raidal, A. Tiko, C. Veelken

Department of Physics, University of Helsinki, Helsinki, Finland

P. Eerola, M. Voutilainen

Helsinki Institute of Physics, Helsinki, Finland

J. Härkönen, V. Karimäki, R. Kinnunen, T. Lampén, K. Lassila-Perini, S. Lehti, T. Lindén, P. Luukka, T. Mäenpää, T. Peltola, E. Tuominen, J. Tuominiemi, E. Tuovinen, L. Wendland

Lappeenranta University of Technology, Lappeenranta, Finland

J. Talvitie, T. Tuuva

DSM/IRFU, CEA/Saclay, Gif-sur-Yvette, France

M. Besancon, F. Couderc, M. Dejardin, D. Denegri, B. Fabbro, J.L. Faure, C. Favaro, F. Ferri, S. Ganjour, A. Givernaud, P. Gras, G. Hamel de Monchenault, P. Jarry, E. Locci, J. Malcles, J. Rander, A. Rosowsky, M. Titov, A. Zghiche

Laboratoire Leprince-Ringuet, Ecole Polytechnique, IN2P3-CNRS, Palaiseau, France

S. Baffioni, F. Beaudette, P. Busson, L. Cadamuro, E. Chapon, C. Charlot, T. Dahms, O. Davignon, N. Filipovic, A. Florent, R. Granier de Cassagnac, L. Mastrolorenzo, P. Miné, I.N. Naranjo, M. Nguyen, C. Ochando, G. Ortona, P. Paganini, S. Regnard, R. Salerno, J.B. Sauvan, Y. Sirois, T. Strebler, Y. Yilmaz, A. Zabi

Institut Pluridisciplinaire Hubert Curien, Université de Strasbourg, Université de Haute Alsace Mulhouse, CNRS/IN2P3, Strasbourg, France

J.-L. Agram[13], J. Andrea, A. Aubin, D. Bloch, J.-M. Brom, M. Buttignol, E.C. Chabert, N. Chanon, C. Collard, E. Conte[13], J.-C. Fontaine[13], D. Gelé, U. Goerlach, C. Goetzmann, A.-C. Le Bihan, J.A. Merlin[2], K. Skovpen, P. Van Hove

Centre de Calcul de l'Institut National de Physique Nucleaire et de Physique des Particules, CNRS/IN2P3, Villeurbanne, France

S. Gadrat

Université de Lyon, Université Claude Bernard Lyon 1, CNRS-IN2P3, Institut de Physique Nucléaire de Lyon, Villeurbanne, France

S. Beauceron, N. Beaupere, C. Bernet[7], G. Boudoul[2], E. Bouvier, S. Brochet, C.A. Carrillo Montoya, J. Chasserat, R. Chierici, D. Contardo, B. Courbon, P. Depasse, H. El Mamouni, J. Fan, J. Fay, S. Gascon, M. Gouzevitch, B. Ille, I.B. Laktineh, M. Lethuillier, L. Mirabito, A.L. Pequegnot, S. Perries, J.D. Ruiz Alvarez, D. Sabes, L. Sgandurra, V. Sordini, M. Vander Donckt, P. Verdier, S. Viret, H. Xiao

Institute of High Energy Physics and Informatization, Tbilisi State University, Tbilisi, Georgia

Z. Tsamalaidze[9]

RWTH Aachen University, I. Physikalisches Institut, Aachen, Germany

C. Autermann, S. Beranek, M. Bontenackels, M. Edelhoff, L. Feld, A. Heister, M.K. Kiesel, K. Klein, M. Lipinski, A. Ostapchuk, M. Preuten, F. Raupach, J. Sammet, S. Schael, J.F. Schulte, T. Verlage, H. Weber, B. Wittmer, V. Zhukov[5]

RWTH Aachen University, III. Physikalisches Institut A, Aachen, Germany

M. Ata, M. Brodski, E. Dietz-Laursonn, D. Duchardt, M. Endres, M. Erdmann, S. Erdweg, T. Esch, R. Fischer, A. Güth, T. Hebbeker, C. Heidemann, K. Hoepfner, D. Klingebiel, S. Knutzen, P. Kreuzer, M. Merschmeyer, A. Meyer, P. Millet, M. Olschewski, K. Padeken, P. Papacz, T. Pook, M. Radziej, H. Reithler, M. Rieger, S.A. Schmitz, L. Sonnenschein, D. Teyssier, S. Thüer

RWTH Aachen University, III. Physikalisches Institut B, Aachen, Germany

V. Cherepanov, Y. Erdogan, G. Flügge, H. Geenen, M. Geisler, W. Haj Ahmad, F. Hoehle, B. Kargoll, T. Kress, Y. Kuessel, A. Künsken, J. Lingemann[2], A. Nowack, I.M. Nugent, C. Pistone, O. Pooth, A. Stahl

Deutsches Elektronen-Synchrotron, Hamburg, Germany

M. Aldaya Martin, I. Asin, N. Bartosik, O. Behnke, U. Behrens, A.J. Bell, K. Borras, A. Burgmeier, A. Cakir, L. Calligaris, A. Campbell, S. Choudhury, F. Costanza, C. Diez Pardos, G. Dolinska, S. Dooling, T. Dorland, G. Eckerlin, D. Eckstein, T. Eichhorn, G. Flucke, J. Garay Garcia, A. Geiser, A. Gizhko, P. Gunnellini, J. Hauk, M. Hempel[14], H. Jung, A. Kalogeropoulos, O. Karacheban[14], M. Kasemann, P. Katsas, J. Kieseler, C. Kleinwort, I. Korol, W. Lange, J. Leonard, K. Lipka, A. Lobanov, R. Mankel, I. Marfin[14], I.-A. Melzer-Pellmann, A.B. Meyer, G. Mittag, J. Mnich, A. Mussgiller, S. Naumann-Emme, A. Nayak, E. Ntomari, H. Perrey, D. Pitzl, R. Placakyte, A. Raspereza, P.M. Ribeiro Cipriano, B. Roland, M.Ö. Sahin, J. Salfeld-Nebgen, P. Saxena, T. Schoerner-Sadenius, M. Schröder, C. Seitz, S. Spannagel, C. Wissing

University of Hamburg, Hamburg, Germany

V. Blobel, M. Centis Vignali, A.R. Draeger, J. Erfle, E. Garutti, K. Goebel, D. Gonzalez, M. Görner, J. Haller, M. Hoffmann, R.S. Höing, A. Junkes, H. Kirschenmann, R. Klanner, R. Kogler, T. Lapsien, T. Lenz, I. Marchesini, D. Marconi, D. Nowatschin, J. Ott, T. Peiffer, A. Perieanu, N. Pietsch, J. Poehlsen, D. Rathjens, C. Sander, H. Schettler, P. Schleper, E. Schlieckau, A. Schmidt, M. Seidel, V. Sola, H. Stadie, G. Steinbrück, H. Tholen, D. Troendle, E. Usai, L. Vanelderen, A. Vanhoefer

Institut für Experimentelle Kernphysik, Karlsruhe, Germany

M. Akbiyik, C. Barth, C. Baus, J. Berger, C. Böser, E. Butz, T. Chwalek, F. Colombo, W. De Boer, A. Descroix, A. Dierlamm, M. Feindt, F. Frensch, M. Giffels, A. Gilbert, F. Hartmann[2], U. Husemann, I. Katkov[5], A. Kornmayer[2], P. Lobelle Pardo, M.U. Mozer, T. Müller, Th. Müller, M. Plagge, G. Quast, K. Rabbertz, S. Röcker, F. Roscher, H.J. Si-

monis, F.M. Stober, R. Ulrich, J. Wagner-Kuhr, S. Wayand, T. Weiler, C. Wöhrmann, R. Wolf

Institute of Nuclear and Particle Physics (INPP), NCSR Demokritos, Aghia Paraskevi, Greece

G. Anagnostou, G. Daskalakis, T. Geralis, V.A. Giakoumopoulou, A. Kyriakis, D. Loukas, A. Markou, A. Psallidas, I. Topsis-Giotis

University of Athens, Athens, Greece

A. Agapitos, S. Kesisoglou, A. Panagiotou, N. Saoulidou, E. Tziaferi

University of Ioánnina, Ioánnina, Greece

I. Evangelou, G. Flouris, C. Foudas, P. Kokkas, N. Loukas, N. Manthos, I. Papadopoulos, E. Paradas, J. Strologas

Wigner Research Centre for Physics, Budapest, Hungary

G. Bencze, C. Hajdu, A. Hazi, P. Hidas, D. Horvath[15], F. Sikler, V. Veszpremi, G. Vesztergombi[16], A.J. Zsigmond

Institute of Nuclear Research ATOMKI, Debrecen, Hungary

N. Beni, S. Czellar, J. Karancsi[17], J. Molnar, J. Palinkas, Z. Szillasi

University of Debrecen, Debrecen, Hungary

M. Bartók[18], A. Makovec, P. Raics, Z.L. Trocsanyi

National Institute of Science Education and Research, Bhubaneswar, India

P. Mal, K. Mandal, N. Sahoo, S.K. Swain

Panjab University, Chandigarh, India

S. Bansal, S.B. Beri, V. Bhatnagar, R. Chawla, R. Gupta, U.Bhawandeep, A.K. Kalsi, A. Kaur, M. Kaur, R. Kumar, A. Mehta, M. Mittal, N. Nishu, J.B. Singh

University of Delhi, Delhi, India

Ashok Kumar, Arun Kumar, A. Bhardwaj, B.C. Choudhary, A. Kumar, S. Malhotra, M. Naimuddin, K. Ranjan, R. Sharma, V. Sharma

Saha Institute of Nuclear Physics, Kolkata, India

S. Banerjee, S. Bhattacharya, K. Chatterjee, S. Dey, S. Dutta, B. Gomber, Sa. Jain, Sh. Jain, R. Khurana, N. Majumdar, A. Modak, K. Mondal, S. Mukherjee, S. Mukhopadhyay, A. Roy, D. Roy, S. Roy Chowdhury, S. Sarkar, M. Sharan

Bhabha Atomic Research Centre, Mumbai, India

A. Abdulsalam, D. Dutta, V. Jha, V. Kumar, A.K. Mohanty[2], L.M. Pant, P. Shukla, A. Topkar

Tata Institute of Fundamental Research, Mumbai, India

T. Aziz, S. Banerjee, S. Bhowmik[19], R.M. Chatterjee, R.K. Dewanjee, S. Dugad, S. Ganguly, S. Ghosh, M. Guchait, A. Gurtu[20], G. Kole, S. Kumar, M. Maity[19], G. Majumder, K. Mazumdar, G.B. Mohanty, B. Parida, K. Sudhakar, N. Sur, B. Sutar, N. Wickramage[21]

Indian Institute of Science Education and Research (IISER), Pune, India

S. Sharma

Institute for Research in Fundamental Sciences (IPM), Tehran, Iran

H. Bakhshiansohi, H. Behnamian, S.M. Etesami[22], A. Fahim[23], R. Goldouzian, M. Khakzad, M. Mohammadi Najafabadi, M. Naseri, S. Paktinat Mehdiabadi, F. Rezaei Hosseinabadi, B. Safarzadeh[24], M. Zeinali

University College Dublin, Dublin, Ireland

M. Felcini, M. Grunewald

INFN Sezione di Bari [a]**, Università di Bari** [b]**, Politecnico di Bari** [c]**, Bari, Italy**

M. Abbrescia[a,b], C. Calabria[a,b], C. Caputo[a,b], S.S. Chhibra[a,b], A. Colaleo[a], D. Creanza[a,c], L. Cristella[a,b], N. De Filippis[a,c], M. De Palma[a,b], L. Fiore[a], G. Iaselli[a,c], G. Maggi[a,c], M. Maggi[a], G. Miniello[a,b], S. My[a,c], S. Nuzzo[a,b], A. Pompili[a,b], G. Pugliese[a,c], R. Radogna[a,b,2], A. Ranieri[a], G. Selvaggi[a,b], A. Sharma[a], L. Silvestris[a,2], R. Venditti[a,b], P. Verwilligen[a]

INFN Sezione di Bologna [a]**, Università di Bologna** [b]**, Bologna, Italy**

G. Abbiendi[a], C. Battilana, A.C. Benvenuti[a], D. Bonacorsi[a,b], S. Braibant-Giacomelli[a,b], L. Brigliadori[a,b], R. Campanini[a,b], P. Capiluppi[a,b], A. Castro[a,b], F.R. Cavallo[a], G. Codispoti[a,b], M. Cuffiani[a,b], G.M. Dallavalle[a], F. Fabbri[a], A. Fanfani[a,b], D. Fasanella[a,b], P. Giacomelli[a], C. Grandi[a], L. Guiducci[a,b], S. Marcellini[a], G. Masetti[a], A. Montanari[a], F.L. Navarria[a,b], A. Perrotta[a], A.M. Rossi[a,b], T. Rovelli[a,b], G.P. Siroli[a,b], N. Tosi[a,b], R. Travaglini[a,b]

INFN Sezione di Catania [a]**, Università di Catania** [b]**, CSFNSM** [c]**, Catania, Italy**

G. Cappello[a], M. Chiorboli[a,b], S. Costa[a,b], F. Giordano[a,c,2], R. Potenza[a,b], A. Tricomi[a,b], C. Tuve[a,b]

INFN Sezione di Firenze [a]**, Università di Firenze** [b]**, Firenze, Italy**

G. Barbagli[a], V. Ciulli[a,b], C. Civinini[a], R. D'Alessandro[a,b], E. Focardi[a,b], E. Gallo[a], S. Gonzi[a,b], V. Gori[a,b], P. Lenzi[a,b], M. Meschini[a], S. Paoletti[a], G. Sguazzoni[a], A. Tropiano[a,b], L. Viliani[a,b]

INFN Laboratori Nazionali di Frascati, Frascati, Italy

L. Benussi, S. Bianco, F. Fabbri, D. Piccolo

INFN Sezione di Genova [a]**, Università di Genova** [b]**, Genova, Italy**

V. Calvelli[a,b], F. Ferro[a], M. Lo Vetere[a,b], E. Robutti[a], S. Tosi[a,b]

INFN Sezione di Milano-Bicocca [a]**, Università di Milano-Bicocca** [b]**, Milano, Italy**

M.E. Dinardo[a,b], S. Fiorendi[a,b], S. Gennai[a,2], R. Gerosa[a,b], A. Ghezzi[a,b], P. Govoni[a,b], M.T. Lucchini[a,b,2], S. Malvezzi[a], R.A. Manzoni[a,b], B. Marzocchi[a,b,2], D. Menasce[a], L. Moroni[a], M. Paganoni[a,b], D. Pedrini[a], S. Ragazzi[a,b], N. Redaelli[a], T. Tabarelli de Fatis[a,b]

INFN Sezione di Napoli [a]**, Università di Napoli 'Federico II'** [b]**, Napoli, Italy, Università della Basilicata** [c]**, Potenza, Italy, Università G. Marconi** [d]**, Roma, Italy**

S. Buontempo[a], N. Cavallo[a,c], S. Di Guida[a,d,2], M. Esposito[a,b], F. Fabozzi[a,c], A.O.M. Iorio[a,b], G. Lanza[a], L. Lista[a], S. Meola[a,d,2], M. Merola[a], P. Paolucci[a,2], C. Sciacca[a,b]

INFN Sezione di Padova [a]**, Università di Padova** [b]**, Padova, Italy, Università di Trento** [c]**, Trento, Italy**

P. Azzi[a,2], N. Bacchetta[a], D. Bisello[a,b], R. Carlin[a,b], A. Carvalho Antunes De Oliveira[a,b], P. Checchia[a], M. Dall'Osso[a,b], T. Dorigo[a], U. Dosselli[a], F. Gasparini[a,b], U. Gasparini[a,b], A. Gozzelino[a], S. Lacaprara[a], M. Margoni[a,b], A.T. Meneguzzo[a,b], J. Pazzini[a,b], M. Pegoraro[a], N. Pozzobon[a,b], P. Ronchese[a,b], F. Simonetto[a,b], E. Torassa[a], M. Tosi[a,b], S. Vanini[a,b], M. Zanetti[a,b], P. Zotto[a,b], A. Zucchetta[a,b], G. Zumerle[a,b]

INFN Sezione di Pavia [a]**, Università di Pavia** [b]**, Pavia, Italy**

M. Gabusi[a,b], A. Magnani[a], S.P. Ratti[a,b], V. Re[a], C. Riccardi[a,b], P. Salvini[a], I. Vai[a], P. Vitulo[a,b]

INFN Sezione di Perugia [a]**, Università di Perugia** [b]**, Perugia, Italy**

L. Alunni Solestizi[a,b], M. Biasini[a,b], G.M. Bilei[a], D. Ciangottini[a,b,2], L. Fanò[a,b], P. Lariccia[a,b], G. Mantovani[a,b], M. Menichelli[a], A. Saha[a], A. Santocchia[a,b], A. Spiezia[a,b,2]

INFN Sezione di Pisa [a]**, Università di Pisa** [b]**, Scuola Normale Superiore di Pisa** [c]**, Pisa, Italy**

K. Androsov[a,25], P. Azzurri[a], G. Bagliesi[a], J. Bernardini[a], T. Boccali[a], G. Broccolo[a,c], R. Castaldi[a], M.A. Ciocci[a,25], R. Dell'Orso[a], S. Donato[a,c,2], G. Fedi, F. Fiori[a,c], L. Foà[a,c†], A. Giassi[a], M.T. Grippo[a,25], F. Ligabue[a,c], T. Lomtadze[a], L. Martini[a,b], A. Messineo[a,b], C.S. Moon[a,26], F. Palla[a], A. Rizzi[a,b], A. Savoy-Navarro[a,27], A.T. Serban[a], P. Spagnolo[a], P. Squillacioti[a,25], R. Tenchini[a], G. Tonelli[a,b], A. Venturi[a], P.G. Verdini[a]

INFN Sezione di Roma [a]**, Università di Roma** [b]**, Roma, Italy**

L. Barone[a,b], F. Cavallari[a], G. D'imperio[a,b], D. Del Re[a,b], M. Diemoz[a], S. Gelli[a,b], C. Jorda[a], E. Longo[a,b], F. Margaroli[a,b], P. Meridiani[a], F. Micheli[a,b], G. Organtini[a,b], R. Paramatti[a], F. Preiato[a,b], S. Rahatlou[a,b], C. Rovelli[a], F. Santanastasio[a,b], L. Soffi[a,b], P. Traczyk[a,b,2]

INFN Sezione di Torino [a]**, Università di Torino** [b]**, Torino, Italy, Università del Piemonte Orientale** [c]**, Novara, Italy**

N. Amapane[a,b], R. Arcidiacono[a,c], S. Argiro[a,b], M. Arneodo[a,c], R. Bellan[a,b], C. Biino[a], N. Cartiglia[a], S. Casasso[a,b], M. Costa[a,b], R. Covarelli[a,b], A. Degano[a,b], N. Demaria[a], L. Finco[a,b,2], B. Kiani[a,b], C. Mariotti[a], S. Maselli[a], G. Mazza[a], E. Migliore[a,b], V. Monaco[a,b], M. Musich[a], M.M. Obertino[a,c], L. Pacher[a,b], N. Pastrone[a], M. Pelliccioni[a], G.L. Pinna Angioni[a,b], A. Romero[a,b], M. Ruspa[a,c], R. Sacchi[a,b], A. Solano[a,b], A. Staiano[a]

INFN Sezione di Trieste ^{a}, Università di Trieste ^{b}, Trieste, Italy

S. Belforte^a, V. Candelise^{a,b,2}, M. Casarsa^a, F. Cossutti^a, G. Della Ricca^{a,b}, B. Gobbo^a, C. La Licata^{a,b}, M. Marone^{a,b}, A. Schizzi^{a,b}, T. Umer^{a,b}, A. Zanetti^a

Kangwon National University, Chunchon, Korea

S. Chang, A. Kropivnitskaya, S.K. Nam

Kyungpook National University, Daegu, Korea

D.H. Kim, G.N. Kim, M.S. Kim, D.J. Kong, S. Lee, Y.D. Oh, H. Park, A. Sakharov, D.C. Son

Chonbuk National University, Jeonju, Korea

H. Kim, T.J. Kim, M.S. Ryu

Chonnam National University, Institute for Universe and Elementary Particles, Kwangju, Korea

S. Song

Korea University, Seoul, Korea

S. Choi, Y. Go, D. Gyun, B. Hong, M. Jo, H. Kim, Y. Kim, B. Lee, K. Lee, K.S. Lee, S. Lee, S.K. Park, Y. Roh

Seoul National University, Seoul, Korea

H.D. Yoo

University of Seoul, Seoul, Korea

M. Choi, J.H. Kim, J.S.H. Lee, I.C. Park, G. Ryu

Sungkyunkwan University, Suwon, Korea

Y. Choi, Y.K. Choi, J. Goh, D. Kim, E. Kwon, J. Lee, I. Yu

Vilnius University, Vilnius, Lithuania

A. Juodagalvis, J. Vaitkus

National Centre for Particle Physics, Universiti Malaya, Kuala Lumpur, Malaysia

Z.A. Ibrahim, J.R. Komaragiri, M.A.B. Md Ali[28], F. Mohamad Idris, W.A.T. Wan Abdullah

Centro de Investigacion y de Estudios Avanzados del IPN, Mexico City, Mexico

E. Casimiro Linares, H. Castilla-Valdez, E. De La Cruz-Burelo, I. Heredia-de La Cruz, A. Hernandez-Almada, R. Lopez-Fernandez, G. Ramirez Sanchez, A. Sanchez-Hernandez

Universidad Iberoamericana, Mexico City, Mexico

S. Carrillo Moreno, F. Vazquez Valencia

Benemerita Universidad Autonoma de Puebla, Puebla, Mexico

S. Carpinteyro, I. Pedraza, H.A. Salazar Ibarguen

Universidad Autónoma de San Luis Potosí, San Luis Potosí, Mexico

A. Morelos Pineda

University of Auckland, Auckland, New Zealand

D. Krofcheck

University of Canterbury, Christchurch, New Zealand

P.H. Butler, S. Reucroft

National Centre for Physics, Quaid-I-Azam University, Islamabad, Pakistan

A. Ahmad, M. Ahmad, Q. Hassan, H.R. Hoorani, W.A. Khan, T. Khurshid, M. Shoaib

National Centre for Nuclear Research, Swierk, Poland

H. Bialkowska, M. Bluj, B. Boimska, T. Frueboes, M. Górski, M. Kazana, K. Nawrocki, K. Romanowska-Rybinska, M. Szleper, P. Zalewski

Institute of Experimental Physics, Faculty of Physics, University of Warsaw, Warsaw, Poland

G. Brona, K. Bunkowski, K. Doroba, A. Kalinowski, M. Konecki, J. Krolikowski, M. Misiura, M. Olszewski, M. Walczak

Laboratório de Instrumentação e Física Experimental de Partículas, Lisboa, Portugal

P. Bargassa, C. Beirão Da Cruz E Silva, A. Di Francesco, P. Faccioli, P.G. Ferreira Parracho, M. Gallinaro, L. Lloret Iglesias, F. Nguyen, J. Rodrigues Antunes, J. Seixas, O. Toldaiev, D. Vadruccio, J. Varela, P. Vischia

Joint Institute for Nuclear Research, Dubna, Russia

S. Afanasiev, P. Bunin, M. Gavrilenko, I. Golutvin, I. Gorbunov, A. Kamenev, V. Karjavin, V. Konoplyanikov, A. Lanev, A. Malakhov, V. Matveev[29], P. Moisenz, V. Palichik, V. Perelygin, S. Shmatov, S. Shulha, N. Skatchkov, V. Smirnov, T. Toriashvili[30], A. Zarubin

Petersburg Nuclear Physics Institute, Gatchina (St. Petersburg), Russia

V. Golovtsov, Y. Ivanov, V. Kim[31], E. Kuznetsova, P. Levchenko, V. Murzin, V. Oreshkin, I. Smirnov, V. Sulimov, L. Uvarov, S. Vavilov, A. Vorobyev

Institute for Nuclear Research, Moscow, Russia

Yu. Andreev, A. Dermenev, S. Gninenko, N. Golubev, A. Karneyeu, M. Kirsanov, N. Krasnikov, A. Pashenkov, D. Tlisov, A. Toropin

Institute for Theoretical and Experimental Physics, Moscow, Russia

V. Epshteyn, V. Gavrilov, N. Lychkovskaya, V. Popov, I. Pozdnyakov, G. Safronov, A. Spiridonov, E. Vlasov, A. Zhokin

P.N. Lebedev Physical Institute, Moscow, Russia

V. Andreev, M. Azarkin[32], I. Dremin[32], M. Kirakosyan, A. Leonidov[32], G. Mesyats, S.V. Rusakov, A. Vinogradov

Skobeltsyn Institute of Nuclear Physics, Lomonosov Moscow State University, Moscow, Russia

A. Baskakov, A. Belyaev, E. Boos, M. Dubinin[33], L. Dudko, A. Ershov, A. Gribushin, V. Klyukhin, O. Kodolova, I. Lokhtin, I. Myagkov, S. Obraztsov, S. Petrushanko, V. Savrin,

A. Snigirev

State Research Center of Russian Federation, Institute for High Energy Physics, Protvino, Russia

I. Azhgirey, I. Bayshev, S. Bitioukov, V. Kachanov, A. Kalinin, D. Konstantinov, V. Krychkine, V. Petrov, R. Ryutin, A. Sobol, L. Tourtchanovitch, S. Troshin, N. Tyurin, A. Uzunian, A. Volkov

University of Belgrade, Faculty of Physics and Vinca Institute of Nuclear Sciences, Belgrade, Serbia

P. Adzic[34], M. Ekmedzic, J. Milosevic, V. Rekovic

Centro de Investigaciones Energéticas Medioambientales y Tecnológicas (CIEMAT), Madrid, Spain

J. Alcaraz Maestre, E. Calvo, M. Cerrada, M. Chamizo Llatas, N. Colino, B. De La Cruz, A. Delgado Peris, D. Domínguez Vázquez, A. Escalante Del Valle, C. Fernandez Bedoya, J.P. Fernández Ramos, J. Flix, M.C. Fouz, P. Garcia-Abia, O. Gonzalez Lopez, S. Goy Lopez, J.M. Hernandez, M.I. Josa, E. Navarro De Martino, A. Pérez-Calero Yzquierdo, J. Puerta Pelayo, A. Quintario Olmeda, I. Redondo, L. Romero, M.S. Soares

Universidad Autónoma de Madrid, Madrid, Spain

C. Albajar, J.F. de Trocóniz, M. Missiroli, D. Moran

Universidad de Oviedo, Oviedo, Spain

H. Brun, J. Cuevas, J. Fernandez Menendez, S. Folgueras, I. Gonzalez Caballero, E. Palencia Cortezon, J.M. Vizan Garcia

Instituto de Física de Cantabria (IFCA), CSIC-Universidad de Cantabria, Santander, Spain

J.A. Brochero Cifuentes, I.J. Cabrillo, A. Calderon, J.R. Castiñeiras De Saa, J. Duarte Campderros, M. Fernandez, G. Gomez, A. Graziano, A. Lopez Virto, J. Marco, R. Marco, C. Martinez Rivero, F. Matorras, F.J. Munoz Sanchez, J. Piedra Gomez, T. Rodrigo, A.Y. Rodríguez-Marrero, A. Ruiz-Jimeno, L. Scodellaro, I. Vila, R. Vilar Cortabitarte

CERN, European Organization for Nuclear Research, Geneva, Switzerland

D. Abbaneo, E. Auffray, G. Auzinger, M. Bachtis, P. Baillon, A.H. Ball, D. Barney, A. Benaglia, J. Bendavid, L. Benhabib, J.F. Benitez, G.M. Berruti, P. Bloch, A. Bocci, A. Bonato, C. Botta, H. Breuker, T. Camporesi, G. Cerminara, S. Colafranceschi[35], M. D'Alfonso, D. d'Enterria, A. Dabrowski, V. Daponte, A. David, M. De Gruttola, F. De Guio, A. De Roeck, S. De Visscher, E. Di Marco, M. Dobson, M. Dordevic, N. Dupont-Sagorin, A. Elliott-Peisert, G. Franzoni, W. Funk, D. Gigi, K. Gill, D. Giordano, M. Girone, F. Glege, R. Guida, S. Gundacker, M. Guthoff, J. Hammer, M. Hansen, P. Harris, J. Hegeman, V. Innocente, P. Janot, M.J. Kortelainen, K. Kousouris, K. Krajczar, P. Lecoq, C. Lourenço, N. Magini, L. Malgeri, M. Mannelli, J. Marrouche, A. Martelli, L. Masetti, F. Meijers, S. Mersi, E. Meschi, F. Moortgat, S. Morovic, M. Mulders, M.V. Nemallapudi, H. Neugebauer, S. Orfanelli, L. Orsini, L. Pape, E. Perez, A. Petrilli, G. Petrucciani, A. Pfeiffer, D. Piparo, A. Racz, G. Rolandi[36], M. Rovere, M. Ruan, H. Sakulin, C. Schäfer,

C. Schwick, A. Sharma, P. Silva, M. Simon, P. Sphicas[37], D. Spiga, J. Steggemann, B. Stieger, M. Stoye, Y. Takahashi, D. Treille, A. Tsirou, G.I. Veres[16], N. Wardle, H.K. Wöhri, A. Zagozdzinska[38], W.D. Zeuner

Paul Scherrer Institut, Villigen, Switzerland
W. Bertl, K. Deiters, W. Erdmann, R. Horisberger, Q. Ingram, H.C. Kaestli, D. Kotlinski, U. Langenegger, T. Rohe

Institute for Particle Physics, ETH Zurich, Zurich, Switzerland
F. Bachmair, L. Bäni, L. Bianchini, M.A. Buchmann, B. Casal, G. Dissertori, M. Dittmar, M. Donegà, M. Dünser, P. Eller, C. Grab, C. Heidegger, D. Hits, J. Hoss, G. Kasieczka, W. Lustermann, B. Mangano, A.C. Marini, M. Marionneau, P. Martinez Ruiz del Arbol, M. Masciovecchio, D. Meister, N. Mohr, P. Musella, F. Nessi-Tedaldi, F. Pandolfi, J. Pata, F. Pauss, L. Perrozzi, M. Peruzzi, M. Quittnat, M. Rossini, A. Starodumov[39], M. Takahashi, V.R. Tavolaro, K. Theofilatos, R. Wallny, H.A. Weber

Universität Zürich, Zurich, Switzerland
T.K. Aarrestad, C. Amsler[40], M.F. Canelli, V. Chiochia, A. De Cosa, C. Galloni, A. Hinzmann, T. Hreus, B. Kilminster, C. Lange, J. Ngadiuba, D. Pinna, P. Robmann, F.J. Ronga, D. Salerno, S. Taroni, Y. Yang

National Central University, Chung-Li, Taiwan
M. Cardaci, K.H. Chen, T.H. Doan, C. Ferro, M. Konyushikhin, C.M. Kuo, W. Lin, Y.J. Lu, R. Volpe, S.S. Yu

National Taiwan University (NTU), Taipei, Taiwan
P. Chang, Y.H. Chang, Y.W. Chang, Y. Chao, K.F. Chen, P.H. Chen, C. Dietz, U. Grundler, W.-S. Hou, Y. Hsiung, Y.F. Liu, R.-S. Lu, M. Miñano Moya, E. Petrakou, J.f. Tsai, Y.M. Tzeng, R. Wilken

Chulalongkorn University, Faculty of Science, Department of Physics, Bangkok, Thailand
B. Asavapibhop, G. Singh, N. Srimanobhas, N. Suwonjandee

Cukurova University, Adana, Turkey
A. Adiguzel, S. Cerci[41], C. Dozen, S. Girgis, G. Gokbulut, Y. Guler, E. Gurpinar, I. Hos, E.E. Kangal[42], A. Kayis Topaksu, G. Onengut[43], K. Ozdemir[44], S. Ozturk[45], B. Tali[41], H. Topakli[45], M. Vergili, C. Zorbilmez

Middle East Technical University, Physics Department, Ankara, Turkey
I.V. Akin, B. Bilin, S. Bilmis, B. Isildak[46], G. Karapinar[47], U.E. Surat, M. Yalvac, M. Zeyrek

Bogazici University, Istanbul, Turkey
E.A. Albayrak[48], E. Gülmez, M. Kaya[49], O. Kaya[50], T. Yetkin[51]

Istanbul Technical University, Istanbul, Turkey
K. Cankocak, Y.O. Günaydin[52], F.I. Vardarlı

Institute for Scintillation Materials of National Academy of Science of Ukraine, Kharkov, Ukraine

B. Grynyov

National Scientific Center, Kharkov Institute of Physics and Technology, Kharkov, Ukraine

L. Levchuk, P. Sorokin

University of Bristol, Bristol, United Kingdom

R. Aggleton, F. Ball, L. Beck, J.J. Brooke, E. Clement, D. Cussans, H. Flacher, J. Goldstein, M. Grimes, G.P. Heath, H.F. Heath, J. Jacob, L. Kreczko, C. Lucas, Z. Meng, D.M. Newbold[53], S. Paramesvaran, A. Poll, T. Sakuma, S. Seif El Nasr-storey, S. Senkin, D. Smith, V.J. Smith

Rutherford Appleton Laboratory, Didcot, United Kingdom

K.W. Bell, A. Belyaev[54], C. Brew, R.M. Brown, D.J.A. Cockerill, J.A. Coughlan, K. Harder, S. Harper, E. Olaiya, D. Petyt, C.H. Shepherd-Themistocleous, A. Thea, I.R. Tomalin, T. Williams, W.J. Womersley, S.D. Worm

Imperial College, London, United Kingdom

M. Baber, R. Bainbridge, O. Buchmuller, A. Bundock, D. Burton, M. Citron, D. Colling, L. Corpe, N. Cripps, P. Dauncey, G. Davies, A. De Wit, M. Della Negra, P. Dunne, A. Elwood, W. Ferguson, J. Fulcher, D. Futyan, G. Hall, G. Iles, G. Karapostoli, M. Kenzie, R. Lane, R. Lucas[53], L. Lyons, A.-M. Magnan, S. Malik, J. Nash, A. Nikitenko[39], J. Pela, M. Pesaresi, K. Petridis, D.M. Raymond, A. Richards, A. Rose, C. Seez, P. Sharp[†], A. Tapper, K. Uchida, M. Vazquez Acosta, T. Virdee, S.C. Zenz

Brunel University, Uxbridge, United Kingdom

J.E. Cole, P.R. Hobson, A. Khan, P. Kyberd, D. Leggat, D. Leslie, I.D. Reid, P. Symonds, L. Teodorescu, M. Turner

Baylor University, Waco, USA

J. Dittmann, K. Hatakeyama, A. Kasmi, H. Liu, N. Pastika, T. Scarborough

The University of Alabama, Tuscaloosa, USA

O. Charaf, S.I. Cooper, C. Henderson, P. Rumerio

Boston University, Boston, USA

A. Avetisyan, T. Bose, C. Fantasia, D. Gastler, P. Lawson, D. Rankin, C. Richardson, J. Rohlf, J. St. John, L. Sulak, D. Zou

Brown University, Providence, USA

J. Alimena, E. Berry, S. Bhattacharya, D. Cutts, Z. Demiragli, N. Dhingra, A. Ferapontov, A. Garabedian, U. Heintz, E. Laird, G. Landsberg, Z. Mao, M. Narain, S. Sagir, T. Sinthuprasith

University of California, Davis, Davis, USA

R. Breedon, G. Breto, M. Calderon De La Barca Sanchez, S. Chauhan, M. Chertok, J. Conway, R. Conway, P.T. Cox, R. Erbacher, M. Gardner, W. Ko, R. Lander, M. Mulhearn,

D. Pellett, J. Pilot, F. Ricci-Tam, S. Shalhout, J. Smith, M. Squires, D. Stolp, M. Tripathi, S. Wilbur, R. Yohay

University of California, Los Angeles, USA

R. Cousins, P. Everaerts, C. Farrell, J. Hauser, M. Ignatenko, G. Rakness, D. Saltzberg, E. Takasugi, V. Valuev, M. Weber

University of California, Riverside, Riverside, USA

K. Burt, R. Clare, J. Ellison, J.W. Gary, G. Hanson, J. Heilman, M. Ivova Rikova, P. Jandir, E. Kennedy, F. Lacroix, O.R. Long, A. Luthra, M. Malberti, M. Olmedo Negrete, A. Shrinivas, S. Sumowidagdo, H. Wei, S. Wimpenny

University of California, San Diego, La Jolla, USA

J.G. Branson, G.B. Cerati, S. Cittolin, R.T. D'Agnolo, A. Holzner, R. Kelley, D. Klein, D. Kovalskyi, J. Letts, I. Macneill, D. Olivito, S. Padhi, C. Palmer, M. Pieri, M. Sani, V. Sharma, S. Simon, M. Tadel, Y. Tu, A. Vartak, S. Wasserbaech[55], C. Welke, F. Würthwein, A. Yagil, G. Zevi Della Porta

University of California, Santa Barbara, Santa Barbara, USA

D. Barge, J. Bradmiller-Feld, C. Campagnari, A. Dishaw, V. Dutta, K. Flowers, M. Franco Sevilla, P. Geffert, C. George, F. Golf, L. Gouskos, J. Gran, J. Incandela, C. Justus, N. Mccoll, S.D. Mullin, J. Richman, D. Stuart, W. To, C. West, J. Yoo

California Institute of Technology, Pasadena, USA

D. Anderson, A. Apresyan, A. Bornheim, J. Bunn, Y. Chen, J. Duarte, A. Mott, H.B. Newman, C. Pena, M. Pierini, M. Spiropulu, J.R. Vlimant, S. Xie, R.Y. Zhu

Carnegie Mellon University, Pittsburgh, USA

V. Azzolini, A. Calamba, B. Carlson, T. Ferguson, Y. Iiyama, M. Paulini, J. Russ, M. Sun, H. Vogel, I. Vorobiev

University of Colorado at Boulder, Boulder, USA

J.P. Cumalat, W.T. Ford, A. Gaz, F. Jensen, A. Johnson, M. Krohn, T. Mulholland, U. Nauenberg, J.G. Smith, K. Stenson, S.R. Wagner

Cornell University, Ithaca, USA

J. Alexander, A. Chatterjee, J. Chaves, J. Chu, S. Dittmer, N. Eggert, N. Mirman, G. Nicolas Kaufman, J.R. Patterson, A. Ryd, L. Skinnari, W. Sun, S.M. Tan, W.D. Teo, J. Thom, J. Thompson, J. Tucker, Y. Weng, P. Wittich

Fermi National Accelerator Laboratory, Batavia, USA

S. Abdullin, M. Albrow, J. Anderson, G. Apollinari, L.A.T. Bauerdick, A. Beretvas, J. Berryhill, P.C. Bhat, G. Bolla, K. Burkett, J.N. Butler, H.W.K. Cheung, F. Chlebana, S. Cihangir, V.D. Elvira, I. Fisk, J. Freeman, E. Gottschalk, L. Gray, D. Green, S. Grünendahl, O. Gutsche, J. Hanlon, D. Hare, R.M. Harris, J. Hirschauer, B. Hooberman, Z. Hu, S. Jindariani, M. Johnson, U. Joshi, A.W. Jung, B. Klima, B. Kreis, S. Kwan[†], S. Lammel, J. Linacre, D. Lincoln, R. Lipton, T. Liu, R. Lopes De Sá, J. Lykken, K. Maeshima, J.M. Marraffino, V.I. Martinez Outschoorn, S. Maruyama,

D. Mason, P. McBride, P. Merkel, K. Mishra, S. Mrenna, S. Nahn, C. Newman-Holmes, V. O'Dell, O. Prokofyev, E. Sexton-Kennedy, A. Soha, W.J. Spalding, L. Spiegel, L. Taylor, S. Tkaczyk, N.V. Tran, L. Uplegger, E.W. Vaandering, C. Vernieri, M. Verzocchi, R. Vidal, A. Whitbeck, F. Yang, H. Yin

University of Florida, Gainesville, USA

D. Acosta, P. Avery, P. Bortignon, D. Bourilkov, A. Carnes, M. Carver, D. Curry, S. Das, G.P. Di Giovanni, R.D. Field, M. Fisher, I.K. Furic, J. Hugon, J. Konigsberg, A. Korytov, T. Kypreos, J.F. Low, P. Ma, K. Matchev, H. Mei, P. Milenovic[56], G. Mitselmakher, L. Muniz, D. Rank, A. Rinkevicius, L. Shchutska, M. Snowball, D. Sperka, S.J. Wang, J. Yelton

Florida International University, Miami, USA

S. Hewamanage, S. Linn, P. Markowitz, G. Martinez, J.L. Rodriguez

Florida State University, Tallahassee, USA

A. Ackert, J.R. Adams, T. Adams, A. Askew, J. Bochenek, B. Diamond, J. Haas, S. Hagopian, V. Hagopian, K.F. Johnson, A. Khatiwada, H. Prosper, V. Veeraraghavan, M. Weinberg

Florida Institute of Technology, Melbourne, USA

V. Bhopatkar, M. Hohlmann, H. Kalakhety, D. Mareskas-palcek, T. Roy, F. Yumiceva

University of Illinois at Chicago (UIC), Chicago, USA

M.R. Adams, L. Apanasevich, D. Berry, R.R. Betts, I. Bucinskaite, R. Cavanaugh, O. Evdokimov, L. Gauthier, C.E. Gerber, D.J. Hofman, P. Kurt, C. O'Brien, I.D. Sandoval Gonzalez, C. Silkworth, P. Turner, N. Varelas, Z. Wu, M. Zakaria

The University of Iowa, Iowa City, USA

B. Bilki[57], W. Clarida, K. Dilsiz, R.P. Gandrajula, M. Haytmyradov, V. Khristenko, J.-P. Merlo, H. Mermerkaya[58], A. Mestvirishvili, A. Moeller, J. Nachtman, H. Ogul, Y. Onel, F. Ozok[48], A. Penzo, S. Sen, C. Snyder, P. Tan, E. Tiras, J. Wetzel, K. Yi

Johns Hopkins University, Baltimore, USA

I. Anderson, B.A. Barnett, B. Blumenfeld, D. Fehling, L. Feng, A.V. Gritsan, P. Maksimovic, C. Martin, K. Nash, M. Osherson, M. Swartz, M. Xiao, Y. Xin

The University of Kansas, Lawrence, USA

P. Baringer, A. Bean, G. Benelli, C. Bruner, J. Gray, R.P. Kenny III, D. Majumder, M. Malek, M. Murray, D. Noonan, S. Sanders, R. Stringer, Q. Wang, J.S. Wood

Kansas State University, Manhattan, USA

I. Chakaberia, A. Ivanov, K. Kaadze, S. Khalil, M. Makouski, Y. Maravin, L.K. Saini, N. Skhirtladze, I. Svintradze

Lawrence Livermore National Laboratory, Livermore, USA

D. Lange, F. Rebassoo, D. Wright

University of Maryland, College Park, USA

C. Anelli, A. Baden, O. Baron, A. Belloni, B. Calvert, S.C. Eno, J.A. Gomez, N.J. Hadley, S. Jabeen, R.G. Kellogg, T. Kolberg, Y. Lu, A.C. Mignerey, K. Pedro, Y.H. Shin, A. Skuja, M.B. Tonjes, S.C. Tonwar

Massachusetts Institute of Technology, Cambridge, USA

A. Apyan, R. Barbieri, A. Baty, K. Bierwagen, S. Brandt, W. Busza, I.A. Cali, L. Di Matteo, G. Gomez Ceballos, M. Goncharov, D. Gulhan, M. Klute, Y.S. Lai, Y.-J. Lee, A. Levin, P.D. Luckey, C. Mcginn, X. Niu, C. Paus, D. Ralph, C. Roland, G. Roland, G.S.F. Stephans, K. Sumorok, M. Varma, D. Velicanu, J. Veverka, J. Wang, T.W. Wang, B. Wyslouch, M. Yang, V. Zhukova

University of Minnesota, Minneapolis, USA

B. Dahmes, A. Finkel, A. Gude, S.C. Kao, K. Klapoetke, Y. Kubota, J. Mans, S. Nour-bakhsh, R. Rusack, N. Tambe, J. Turkewitz

University of Mississippi, Oxford, USA

J.G. Acosta, S. Oliveros

University of Nebraska-Lincoln, Lincoln, USA

E. Avdeeva, K. Bloom, S. Bose, D.R. Claes, A. Dominguez, C. Fangmeier, R. Gonzalez Suarez, R. Kamalieddin, J. Keller, D. Knowlton, I. Kravchenko, J. Lazo-Flores, F. Meier, J. Monroy, F. Ratnikov, J.E. Siado, G.R. Snow

State University of New York at Buffalo, Buffalo, USA

M. Alyari, J. Dolen, J. George, A. Godshalk, I. Iashvili, J. Kaisen, A. Kharchilava, A. Kumar, S. Rappoccio

Northeastern University, Boston, USA

G. Alverson, E. Barberis, D. Baumgartel, M. Chasco, A. Hortiangtham, A. Massironi, D.M. Morse, D. Nash, T. Orimoto, R. Teixeira De Lima, D. Trocino, R.-J. Wang, D. Wood, J. Zhang

Northwestern University, Evanston, USA

K.A. Hahn, A. Kubik, N. Mucia, N. Odell, B. Pollack, A. Pozdnyakov, M. Schmitt, S. Stoynev, K. Sung, M. Trovato, M. Velasco, S. Won

University of Notre Dame, Notre Dame, USA

A. Brinkerhoff, N. Dev, M. Hildreth, C. Jessop, D.J. Karmgard, N. Kellams, K. Lannon, S. Lynch, N. Marinelli, F. Meng, C. Mueller, Y. Musienko[29], T. Pearson, M. Planer, R. Ruchti, G. Smith, N. Valls, M. Wayne, M. Wolf, A. Woodard

The Ohio State University, Columbus, USA

L. Antonelli, J. Brinson, B. Bylsma, L.S. Durkin, S. Flowers, A. Hart, C. Hill, R. Hughes, K. Kotov, T.Y. Ling, B. Liu, W. Luo, D. Puigh, M. Rodenburg, B.L. Winer, H.W. Wulsin

Princeton University, Princeton, USA

O. Driga, P. Elmer, J. Hardenbrook, P. Hebda, S.A. Koay, P. Lujan, D. Marlow, T. Medvedeva, M. Mooney, J. Olsen, P. Piroué, X. Quan, H. Saka, D. Stickland, C. Tully, J.S. Werner, A. Zuranski

Purdue University, West Lafayette, USA

V.E. Barnes, D. Benedetti, D. Bortoletto, L. Gutay, M.K. Jha, M. Jones, K. Jung, M. Kress, N. Leonardo, D.H. Miller, N. Neumeister, F. Primavera, B.C. Radburn-Smith, X. Shi, I. Shipsey, D. Silvers, J. Sun, A. Svyatkovskiy, F. Wang, W. Xie, L. Xu, J. Zablocki

Purdue University Calumet, Hammond, USA

N. Parashar, J. Stupak

Rice University, Houston, USA

A. Adair, B. Akgun, Z. Chen, K.M. Ecklund, F.J.M. Geurts, W. Li, B. Michlin, M. Northup, B.P. Padley, R. Redjimi, J. Roberts, J. Rorie, Z. Tu, J. Zabel

University of Rochester, Rochester, USA

B. Betchart, A. Bodek, P. de Barbaro, R. Demina, Y. Eshaq, T. Ferbel, M. Galanti, A. Garcia-Bellido, P. Goldenzweig, J. Han, A. Harel, O. Hindrichs, A. Khukhunaishvili, G. Petrillo, M. Verzetti, D. Vishnevskiy

The Rockefeller University, New York, USA

L. Demortier

Rutgers, The State University of New Jersey, Piscataway, USA

S. Arora, A. Barker, J.P. Chou, C. Contreras-Campana, E. Contreras-Campana, D. Duggan, D. Ferencek, Y. Gershtein, R. Gray, E. Halkiadakis, D. Hidas, E. Hughes, S. Kaplan, R. Kunnawalkam Elayavalli, A. Lath, S. Panwalkar, M. Park, S. Salur, S. Schnetzer, D. Sheffield, S. Somalwar, R. Stone, S. Thomas, P. Thomassen, M. Walker

University of Tennessee, Knoxville, USA

M. Foerster, K. Rose, S. Spanier, A. York

Texas A&M University, College Station, USA

O. Bouhali[59], A. Castaneda Hernandez, M. Dalchenko, M. De Mattia, A. Delgado, S. Dildick, R. Eusebi, W. Flanagan, J. Gilmore, T. Kamon[60], V. Krutelyov, R. Montalvo, R. Mueller, I. Osipenkov, Y. Pakhotin, R. Patel, A. Perloff, J. Roe, A. Rose, A. Safonov, I. Suarez, A. Tatarinov, K.A. Ulmer

Texas Tech University, Lubbock, USA

N. Akchurin, C. Cowden, J. Damgov, C. Dragoiu, P.R. Dudero, J. Faulkner, K. Kovitanggoon, S. Kunori, K. Lamichhane, S.W. Lee, T. Libeiro, S. Undleeb, I. Volobouev

Vanderbilt University, Nashville, USA

E. Appelt, A.G. Delannoy, S. Greene, A. Gurrola, R. Janjam, W. Johns, C. Maguire, Y. Mao, A. Melo, P. Sheldon, B. Snook, S. Tuo, J. Velkovska, Q. Xu

University of Virginia, Charlottesville, USA

M.W. Arenton, S. Boutle, B. Cox, B. Francis, J. Goodell, R. Hirosky, A. Ledovskoy, H. Li, C. Lin, C. Neu, E. Wolfe, J. Wood, F. Xia

Wayne State University, Detroit, USA

C. Clarke, R. Harr, P.E. Karchin, C. Kottachchi Kankanamge Don, P. Lamichhane, J. Sturdy

University of Wisconsin, Madison, USA

D.A. Belknap, D. Carlsmith, M. Cepeda, A. Christian, S. Dasu, L. Dodd, S. Duric, E. Friis, R. Hall-Wilton, M. Herndon, A. Hervé, P. Klabbers, A. Lanaro, A. Levine, K. Long, R. Loveless, A. Mohapatra, I. Ojalvo, T. Perry, G.A. Pierro, G. Polese, I. Ross, T. Ruggles, T. Sarangi, A. Savin, N. Smith, W.H. Smith, D. Taylor, N. Woods

30: Also at Institute of High Energy Physics and Informatization, Tbilisi State University, Tbilisi, Georgia

31: Also at St. Petersburg State Polytechnical University, St. Petersburg, Russia

32: Also at National Research Nuclear University 'Moscow Engineering Physics Institute' (MEPhI), Moscow, Russia

33: Also at California Institute of Technology, Pasadena, USA

34: Also at Faculty of Physics, University of Belgrade, Belgrade, Serbia

35: Also at Facoltà Ingegneria, Università di Roma, Roma, Italy

36: Also at Scuola Normale e Sezione dell'INFN, Pisa, Italy

37: Also at University of Athens, Athens, Greece

38: Also at Warsaw University of Technology, Institute of Electronic Systems, Warsaw, Poland

39: Also at Institute for Theoretical and Experimental Physics, Moscow, Russia

40: Also at Albert Einstein Center for Fundamental Physics, Bern, Switzerland

41: Also at Adiyaman University, Adiyaman, Turkey

42: Also at Mersin University, Mersin, Turkey

43: Also at Cag University, Mersin, Turkey

44: Also at Piri Reis University, Istanbul, Turkey

45: Also at Gaziosmanpasa University, Tokat, Turkey

46: Also at Ozyegin University, Istanbul, Turkey

47: Also at Izmir Institute of Technology, Izmir, Turkey

48: Also at Mimar Sinan University, Istanbul, Istanbul, Turkey

49: Also at Marmara University, Istanbul, Turkey

50: Also at Kafkas University, Kars, Turkey

51: Also at Yildiz Technical University, Istanbul, Turkey

52: Also at Kahramanmaras Sütcü Imam University, Kahramanmaras, Turkey

53: Also at Rutherford Appleton Laboratory, Didcot, United Kingdom

54: Also at School of Physics and Astronomy, University of Southampton, Southampton, United Kingdom

55: Also at Utah Valley University, Orem, USA

56: Also at University of Belgrade, Faculty of Physics and Vinca Institute of Nuclear Sciences, Belgrade, Serbia

57: Also at Argonne National Laboratory, Argonne, USA

58: Also at Erzincan University, Erzincan, Turkey

59: Also at Texas A&M University at Qatar, Doha, Qatar

60: Also at Kyungpook National University, Daegu, Korea